EPOXIDATION REACTIONS OF SMALL ALKENES ON CATALYTIC SURFACES

A THESIS SUBMITTED TO
THE GRADUATE SCHOOL OF NATURAL AND APPLIED SCIENCES
OF
MIDDLE EAST TECHNICAL UNIVERSITY

BY

EMİNE KURNAZ

IN PARTIAL FULLFILMENT OF THE REQUIREMENTS
FOR
THE DEGREE OF MASTER OF SCIENCE
IN
CHEMICAL ENGINEERING

NOVEMBER 2011

Approval of the thesis:

EPOXIDATION REACTIONS OF SMALL ALKENES ON CATALYTIC SURFACES

submitted by **EMİNE KURNAZ** in partial fulfillment of the requirements for the degree of **Master of Science in Chemical Engineering Department, Middle East Technical University** by,

Prof. Dr. Canan Özgen
Dean, Graduate School of **Natural and Applied Sciences** _____

Prof. Dr. Deniz Üner
Head of Department, **Chemical Engineering** _____

Prof. Dr. Işık Önal
Supervisor, **Chemical Engineering Department**, **METU** _____

Examining Committee Members:
Prof. Dr. İnci Eroğlu
Chemical Engineering Department, METU _____

Prof. Dr. Işık Önal
Chemical Engineering Department, METU _____

Assoc. Prof. Dr. Görkem Külah
Chemical Engineering Department, METU _____

Prof. Dr. Şakir Erkoç
Physics Department, METU _____

Dr. Derya Düzenli
Engineer, General Directorate of Mineral Res. and Explor. _____

Date: 28.11.2011

I hereby declare that all information in this document has been obtained and presented in accordance with academic rules and ethical conduct. I also declare that, as required by these rules and conduct, I have fully cited and referenced all material and results that are not original to this work.

Name, Last name : Emine Kurnaz

Signature :

ABSTRACT

EPOXIDATION REACTIONS OF SMALL ALKENES ON CATALYTIC SURFACES

Kurnaz, Emine
M.Sc., Department of Chemical Engineering
Supervisor: Prof. Dr. Işık Önal

November 2011, 104 pages

Propylene epoxidation reaction was investigated on catalytic surfaces of chlorinated copper(I) oxide and ruthenium(IV) oxide using periodic density functional theory (DFT). Cu_2O(001) and (110) surface of RuO_2 was selected to generate chlorinated surfaces to be used in the study. Besides epoxidation, other reactions that compete with epoxidation were also studied such as formations of allyl-radical, acrolein, acetone on chlorinated Cu_2O(001) and formations of propionaldehyde, allyl-radical and acetone on chlorinated RuO_2(110) surface. Path of each reaction was determined by CI-NEB method and transition state analyses. Generally accepted stable surface intermediate mechanism was utilized in reactions to final products. The surface intermediate favorable on the surfaces in this study was determined to be the intermediate that is not preferable on metallic surfaces under low oxygen.

On chlorinated Cu_2O(001) surface, formation of propylene oxide, acetone and acrolein have higher probability than gas phase allyl-radical since the desorption energy of allyl-radical was calculated to be 70kcal/mol which is a relatively high value. In fact it is desirable since gas phase allyl-radical is known to be the precursor of combustion products. On chlorinated RuO_2(110) surface, desorption

energies of the products were found to be less than that of corresponding values on chlorinated $Cu_2O(001)$. Furthermore, direct propylene formation mechanism was observed to be possible on chlorinated $RuO_2(110)$ surface but not possible on chlorinated $Cu_2O(001)$. When activation barriers and desorption energies of all possible reactions are compared on chlorinated $RuO_2(110)$ surface; gas phase propylene oxide generated directly seems as the preferable product with allyl-radical although it was computed to have high desorption energy.

Comparison of activation barriers obtained in this study on chlorinated $Cu_2O(001)$ with the barriers of nonchlorinated surface revealed chlorine slightly increases the activation barrier of unwanted allylic hydrogen stripping and hence slightly decreases the probability of occurance. When chlorine is placed closer to reaction site, activation barrier of allylic hydrogen stripping reaction increases further. The effect of chlorine might be electronic since the charge of oxygen at reaction site slightly becomes less negative when the place of chlorine gets closer to the reaction site on the surface. Similar comparison between chlorinated and nonchlorinated $RuO_2(110)$ surfaces revealed that chlorine addition does not improve the surface toward propylene oxide formation, rather it is detrimental as chlorine addition caused a decrease in unwanted allylic hydrogen stripping reaction.

Keywords: chlorine, copper oxide, ruthenium oxide, DFT, propylene, partial oxidation

ÖZ

KÜÇÜK ALKENLERİN KATALİTİK YÜZEYLER ÜZERİNDEKİ KISMİ OKSİDASYONU

Kurnaz, Emine
Yüksek Lisans, Kimya Mühendisliği Bölümü
Tez Yöneticisi: Prof. Dr. Işık Önal

Kasım 2011, 104 sayfa

Propilen epoksidasyon reaksiyonu klor eklenmiş bakır(I) oksit ve rutenyum(IV) oksit katalitik yüzeylerinde periyodik DFT kullanılarak incelenmiştir. $Cu_2O(001)$ ve RuO_2'in (110) yüzeyleri bu çalışmada kullanılacak olan klorlanmış yüzeyleri oluşturmak için seçilmiştir. Epoksidasyonun yanı sıra, bu reaksiyonla yarışan klorlu $Cu_2O(001)$ yüzeyinde alil-radikali, akrolein, ve aseton oluşumları; klorlu $RuO_2(110)$ yüzeyinde propion aldehit, alil-radikali ve aseton oluşumları incelenmiştir. Her reaksiyonun oluşum yolu CI-NEB analizi ve geçiş durumu analizleri yapılarak belirlenmiştir. Genel olarak kabul görmüş olan kararlı yüzey ara maddesi oluşumu mekanizması son ürün oluşum reaksiyonları için kullanılmıştır. Bu çalışmada incelenen yüzeyler için avantajlı olduğu ortaya çıkarılan yüzey ara maddesi az oksijen ortamında bulunan metal yüzeyleri için avantajlı olmayan yüzey ara maddesidir.

Klorlu $Cu_2O(001)$ yüzeyinde alil-radikalinin gaz fazına salınma enerjisi yaklaşık 70kcal/mol gibi yüksek bir değerde olduğu için propilen oksit, aseton ve akroelin oluşumları gaz faz alil-radikali oluşumuna göre daha fazla olasılığa sahiptir. Bu avantajlı bir durumdur çünkü gas fazındaki alil-radikalinin yanma reaksiyonunun

öncüsü olduğu bilinmektedir. Klorlu RuO_2(110) yüzeyinde ürünlerin gaz fazına salınma enerjileri klorlu Cu_2O(001) yüzeyindekilere göre daha düşüktür. Ayrıca, direk olarak propilen oksit oluşumu klorlu Cu_2O(001) yüzeyinde mümkün olmadığı halde klorlu RuO_2(110) yüzeyinde mümkündür. Aktivasyon eşikleri ve gaz fazına salınım enerjileri karşılaştırıldığında klorlu RuO_2(110) yüzeyinde yüzey ara ürünü olmadan oluşan propilen oksit ve gaz faza salınma enerjisi yüksek olmasına rağmen alil-radikali tercih edilen ürünlerdir.

Bu çalışmada kullanılan klorlu Cu_2O(001) yüzeyi üzerinde elde edilen aktivasyon eşiklerinin klorsuz yüzeylerdeki eşikler ile karşılaştırılması sonucunda klorun istenmeyen alilik hidrojen koparımı reaksiyonun aktivasyon eşiğini hafifçe arttırdığını ve bunun sonucunda bu reaksiyonun olma olasılığını hafifçe düşürdüğünü ortaya çıkarmıştır. Klor reaksiyon konumuna daha yakın olacak şekilde yerleştirildiğinde, alilik hidrojen koparımı reaksiyonun eşiğini daha da arttırmıştır. Klorün etkisinin elektronik olma ihtimali vardır çünkü reaksiyon konumundaki oksijenin yükü klor daha yakına getirildiğinde daha az negatif olmaktadır. Klorlu ve klorsuz RuO_2(110) yüzeylerindeki benzer karşılaştırma klorun bu yüzeydeki propilen oksit oluşumunu iyileştirmediği aksine istenmeyen alil hidrojeni koparımı reaksiyonunun bariyerini düşürerek kötüleştirdiğini ortaya çıkarmıştır.

Anahtar kelimeler: klor, bakır oksit, rutenyum oksit, DFT, propilen, kısmi oksidasyon

ACKNOWLEDGEMENTS

I wish to express my sincere thanks to my supervisor Prof. Dr. Işık Önal for his guidance and interest throughout this study.

I would like to thank my colleague Deniz Onay, for her helps, support, and sharing part of her results enabling me to improve my studies; Dr. M. Ferdi Fellah for his guidance; Dr. M. Oluş Özbek for his supports and guidance about VASP. Furthermore, I would like to thank İlker Tezsevin for his friendship and quick solutions to technical problems.

I am thankful to my friend Özge Mercan for her invaluable friendship, encouragement and all the discussions we have made. I would like to thank to Sevgi Ünel, Selin Noyan, Duygu Gerçeker, Merve Çınar, Eda Açık, Gülay Yazıcı, Duygu Şengün and all my friends for all of the times spent together. Without them this period would be much tougher. I would like to thank Murat Tınas for his patience and encouragement. I would like to thank my dear housemate Yelda İbadi for her psycohological support.

Above all, I would like to thank my family for their endless love, encouragement and support in all aspects all through my life.

TABLE OF CONTENTS

LIST OF TABLES

TABLES

LIST OF FIGURES

FIGURES

CHAPTER 1

INTRODUCTION

1.1. Propylene Oxide

Propylene oxide (PO) is a colorless liquid with a low-boiling point. As other epoxides, PO is a reactive compound and epoxide ring can be opened by compounds with unstable hydrogen like water, alcohols or organic acids. Another common reaction is the PO's supply of hydroxyl propyl group into compounds which can be generally observed in polymerization reaction of PO (McKetta 1993).

Reactive nature of propylene oxide makes it a very important intermediate since it can be used to produce a large variety of products in chemical industry. Main products that use propylene oxide as a building block include polyether polyols, propylene glycol and propylene glycol ethers. Polyether polyols, the mostly used application area of propylene oxide, are generated by propylene oxide polymerization on polyhydric alcohols (Kirk-Othmer and Kroschwitz 1992). They are utilized in manufacturing of polyurethane foams that have applications as foams, coatings, adhesives and sealants. In addition to that, polyether polyols are used as surfactants and oil demulsifiers. The other main product propylene glycol is generated with the hydrolysis reaction of propylene oxide by water. It has wide application areas such as cosmetic, food or pharmaceutical industries as a solvent; automotive and aircraft industries as hydraulic fluid or de-icer. Furthermore,

propylene glycol is also used for the generation of unsaturated polyester resins to be used in construction, transportation industries (APPE ; SHELL). Propylene glycol ethers are created via the interaction of different types of alcohol i.e. methanol, ethanol, butanol with propylene oxide. They have an application as solvents in paints, coatings, waxes and cleaners.

PO has been gained much of its importance since 1950s due to its reactivity and its being a building block of many important chemicals in industry. According to published data, approximately 6.6 million tons of propylene oxide was consumed in the chemical industry in 2010. Around 90 percentage of produced propylene oxide was used in order to obtain the three main products mentioned above (LyondellBasell)**.**

Propylene oxide is one of the products derived from the partial oxidation reaction of propylene, one of the most abundant olefins. It is generated as a side-product in the cracking processes of oil in refineries. It is the smallest unsaturated hydrocarbon having both a double bond and allylic hydrogen species. Besides partial oxidation reaction, propylene can undergo polymerization reaction with the aid of catalysts to obtain polypropylene or etc.; can be alkylated to get isobutene or higher molecular weight paraffins to be utilized as a blending in gasoline to increase octane number of gasoline; can undergo catalytic ammoxidation reaction to get acrylonitrile to be used in manufacturing of plastics; or can be hydrated by water to get isopropyl alcohol.

1.2. Industrial Propylene Oxide Production

Currently, in industry propylene oxide is produced by basically two processes: i) CHPO (chlorohydrin) ii) Hydroperoxide processes i.e. PO/TBA (tert-butylalcohol) and PO/SM (styrene monomer).

1.2.1. CHPO process

This method is also called as chlorohydrin process. The method was introduced by Wurtz in 1859 and also used for ethylene oxide production before catalytic process with silver is introduced. In the process in addition to propylene, chlorine and

calcium hydroxide are needed as raw materials as 1.4 times of PO and the same amount with PO produced, respectively. Water need is 40 times higher than PO (Cavani and Teles 2009). In the process, propene reacts with chlorine in aqueous environment and a chlorohydrin species is generated. Dehydrochlorination of chlorohydrin is achieved by aqueous potassium hydroxide and the result is the generation of propylene oxide. The overall reaction with the utilization of NaOH used as base is in Figure 1.1:

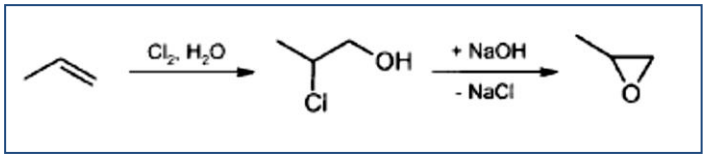

Figure 1.1 Overall reaction of chlorohydrin process with NaOH utilized as the base (Cavani and Teles 2009)

Essential steps of chlorohydrin process can be observed in the flow chart of a chlorohydrin process plant in Figure 1.2.

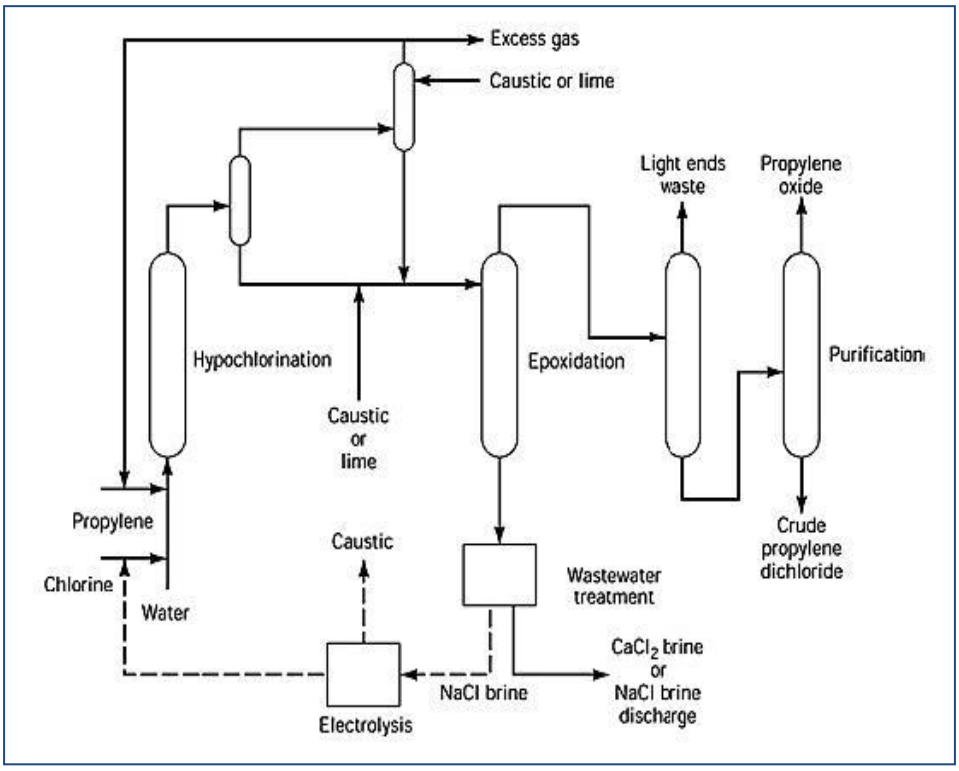

Figure 1.2 Flow chart of a propylene oxide production plant with chlorohydrin process (Trent 2000)

In the first reactor, labeled as “Hypochlorination” in Figure 1.2 chlorohydrin generation is achieved in two steps. In the first step, propylene and chlorine is reacted in the presence of water and generate the propene chloronium complex. The reaction is represented in Figure1.3. By-products 1,2-dichloropropane, the mostly produced species, and allyl chloride which further reacts generate dichloropropanols are produced in two side reactions of this step.

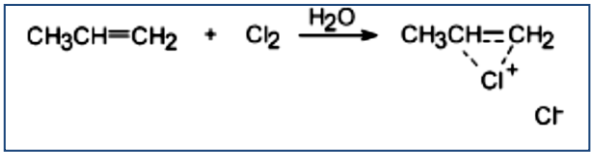

Figure 1.3 Chloronium generation reaction in chlorohydrin process (Kahlich, Wiechern et al. 2000)

Subsequently, two propene chlorohydrin isomers are produced by the interaction of previously generated propene chloronium complex. The first isomer in Figure 1.4 constitutes 90% of chlorohydrin product and the selectivity of the reaction is above 90%. Dichloroisopropyl ethers are also generated by the reaction of propene chlorohydrin and propene-chloronium complex as by-products. Excess water is fed to the system in order to avoid side reactions and minimize by-products (Kahlich, Wiechern et al. 2000)

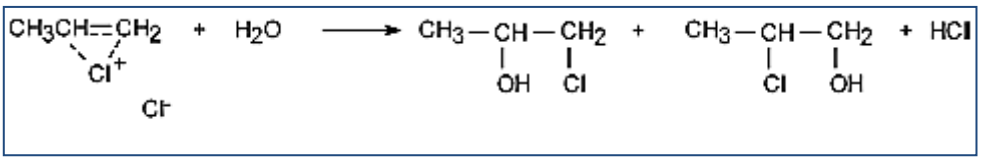

Figure 1.4 Chlorohydrin isomers production from chloronium in chlorohydrin process (Kahlich, Wiechern et al. 2000)

The major by-product 1,2-dichloropropane is sold since it can be used as a solvent, or incinerated with other chlorine containing off-gases to produce HCl (Cavani and Teles 2009).

In the second reactor shown in flow sheet, propylene oxide is produced by reaction of propylene chlorohydrin with $Ca(OH)_2$ or another base. Propylene epoxidation reaction is represented in Figure 1.5.

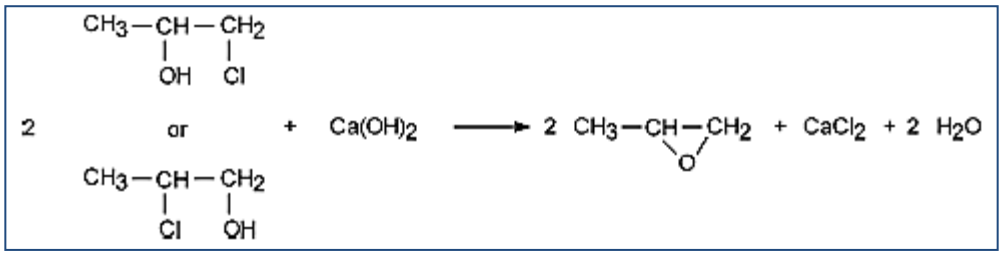

Figure 1.5 Epoxidation of chlorohydrin isomers in the presence of calcium hydroxide as the base (Nijhuis, Makkee et al. 2006)

The side reaction in this reactor is the further hydrolysis of propene oxide to propene glycol. Propene oxide is removed from the reactor by steam to avoid side reaction. Calcium chloride, $CaCl_2$ is also generated as a co-product approximately 2 times of the propylene oxide produced. $CaCl_2$ containing wastewater is 40 times higher than PO and it is one of major problems of chlorohydrin technology. Crude propylene coming from top of second reactor is mixed with some organic by-products and water. In a distillation column propene oxide is separated from its impurities and purified (Nijhuis, Makkee et al. 2006). The construction of a new plant is economically unfeasible due to mostly high cost of first implementation of the plant but also waste water problems (Cavani and Teles 2009).

1.2.2. Hydroperoxide processes

In hydroperoxide processes propylene is reacted with alkyl-hydroperoxides generated by peroxidation of an alkane. Various types of alkanes can be used for this purpose as can be seen in Table 1.1, nevertheless only two of them are industrially implemented since economies of the method is highly dependent on economy of the co-product. The reason of the dependence is the fact that co-products are generated in larger amounts than propylene oxide. Industrially, the propylene oxide- tert-butyl alcohol (PO-TBA) process and the propylene oxide-

styrene monomer (PO-SM or SMPO) process are utilized and will be explained in the following sections.

Table 1.1 Reaction systems used for PO with co-product synthesis (Kahlich, Wiechern et al. 2000)

Raw material	Peroxide	Intermediate	Coproduct
Acetaldehyde	peracetic acid	-	acetic acid
2-Propanol	peracetic acid	acetone	2-propanol
Isobutane	tert-butyl hydroperoxide	tert-butyl alcohol	isobutene
Isopentane	tert-butyl hydroperoxide	tert-pentyl alcohol	isoprene
Ethylbenzene	ethylbenzene hydroperoxide	α-phenylethanol	styrene
Cumene	cumene hydroperoxide	dimethylphenylmethanol	α-methylstyrene
Cyclohexen	cyclohexene hydroperoxide	cyclohexanol	cyclohexanone

1.2.2.1. PO-TBA process

The PO-TBA process utilizes isobutane for the peroxidation step and tert-butyl hydroperoxide is generated by the reaction in Figure 1.6 in liquid-phase. Tert-butyl alcohol is also created in this step approximately in half amount of tert-butyl hydroperoxide. Aldehydes and ketones are minutely produced by-products (Kahlich, Wiechern et al. 2000).

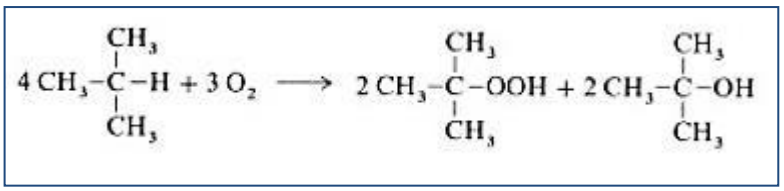

Figure 1.6 Tert-butyl hydroperoxide production reaction from isobutane, hydroperoxide generation step in PO-TBA process (Kahlich, Wiechern et al. 2000)

Afterwards, tert-butyl hydroperoxide is interacted with propylene in the presence of a homogeneous catalyst, organometallics in most cases molybdenum, tungsten or vanadium to generate propylene oxide and co-product tert-butyl alcohol (Figure

1.7). Metal supported heterogeneous catalysts can also be used but metal atoms on the surface are removed in the process (Kirk-Othmer and Kroschwitz 1992; Nijhuis, Makkee et al. 2006).

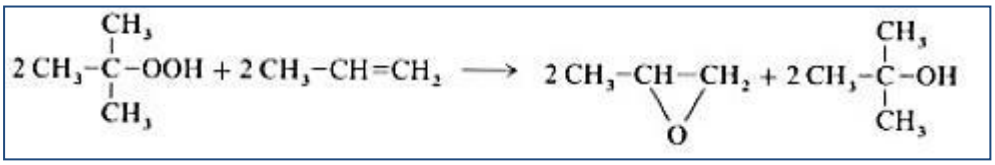

Figure 1.7 Propylene oxide production reaction from tert-butyl hydroperoxide, epoxidation step in PO-TBA process (Kahlich, Wiechern et al. 2000)

Epoxidation is achieved in a series of up to five reactors in the process. Product of epoxidation step is crude propylene oxide and contains tert-butyl alcohol, catalyst and by-products (Kahlich, Wiechern et al. 2000). In order to separate propylene oxide from the crude propylene oxide mixture, a distillation step is employed. Co-product tert-butyl alcohol used to be utilized as a gasoline additive however; that application vanished in recent years (Trent 2000; Nijhuis, Makkee et al. 2006)

1.2.2.2. PO-SM process

The PO-SM process utilizes ethylbenzene for the peroxidation step and styrene monomer is formed as a co-product at 2.5-3 times larger than PO. In the first reactor, ethylbenzene is employed with air to produce ethylbenzene hydroperoxide.

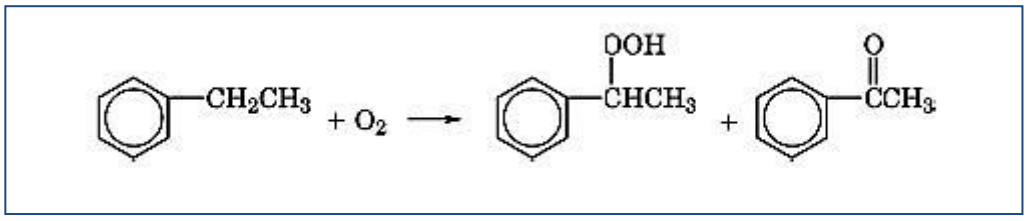

Figure 1.8 Ethylbenzene hydroperoxide production reaction in PO-SM process (Trent 2000)

In the second reactor, ethylbenzene hydroperoxide is catalytically reacted with propene. The reactor products are propene oxide, α-phenylethanol and acetophenone together with other organic impurities.

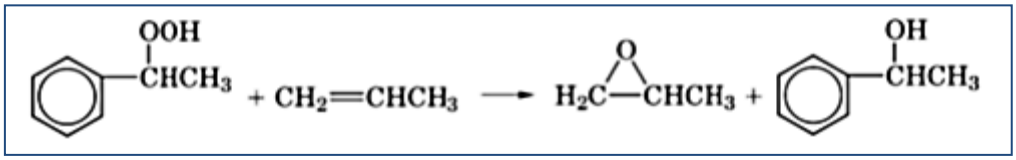

Figure 1.9 Propylene epoxidation reaction in PO-SM process (Trent 2000)

Crude products from second reactor are separated similar to PO-TBA process in a distillation column. α-Phenylethanol at the bottom of the distillation column is further dehydrated in the presence of alumina catalyst in triphenylmethane solvent to produce the co-product styrene.

There are two variants of PO-SM process with respect to type of the catalyst utilized. One is named as Halcon process and uses homogeneous molybdenum based catalyst and Shell process utilizes titanium-based heterogeneous catalyst. Recovery of homogenous catalyst from the product mixture is more problematic than heterogeneous so Shell process is preferred in building new PO plants based on hydroperoxide method. Furthermore, Shell has done many improvements in the process to increase the selectivity and to reduce the first investment cost of the process such as removal of by-products, addition of recycle stream in order to decrease side reactions (Buijink, Lange et al. 2008)

1.2.2.3. PO-only process by cumene

In 2003, Sumitomo Chemical Company in Japan implemented a PO production plant similar to PO-SM process with fewer co-products. In the procedure, cumene species is used instead of ethylbenzene to generate cumene hydroperoxide compound. Cumene hydroperoxide is employed to react with propylene in the presence of highly reactive Ti/SiO_2 catalysts in a fixed bed reactor. Propylene oxide is produced and cumyl alcohol is obtained as a co-product. Cumyl alcohol is dehydrated to α-methylstyrene and hydrogenated to get cumene or it is directly

hydrogenolysed to cumene. The overall reaction scheme of the process can be seen in Figure 1.10.

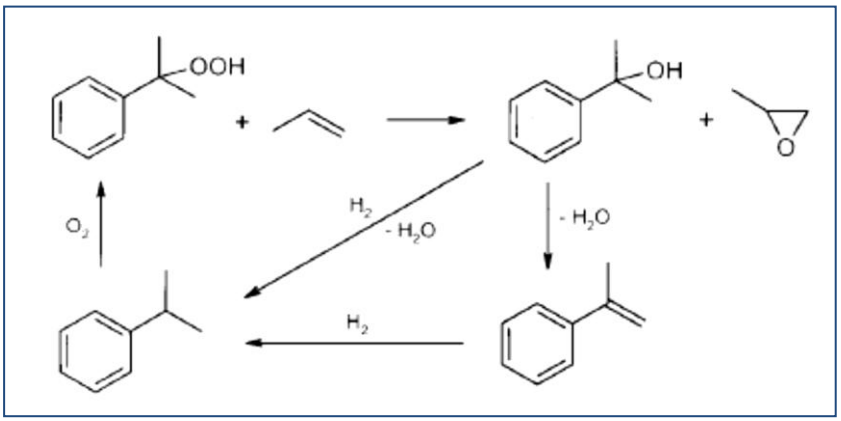

Figure 1.10 Overall reaction scheme in PO-only process by cumene

By those reactions, co-product is converted to a raw material and supplied to the system making the process advantageous over PO-SM process. Another advantage comes from the cumene hydroperoxidation reaction that, it is a fast autoxidation process with a selectivity of 95-98% with respect to cumene whereas ethylbenzene hydroperoxidation has 72-77% selectivity (Sumitomo Chemical Co.).

1.2.3. Direct Oxidation

All of the industrial PO production methods are problematic. They are inefficienct, require high implementation cost, their economy depend on the co-product produced more than PO in the process, and they produce high amounts of environmentally unfriendly wastes.

The desired method for propylene epoxidation is the direct selective oxidation of propylene with oxygen with the aid of a heterogeneous catalyst in analogy with ethylene direct epoxidation route on silver based heterogeneous catalysts. Direct epoxidation of ethylene on silver based catalysts give selectivities around 50% and the selectivity increases close to 90% when tiny amounts of hydrochlorinated species are added to the feedstream. However, an epoxidation catalyst could not been developed yet for the propylene epoxidation reaction.

1.3. Catalysis Phenomena

Catalysis has very important contribution to our lives. Catalytic processes are everywhere in production of food, generation of energy, building up materials and in almost all biological reactions in bodies like digesting food, functioning of organs, fighting for diseases, breathing. Furthermore, catalytic processes comprise a very big portion of the world's economy. Those processes are responsible of production of the 60% of all chemicals (Ertl, Knözinger et al. 1997). More than 80% of the industrial processes developed after 1980 depend on catalytic reactions. Moreover, around 15 companies in the world just work in the area of producing catalysts (Deutschmann, Knözinger et al. 2000). Catalyst usage is dominant in four major sector; refining, chemicals, polymerization and exhaust emission.

Catalyst is defined as the substance that changes the speed of conversion of reactants into products by participating elementary steps of reaction and being regenerated so that it returns to its original state at the end of the catalytic cycle. (Cornils 2003). They can be active in a wide temperature and pressure ranges; between 78K and 1500K and between of 10^{-9} and 100MPa pressures (Deutschmann, Knözinger et al. 2000). Catalysts are basically classified into three categories; homogeneous catalysts, biocatalysts and heterogeneous catalysts. Homogeneous catalysts are those in the same phase with the reactants and products. Generally, homogeneous catalysts are transition metals combined with an organic ligand and they are involved in reactions taking place in a liquid solvent. Biocatalysts are specific kind of catalysts that has similarities with both homogeneous and heterogeneous catalysts and are active in organisms or bioreactors. Enzymes are classified as biocatalysts and they are the most efficient of all catalysts.

Heterogeneous catalysts' phase is different than the phase of reactants and products. As a result, heterogeneously catalyzed processes has an advantage over homogenously catalyzed or biocatalyzed systems since distinct phases makes the separation of the catalyst from the system easier (Ertl, Knözinger et al. 1997). Well-known examples of heterogeneous catalytic systems are gas-solid systems where the catalysts are solid and the reactants with products are in gas phase.

Reaction mechanism on a heterogeneous catalyst begins with the travel of the reactants from feed stream to catalyst surface. Reactant molecules should diffuse into pores of catalyst particles to reach active site where they adsorbed prior to reaction. The reaction on the active site may take place either directly or through formation of stable surface intermediates. After the reaction, products are adsorbed on the active site. Subsequently, products desorb from actives site, diffuse to catalyst surface through pores and mixed with flow to reactor outlet. Some of these phenomena occurs at macroscopic level while the other at microscopic level making the situation harder to understand (Ertl, Knözinger et al. 1997; Rothenberg 2008)

An important concept in understanding the reaction mechanism analysis is the **transition state theory**. It is an alternative to Arrhenius equation and collision theory. Transition state theory claims the existence of a potential energy barrier that reactants should pass through to give products. At the maximum point of the energy barrier an activated complex, the transition state, is generated (Chorkendorff and Niemantsverdriet 2007). Transition states are at the saddle points of the reaction potential energy diagrams. Furthermore, they are in quasi-equilibrium state with reactants. In other words, transition state formation is a reversible process; activated complexes can proceed either to products side or go in reverse direction and form reactants again. On the other hand, path from transition state to products is irreversible, once the system passed through the transition state point it can only continue in the direction towards products.

Another important notion in catalytic reaction mechanism is the active site concept. **Active sites** are parts of the catalytic surface where the reactants are adsorbed and reaction takes place. They have distinct characteristics than the other parts of the substance that provide the catalytic activity. For example, atoms on the active site are not fully coordinated thus have more affinity to interact with adsorbates. Defect sites, step sizes and vacancies are candidates for active sites as atoms at those sites have less coordinated than bulk. Additionally, specific surfaces of the material may provide uncoordinated sites as some of the surface atoms have less coordination than corresponding bulk atoms. All in all, active sites can have different sizes, shapes and orientations on the surface and they might be heterogeneously

distributed over the surface. Those dissimilarities of active sites make each site unique in terms of interaction affinity with adsorbents.

The interaction between reactants and catalyst surface on the active site affects the rate of the reaction on catalytic surface. That effect is explained by **Sabatier's principle** which claims that the interaction shouldn't be so weak or so strong. In the case of so weak interactions, reactants leave the surface so easily without reacting to give products. The other case is the interaction being so strong that the products do not leave the catalyst surface and block the active sites causing decrease in reaction rate and eventually deactivating the catalyst. Therefore, there is an optimum point in the reactant-surface interaction where the reaction rate is at maximum which is called Sabatier's maximum. Rate of reaction is related to the heat of adsorption of reactants. At low heats of adsorption there is a direct relationship, as heat of adsorption increases, reaction rate also increases reaching Sabatier's maximum. After that point, reaction rate starts to decrease with increase in heat of adsorption since the products do not desorb. This trend gives a volcano plot and a good catalyst should have surface that provides a mild interaction with reactants, intermediates that are formed during reaction and the products of the reaction (Rothenberg 2008).

A good catalyst should have more features than just providing the increase in reaction rates of all possible reactions between the reactants. It should enhance formation of the desired products by increasing selectivity of the system towards them.

1.3.1. Promoters and Poisons

Selectivity increase can be achieved by adding tiny amounts of specific compounds i.e. promoters or poisons to the catalyst. They may be present on the surface as impurities or can be fed to the system by reactant stream. They are also called performance adjuster and may have also effect on activity and/or lifetime of the catalyst. These species may not be catalytically active on their own but just alter the performance of the catalyst or they can act separately as a catalyst and make the

catalyst bifunctional. Promotion or poisoning effects are not only catalyst species dependent but also reaction dependent (Ertl, Knözinger et al. 1997).

Promoters provide an improvement effect on catalytic properties. They are classified as structural promoters or electronic promoters according to the nature of the effect. Structural promoters deal with surface configuration, change surface area, increase dispersion of the catalyst on support, prevent sintering etc. Structural promoters are also known as textural modifiers (Rothenberg 2008). Electronic promoters whose most well-known examples are alkali metals change binding characteristics of the surface and hence affects adsorption kinetics, dissociation of products from the surface. Change in bond strength of a reactant and the surface can significantly modify catalytic activity as Sabatier's Principle suggests (Chorkendorff and Niemantsverdriet 2007).

Poisons may block sites on the surface and/or alters the interaction between substrate and catalytic surface and decreases the activity of catalyst. Poisoning effect can be reversible or irreversible for example high doping of chlorine promoter to silver catalyst in ethylene epoxidation can lead to irreversible formation of bulk AgCl phase which is inactive. When there exists more than one reaction occurring on the surface, poisons can be used to increase selectivity by decreasing activity of the catalyst towards undesired reaction (Rothenberg 2008). Poisons can also be used to decrease the reaction rate of excessively exothermic reactions that can produce hot-spots that make the catalytic system unstable. In this case, poisons act also as promoters by making the system more stable.

1.3.2. Metal Oxide Catalysts

Metal oxides have great and even increasing importance in catalytic processes in petroleum, environmental and chemical industries due to their versatile properties. They are either employed on their own as catalysts or as supports of metals or even supports of other metal oxides. Bulk metal oxides are utilized as heterogeneous catalysts in selective oxidation reactions to produce chemical intermediates that are important for chemical industry (Fierro 2006). Metal oxides as supports can enhance catalyst's activity since interaction of supports and catalysts may result in

the change of adsorption properties. Furthermore, addition of support can alter the structure of the catalyst by increasing production of some specific crystal surfaces and increasing surface area which also contribute to catalytic affinity (Henrich and Cox 1996).

The most important concern of researchers employing metal oxides in their study is to find out the origin of their properties and to learn how to manipulate these properties to get desired behavior. Determination of structure-function relationships is of invaluable importance to be able to smartly design the catalysts. Features of the surface are crucial for particular reactions i.e. selective oxidation reactions. Catalytic surface should be active enough to actuate reactants and the oxygen on the surface but it shouldn't provoke breaking C-H bonds and facilitate total oxidation. Some particular characteristics have more influence on catalytic performance especially for selective oxidation reactions:

Characteristics of oxygen species on the oxidized surface have particular importance for selective oxidation catalysts. Basically four types of adsorbed oxygen are identified on oxide surfaces. The first one (O_2^*) is molecular oxygen adsorbed to the catalytic surface. Oxygen shows that kind of behavior on stoichiometric, fully oxidized metallic oxides. The second one (O_2^-) is bound molecularly and gained a negative charge. The third (O^-) and fourth (O^{2-}) are atomic oxygens with -1 and -2 charges, respectively. Although O_2^{2-} and O_3^- species were observed in studies of alkali, alkaline earth oxides and TiO_2, the four oxygen species mentioned above are the most common ones in transition metal oxides. The last three take part in increasing oxidation state of cations on the surface to some extent depending on charge transfer (Kung 1989). First three oxygens show electrophilic character and so active that they facilitate C-H bond activation and combustion reaction. O^{2-} is more nucleophilic and can assist selective oxygenation reactions (Santen and Neurock 2006).

Oxidation state of the metals in the structure is crucial and related to acid base properties and redox characteristics, hence metal oxides with different oxidation states function differently. A cation should have capability to change its oxidation state to be able to take part in redox reactions. Transition metals are potential

candidates for redox reactions since they can be in more than one oxidation state. Specifically, cations in lower oxidation state are more active.

Degree of coordination of surface atoms determines the willingness of surface atoms to interact with adsorbates. Surface atoms have smaller number of neighbors than the atoms in bulk. Therefore, they have fewer bonds, lower coordination number than bulk atoms and labeled as coordinatively unsaturated. Generally, coordinatively unsaturated atoms have tendency to make bonds with adsorbates. On a surface of metal oxide, coordinatively unsaturated metal ions behave like a Lewis acid while coordinatively unsaturated oxygen ions' basicity is higher than bulk oxygens. Coordinatively unsaturated sites are important in surface chemistry due to their active nature. They may be removed easily than bulk materials. Adsorbate molecules are chemisorbed and make bonds on these sites. Prior to utilization of oxide, activation of surfaces are required by heating since some water might be adsorbed on coordinatively unsaturated sites (cus) of oxides making them saturated and unwilling to make more bonds (Kung 1989). Surface coordination can be controlled by choosing the exposed crystal plane and utilizing proper preparation methods to produce it (Fierro 2006).

Width of band gap is another feature to address oxidation reduction capabilities of materials. The term band gap is used to define the energy state between valence band and conduction band of a material. In band gap, no electron states can exist, and it is a property that determines the electrical conductivity of material together with many physical or chemical properties. Materials having a large band gap are insulators since it is hard to excite an electron to a conduction band. Smaller band gap means that the material is a semiconductor and very little or no band gap indicates conductors. Band gap is also a sign of oxide species' reducibility which can affect activity or selectivity of catalyst towards oxidation reactions.

Various acid-base characteristics should be present at the surface due to the fact that adsorption of a molecule to a site is controlled by Lewis and Bronsted acid-base properties. Concept of hard and soft acid-base is not used in the studies of heterogeneous catalyst. Coordinatively unsaturated cation on the surface behave like a Lewis acid site and they tend to make bonds accepting electrons while oxygen

ions accept protons and act like a Bronsted base (Fierro 2006). For this reason, surfaces are treated with various probe molecules to determine whether acid-base properties are suitable for specific reactions before analysis with real reactants. Probe molecules are selected according to their ability to identify specific surface properties for specific reactions. Surface acidity or basicity can be altered in order to change the reactivity of the surface as desired.

Types of chemical bonds that connect the oxide are also related with its properties since oxidation state of the metal is determined according to the types of bonds that makes with neighboring atom.

Defect sites in various types of abnormal structures can exist within oxide material. Vacancies, interstitials, trapped electrons or holes are some examples of abnormalities. Defect sites have different electronic structures which can affect surrounding atoms and can significantly change surface reactivity and many reactions on surface occur at defect sites. Coordinatively unsaturated nature of atoms in defect sites is the reason of their high activity (Santen and Neurock 2006). For instance, rock salt structured MgO(100) is almost inactive but oxygen vacancies on surface creates sites that compounds can adsorb and reacts (Chorkendorff and Niemantsverdriet 2007).

Surface morphology and structure, particle size and shape are also factors that can alter catalytic properties of a material. Furthermore, they can be tuned with the addition of support or textural modifiers but at the same time they are dynamic properties and modifications can be observed in the process of reaction depending on the reaction conditions. Along with mentioned in this paragraph, part of the characteristics of the oxide surfaces described above are sensitive to reaction conditions, could be destroyed or changed in the high temperature and high oxygen concentrations in the reactors.

1.4. Computational Chemistry Application to Catalysis

Computational models at microscopic level help to understand or to predict the catalytic phenomena. Computational approach can be used to completely understand the reaction mechanism in combination with the foundations of

experimental work. Experimental methods may be insufficient for the identification of some surface intermediates due to their rapid formation and disappearance which can lead to miss the exact reaction mechanism. Additionally, computational methods can be used to predict the properties of the substances prior to synthesizing them since some properties of compounds are easier, quicker or cheaper to be found computationally than experimentally (Young 2001).

Theoretical computational methods depend on quantum mechanics which is the exact mathematical description of the behavior of electrons. In principle, using quantum mechanics tools, every property of an atom or molecule can be correctly estimated. Schrödinger's equation is the way to calculate properties of a system which is the description of the quantum state of a system with time. Time-independent form of Schrödinger's equation describes stationary state systems and it is formulated as follows:

$$\hat{\mathrm{H}}\Psi_i(\boldsymbol{x}_1, \boldsymbol{x}_2, \ldots, \boldsymbol{x}_N) = E_i\Psi_i(\boldsymbol{x}_1, \boldsymbol{x}_2, \ldots, \boldsymbol{x}_N) \tag{1.1}$$

Where $\boldsymbol{x}_i$ contains both space coordinates r_i and spin coordinates s_i. $\hat{\mathrm{H}}$ is the Hamiltonian operator for a system having M nuclei and N electrons. Hamiltonian operator consists of all the energy terms required to define the molecule:

$$\hat{\mathrm{H}} = -\frac{1}{2}\sum_{\mathrm{i}=1}^{\mathrm{N}}\nabla_{\mathrm{i}}^2 - \frac{1}{2}\sum_{\mathrm{A}=1}^{\mathrm{M}}\frac{1}{\mathrm{M_A}}\nabla_{\mathrm{A}}^2 + \sum_{\mathrm{i}=1}^{\mathrm{N}}\vartheta(\mathbf{r}_{\mathrm{i}}) + \sum_{\mathrm{i}=1}^{\mathrm{N}}\sum_{\mathrm{j}>\mathrm{i}}^{\mathrm{N}}\frac{1}{\mathrm{r_{ij}}} + \sum_{\mathrm{A}=1}^{\mathrm{M}}\sum_{\mathrm{B}>\mathrm{A}}^{\mathrm{M}}\frac{\mathrm{Z_A Z_B}}{\mathrm{R_{AB}}} \tag{1.2}$$

where $\vartheta(\boldsymbol{r}_i)$ is the external potential on electron i due to the nuclei of A with charges Z_A, which is formulated below:

$$\vartheta(\boldsymbol{r}_i) = -\sum_{A=1}^{M}\frac{Z_A}{\boldsymbol{r}_{iA}} \tag{1.3}$$

where A, B are related to nuclei and i, j are related to electrons. However, in reality quantum equations can only be solved for systems having a few electrons. The reason is the enormous increase in number of equations to be solved as the number of electrons in the system increases (Parr and Yang 1994; Koch and Holthausen 2001).

Calculations are simplified by the Born-Oppenheimer approximation which is based on the fact that nuclei of molecules' movement are much slower than electrons' which are nearly 1800 times lighter. Electrons take their positions instantaneously with respect to the displacement of nucleus. Therefore, it is appropriate to separate nucleus movement calculations and electron movement calculations. Electronic energy calculations can be performed at fixed nucleus and compute kinetic energy independent of electrons. By this way, term for nuclear kinetic energy vanishes and nuclear-nuclear repulsion energy becomes a constant for a specified geometry (Cramer 2004). Application of the Born-Oppenheimer approximation makes Hamiltonian operator as follows:

$$\hat{\mathrm{H}} = -\frac{1}{2}\sum_{i=1}^{N}\nabla_i^2 + \sum_{i=1}^{N}\vartheta(\mathbf{r}_\mathrm{i}) + \sum_{i=1}^{N}\sum_{j>i}^{N}\frac{1}{r_{ij}} \tag{1.4}$$

where the first term is kinetic energy of electrons, the second is attractive interaction of electrons with stationary nuclei and the last one stands for the repulsive electron-electron interactions (Young 2001).

Hamiltonian operator can be expressed in more compact form as follows:

$$\hat{\mathrm{H}} = \hat{T} + \hat{V}_{ne} + \hat{V}_{ee} \tag{1.5}$$

in which kinetic energy is expressed as;

$$\hat{T} = -\frac{1}{2}\sum_{i=1}^{N}\nabla_i^2 \tag{1.6}$$

energy comes from nucleus-electron interaction as;

$$\hat{V}_{ne} = \sum_{i=1}^{N}\vartheta(\mathbf{r}_\mathrm{i}) = -\sum_{i=1}^{N}\sum_{A=1}^{M}\frac{Z_A}{\boldsymbol{r}_{iA}} \tag{1.7}$$

and finally electron-electron interaction as;

$$\hat{V}_{ee} = \sum_{i=1}^{N}\sum_{j>i}^{N}\frac{1}{r_{ij}} \tag{1.8}$$

1.4.1. Molecular Mechanics

Molecular mechanics simulations use classical expressions rather than quantum mechanical technique to calculate the energy of a compound. Molecular mechanics methods approximate nuclei and electrons together as spherical atom-like species and molecule as a group of weights symbolizing nuclei that are connected by springs as symbols of the bonds. Calculations of the structure and energy of the molecules are done with force fields which are functions and parameters based on experimental data and/or theoretical concept. Force fields are used to compute nuclear interactions between the particles and a classical mechanics' concept potential functions which are constructed based on empirical parameters.

Electron movements are not considered by an assumption similar to the Born-Oppenheimer approximation; they are accepted to be settled so fast after nucleus of an atom finds its position (Ramachandran, Deepa et al. 2008).

1.4.2. Molecular Dynamics and Monte Carlo Simulations

Molecular Dynamics and Monte Carlo simulations utilize statistical mechanics principles to determine the macroscopic properties of a bulk material. Statistical mechanics methods calculate thermodynamic properties of bulk materials employing molecular description of the material.

Molecular Dynamics simulations model the molecular system in a time-dependent manner. Energy calculations are made by means of molecular mechanics and used in order to evaluate the forces acting on atoms (Young 2001). Generally, molecular systems contain hundreds or thousands of atoms in a constant volume. Time variable is included over millions of iterations with very small time steps in femtoseconds. Simulations result in time-averaged properties which are comparable to experimentally obtained ones.

Monte Carlo calculations are performed by random generation of location, orientation and structural geometry of atoms or molecules by choosing a value of a variable randomly. The results of high numbers of iterations are refined by a convergence criterion in terms of energy in accordance with the statistical analysis

(Dronskowski 2005). Monte Carlo simulations are computationally less expensive than Molecular Dynamics but cannot estimate properties requiring time-dependent calculations (Young 2001).

1.4.3. Ab-initio Methods

Ab-initio calculations are dependent on only theoretical basis that no experimental correlations or parameters are introduced as the name ab-initio, "from the beginning" in Latin, implies.

Ab-initio methods describe the systems using just some basic information; the speed of light, Planck's constant, the mass and the charge of the electron. Chemical properties, sizes and structure of the molecule are obtained first by calculating the wavefunction, a mathematical constraint that does not exist in real life, and then using the correlations between wavefunction and the properties of the system. However, ab-initio calculations can be practically applied molecules having 50 atoms or less due to the enormous increase of equations to be solved when the number of the atoms in the system increases and hence computational time required for calculations increase. In order to make the system of equations practically solvable some simplifications should be involved.

The mostly used method for simplifications is the Hartree-Fock (HF) approximation. The fundamental assumption in this method is the neglect of correlations between electrons which can have significant consequences on accuracy of wavefunctions. Some methods start with HF calculations and include corrections for electron correlation afterwards. The most common methods are Moller-Plesset (MPn, n is the degree of correction) perturbation theory, generalized valence bond (GVB) method and coupled cluster (CC) theory. As the magnitude of the assumptions decrease, the accuracy of ab-initio calculations increase and calculated energy decreases converging to the real energy. On the other hand, reduce in approximations makes the method computationally more costly (Young 2001).

1.4.4. Semiempirical Methods

Semiempirical methods are modified versions of computationally expensive Hartree-Fock (HF) calculations. Some approximations based on empirical parameters are made on HF to simplify the calculations. Three major approximations are applied. The first one is to consider only valence shell electrons and eliminate core electrons from calculations. This does not affect accuracy of the results too much since core electrons do not contribute chemical activity. Core electrons are considered together with nucleus of the atom. The second simplification is the use of minimum number of basis sets possible (Jensen 1999). The third major assumption is the reduction of the number of two-electron integrals (Coulomb and exchange) which decreases complexity of the calculations. Modified neglect of differential overlap (MNDO) approach and the zero differential approach (ZDO) are the mostly implemented methods for this purpose. (Ramachandran, Deepa et al. 2008).

1.4.5. Density Functional Theory

Density functional theory brings an alternative, easier way to calculate properties of a system and replaces the complicated N-electron wave function and Schrödinger equation by a much simpler method. The theory introduces a calculation method through a real property, electron density which is defined as the number of electrons per unit volume in a given state.

Thomas and Fermi proposed that statistical methods can be used to approximately determine the distributions of electrons in an atom and developed a method to calculate total energy of a system as below:

$$E_{TF}[\rho(\mathbf{r})] = \frac{3}{10}(3\pi^2)^{2/3}\int \rho^{5/3}(\mathbf{r})d\mathbf{r} - Z\int \frac{\rho(\mathbf{r})}{r}d\mathbf{r} + \frac{1}{2}\iint \frac{\rho(\mathbf{r}_1)\rho(\mathbf{r}_2)}{|\mathbf{r}_1 - \mathbf{r}_2|}d\mathbf{r}_1 d\mathbf{r}_2 \qquad (1.9)$$

Hohenberg and Kohn developed two important theorems and one of which proved that Thomas and Fermi model can be considered as an approximation to the exact density functional theory.

The first Hohenberg and Kohn theorem proves the usability of electron density to find ground state energy of systems. They proposed the existence of a relation between external potential, $\vartheta(r)$, and electron density, $\rho(r)$. Therefore, as external potential, $\vartheta(r)$, can be obtained by electron density, ground state wave functions and hence all properties of a system can be calculated. By this theorem, total energy of a system can be approximated by equation (1.2):

$$\mathrm{E}[\rho] = \mathrm{T}[\rho] + \mathrm{V_{ne}}[\rho] + \mathrm{V_{ee}}[\rho] \tag{1.10}$$

where $T[\rho]$ is kinetic energy term, $V_{ne}[\rho]$ is nucleus-electron interaction portion of potential energy and $V_{ee}[\rho]$ is the potential energy that comes from electron-electron interaction. The approximate form is given below:

$$\mathrm{E}[\rho] = \int \rho(\mathbf{r})\vartheta(\mathbf{r})\mathrm{d}\mathbf{r} + \mathrm{F_{HK}}[\rho] \tag{1.11}$$

where $F_{HK}[\rho]$ is the Hohenberg and Kohn functional and it can be expressed as:

$$\mathrm{F_{HK}}[\rho] = \mathrm{T}[\rho] + \mathrm{V_{ee}}[\rho] \tag{1.12}$$

$$\mathrm{V_{ee}}[\rho] = \mathrm{J}[\rho] + \text{nonclassical term} \tag{1.13}$$

in which potential energy of electron-electron $V_{ee}[\rho]$ can be expressed as the sum of classical electron electron repulsion term, $J[\rho]$, and non-classical term which is a very important parameter, exchange and correlation energy.

The second Hohenberg and Kohn theorem provides a methodology to calculate total energy by variation of an initial guess of electron density. Basically, it calculates the electron density that minimizes the total energy. Furthermore, second theorem proves that total energy calculated by Thomas and Fermi as eqn 1.9 is an approximation to energy equation proposed by the first Hohenberg and Kohn theorem.

Kohn and Sham suggested a practical methodology that the system containing N particles can be approximated as n-electron problems and be solved similar to Hartree-Fock method to calculate the energy of the system. The theorem considers a system with N non-interacting electrons under an external potential, calculates

electron density and kinetic energy exactly. They introduce terms related to interactions to exchange and correlation energy.

$$E[\rho] = T_s[\rho] + J[\rho] + E_{XC}[\rho] + \int \rho(\mathbf{r})\vartheta(\mathbf{r})d\mathbf{r} \quad (1.14)$$

where $T_s[\rho]$ is kinetic energy term of a system with N non-interacting electrons, and $E_{XC}[\rho]$ is the exchange and correlation energy which both contains non-classical interaction energy between electrons and kinetic energy difference between a system with N interacting electrons and a system with N non-interacting electrons (Parr and Yang 1994).

On the other hand, the exact form of exchange and correlation energy is not known. Therefore, approximations are implemented to take exchange and correlation energy into account.

1.4.5.1. Local Density Approximation (LDA)

Local density approximation (LDA) is the simplest approximation to the exchange and correlation energy. It assumes that the electron density is a uniform electron cloud at a local space. Furthermore, exchange and correlation energy of the system is only correlated with that mostly uniform electron density. It can be formulated as follows:

$$E_{XC}[\rho] = \int \varepsilon_{XC}^{hmg}(\rho)\rho(\mathbf{r})d\mathbf{r} \quad (1.15)$$

where $\varepsilon_{XC}^{hmg}(\rho)$ is the exchange and correlation energy of a particle of a uniform electron gas with ρ electron density.

Although it can be acceptable for simple metals, electron density is certainly not uniform in molecules and LDA gives poor results.

1.4.5.2. Generalized Gradient Approximation (GGA)

Generalized gradient approximation (GGA) is one of the gradient-corrected methods and consists of a gradient correction factor together with electron density

calculations. As gradient is a measure of rate of change, gradient-corrected factors provide a degree of non-homogeneous electron density (Jensen 1999). The formula that calculates exchange and correlation energy by GGA is as follows:

$$E_{XC}[\rho] = \int \varepsilon_{XC}[\rho, \nabla\rho]\rho(\mathbf{r})d\mathbf{r} \quad (1.16)$$

This method is more accurate than LDA. There are other methods approximating exchange and correlation energy. For instance, hybrid functional methods (HDFT) combining Hartree-Fock approximation and Kohn-Sham method exist to calculate exchange and correlation energy and they give even more accurate results than GGA.

1.4.5.3. Periodic Density Functional Theory Applications

Density functional theory calculations of periodic systems require special attention as there exists infinite number of electrons in the system. Periodic calculations are necessary to determine properties of solid-state materials for instance metals and metal oxides. Modeling of the surfaces is achieved by implementing supercell approach in which a unit cell is constructed based on the bulk phase lattice parameters. Unit cell is the smallest repeating structure in a crystal structure and the periodic surface is considered as the infinite repetition of the unit cell.

As the periodic system contains infinite number of electrons, there are infinite numbers of wavefunctions to be calculated to describe the system. Furthermore, the basis sets should also be infinite which is not possible. Blöch's theorem helps to expand wavefunctions over the infinite surface using crystal periodicity. Theorem assumes that wavefunction does not change much in a close region of a k-point. Therefore, it is sufficient to find a wavefunction for each k-point to approximate infinite wavefunctions. Approximation to requirement of infinite basis set is done by pseudopotential approach. In that concept, only outer shell electrons are used in the calculations based on the fact that core electrons and nucleus do not have much contribution to bonding characteristics of an atom. Core electrons and the nuclear potential are approximated by smoother pseudopotentials. That decreases the computational cost of calculations as numbers of electrons to be considered are reduced. On the other hand, accuracy of the results might reduce by the

pseudopotential utilization. Reduction in accuracy could be overcome partly since it is possible to determine which portion of the core electrons are included in the core radius and replaced by pseudopotentials. Cut-off energy is the parameter for that decision. When cut-off energy is adjusted high that means lower portion of the core electrons are replaced by pseudopotentials and higher portion are taken into account in calculations which increases the accuracy of the results.

1.5. Objectives of This Study

In this study, we aimed to determine the reactivity of chlorinated $Cu_2O(001)$ and chlorinated $RuO_2(110)$ surfaces for propylene oxide formation by partial oxidation reaction of propylene with the use of DFT calculations. In this aspect, reactions that compete with the propylene epoxidation reactions i.e. formations of allyl-radical, acetone, acrolein on chlorinated $Cu_2O(001)$; formations of propionaldehyde, allyl-radical, acetone on $RuO_2(110)$ are investigated. Analysis of formation reactions to each product enables the identification of specific paths to generate corresponding product. Furthermore, determination and characterization surface intermediates which may not be achieved by current characterization method can also be accomplished via this method. Activation barriers to obtain each product can also be discovered. Performances of two chlorinated surfaces towards propylene epoxidation reaction are to be compared.

CHAPTER 2

LITERATURE SURVEY

Heterogeneous epoxidation of olefins is an important goal in chemical industry since epoxides are used as intermediates in the production of many industrially important chemicals due to their high reactivity. For instance, ethylene oxide (EO), epoxide of the simplest alkene ethylene, is used in the production of ethylene glycol, ethoxylates etc. (Thomas J.M. 1997) whereas propylene oxide (PO) is utilized mostly for the production of polyether polyols as solvents and propylene glycol used in polyester process (Nijhuis, Makkee et al. 2006). In industrial scale, PO is produced via chlorohydrin and hydroperoxide processes. However, chlorohydrin process has environmental problems concerning the disposal of chlorinated side-products and brine. Hydro peroxide process suffers from high production rates of co-products (i.e. 2-4 times of production rate of propylene oxide). Relatively new commercial production technology is the PO/SM method in which styrene monomer, also a valuable product, is produced in more than the amount of PO (Cavani and Teles 2009).

The ultimate aim in propylene oxide (PO) production is direct epoxidation of propylene with oxygen by the help of heterogeneous catalysts. The method works successfully in ethylene oxide (EO) production from ethylene by silver catalysts with selectivity around 50%. Additives to silver catalyst have enormous

improvement to performance on ethylene epoxidation. Addition of alkalis and halogens to silver further increases selectivity over 85% and conversion near 10%. Halogen incorporation to the catalysts are achieved via trace amounts chlorinated hydrocarbons such as dichloroethane(DCE), 2-chlorobutane, EtCl etc. addition to the feedstream. Both activity and selectivity increase was observed at low composition, activity decrease occurred at higher compositions because excess chloride might block active sites (Dever, George et al. 2000).

Understanding the mechanism of ethylene epoxidation reaction and characteristics of the catalyst, especially its surface is of great importance in the way to achieve the intelligent catalyst design for propylene epoxidation reaction. Several experimental and theoretical studies have been conducted in order to find out the underlying mechanism of ethylene epoxidation and the promoter effect of halogens on silver based catalysts.

Earlier ethylene epoxidation study on Ag(111) and Ag(110) surfaces under UHV conditions resulted in similar catalytic changes on both of the surfaces when chlorine is added to the system. Researchers proposed that the decrease in probability of acetaldehyde formation by blockage of sites as acetaldehyde formation requires more sites than ethylene oxide formation. Therefore selectivity is increased on chlorinated surfaces. Effect of chlorine was stated electronic in nature at low ($\theta<0.4$ ML) surface coverage but selectivity increase due to vacancy blocking was proposed at high coverage (Campbell and Koel 1985; Campbell 1986).

In addition to the studies of chlorine as promoter different halogens, i.e. Br, F, were considered as additives to the Ag catalysts in an experimental ethylene epoxidation investigation. The effect of halogens to the selectivity was claimed to be electronic rather than geometric based on the observation that selectivity enhancement increases with an increase in affinity of halogen. Chlorine is proved to be the best halogen promoter for ethylene epoxidation on silver catalyst (Lambert, Cropley et al. 2003). Computational chemistry methods are also used to determine the promoting effect of halogens. DFT was implemented in a relatively recent study and researchers observed that adsorbed chlorine decreases the activation barriers for

both acetaldehyde and ethylene oxide formation and enhance desorption of ethylene oxide from the catalytic surface. Presence of subsurface chlorine, and its superior effect to desorption of EO was declared. Other halogens had also influence in terms of reducing activation barriers but they do not affect desorption energies. Hence the overall impact of chlorine is higher (Torres, Illas et al. 2008).

Despite vast number of studies devoted to the area, still there is no agreement on the reason of chlorine effect on silver catalysts. One theory is the geometric effect (Force and Bell 1976; Campbell and Koel 1985; Serafin, Liu et al. 1998) namely, chlorine's blocking of the vacant sites which could break C-H bonds of ethylene and therefore favor acetaldehyde formation after which combustion occurs. Another theory is concerned with the electronic effect (Serafin, Liu et al. 1998; Lambert, Cropley et al. 2003) that occurs since chlorine is more electronegative than the oxygen with which it competes for the electrons of the same metal atom. Chlorine, due to its higher electronegativity, weakens the strength of metal-oxygen bond thereafter adsorbed oxygen becomes more electrophilic and more active for epoxidation reaction. The influence of alkali promoters is not very clear as well. Cesium donates electrons to adsorbed oxygen species and reduce their affinity towards ethylene oxide production and increases ethylene combustion but at the same time it inhibits the combustion of ethylene oxide (Serafin, Liu et al. 1998).

In a recent DFT computational study, epoxidation procedure of ethylene has been investigated on both silver and silver oxide surfaces. On Ag_2O surfaces, ethylene adsorption was proposed to occur on oxygen on the 2-fold bridge sites where it may provide high activity due to its low binding energy. Ethylene oxide formation has a lower activation barrier on Ag_2O than that on metallic Ag. On Ag_2O, ethylene oxide formation mechanism is suggested to be different than that on metallic Ag. It is also stated that surface oxygen vacancies should be removed for better performance of silver oxide. Chlorine role for increase in selectivity is proposed to be the block of vacant sites (Özbek, Önal et al. 2011).

The analogy between Au and Ag brought the idea that chlorine may improve the performance of Au catalysts. Chlorine pre-covered metallic Au was utilized as a catalyst for styrene epoxidation reaction and its selectivity is higher than non-

chlorinated Au, due to very little CO_2 formation. The proposed reason for chlorine effect is the alteration of O bond to Au surface and hence adjustment in the geometry of oxygenated Au surface (Pinnaduwage, Zhou et al. 2007).

Addition of chlorine containing compounds also improves the system where butadiene epoxidation reaction took place on Ag catalysts as stated in the results of an experimental study. For example, it eliminates thermal runaway by inhibiting combustion reaction, contributing to sustain stable performance for long hours, increase selectivity and yield towards epoxy butadiene. Tests on chlorine pretreated catalysts reveal the continuous loss of chlorine from the surface during the reaction which brings the need of continuous feed of chlorine to the system which was achieved by feeding organic chlorides before reactants. Different organic chlorides are investigated for this purpose and higher concentrations of less reactive organic chloride species is needed in order to achieve same surface coverage. Although highly covered surfaces have higher steady state activity, they reach steady state later due to the need of removal of excess chlorine from surface. Excessively high chlorine on the catalyst may lead to irreversible formation of the catalytically inactive AgCl. Researchers could not decide on whether improvement on the catalysts depends on electronic effect or physical effect (Monnier, Stavinoha et al. 2004).

The success of silver catalysts on both ethylene epoxidation and butadiene epoxidation led to the idea of utilization of them as propylene epoxidation catalysts. A catalytic route similar with ethylene epoxidation has been proposed for propylene epoxidation. Silver catalysts supported on $CaCO_3$ are investigated for propylene epoxidation reaction in an experimental study. Catalysts with changing silver weight percentages from 0.5% to 56% are tested. Highest selectivity was achieved as 10% when metal loading was 14%, and overall conversion was also low. Catalysts' steady state performance was achieved 3-4 hours after the start-up, which is relatively quick. An increasing trend of Ag^+/Ag ratio with decrease in silver loading was observed in UV-vis spectroscopy analysis. Propylene epoxidation was proven to be size-dependent and less selective on silver catalysts (Lu, Bravo-Suárez et al. 2005).

For the sake of increase in selectivity, promoters are implemented to catalysts. Potassium was considered as a promoter for $CaCO_3$ supported silver catalysts. Addition of alkali promoter tripled propylene oxide selectivity to 15% with around 4% conversion which are maximum values at 2% promoter loading. Particle size alteration was observed proportional to K doping to catalysts (Zemichael, Palermo et al. 2002). Higher selectivity was achieved when $Ag/CaCO_3$ and $Ag/\alpha\text{-}Al_2O_3$ catalysts are modified by NaCl. Kinetic tests with all unpromoted catalysts gave selectivities under 6% with best values achieved by $Ag/\alpha\text{-}Al_2O_3$ and $Ag/CaCO_3$ catalysts whose silver doping was around 56 wt%. Introduction of NaCl to catalysts significantly improved selectivity towards propylene oxide with the expense of activity decrease. Highest selectivity was observed at 1 wt% NaCl loading. Most promising catalysts in that study, namely $Ag/\alpha\text{-}Al_2O_3$ and $Ag/CaCO_3$ achieved 1.4 - 4.4% conversions and 39.5 – 30.1% selectivities, respectively. Small amounts of gas phase organic chloride containing species in feedstream improved catalyst's stability and slightly contributed to selectivity although compositions higher than 500ppm worsened both activity and selectivity. UV-vis analysis determined the increase in Ag^+ species by NaCl addition. Researchers' claim for NaCl effect was that electronic property changes occurred on surface so adsorbed oxygen species became more electrophilic on the surface (Lu, Bravo-Suárez et al. 2006).

NaCl effect for unsupported silver catalysts was similar to the effect on supported silver catalysts. Different promoters' involvement pointed out the highest performance contribution of NaCl followed by NaBr both of which contain halogens with moderate electronegativities. NaF led the system to complete combustion. Those findings also suggest the electronic effect (Lu, Luo et al. 2002). Comparative kinetic study of alkali chlorides with alkaline earth chlorides as promoters for unsupported silver catalysts for propylene epoxidation revealed that $BaCl_2$ also act as promoters but not as effective as NaCl. NaCl content that gave the highest selectivity (around 33%) was 3.8 wt% and achieved 20% conversion (Lu and Zuo 1999). To sum up the implantation of silver catalysts, they are not as effective in propylene epoxidation as ethylene epoxidation. The reason of low efficiency of silver catalysts in epoxidation of propylene may be the presence of allylic hydrogens on propylene structure. Allylic hydrogens are so active that C-H

bond activation is more favorable than epoxide ring formation reaction by C-C bond activation.

Besides silver catalysts, many different attempts were done to make propylene epoxidation yield higher. Molten salts of alkali nitrates having low melting point such as potassium and lithium nitrates were implemented as catalysts to propylene epoxidation system. Reactions with molten salts and reactions in blank reactor without any catalyst gave a variety of products i.e., propene oxide, carbon monoxide, carbon dioxide, propionaldehyde, acetone, and trace amounts of formaldehyde, 2-propanol and dioxanes. The conversion, selectivity values and product distribution of blank experiments were similar to those obtained by experiments with molten salts indicating the same reaction mechanism. However, the residence times of blank experiments were much higher. Therefore, author's reported that molten salts increased reaction rate. Similar results of tests with different salts suggest that molten salts act as a reaction medium rather than catalyst. The reaction was proposed to take place inside the molten salt phase or at the gas-salt interface (Nijhuis, Musch et al. 2000).

Due to its potential for the generation of mildly electrophilic oxygen species, N_2O was utilized as oxidant for silica supported iron catalysts in propene epoxidation reaction. The catalyst achieved 40-60% selectivity towards propylene oxide with 6-12% conversion of propylene. Although there were slight decreases of reaction rate, catalyst was stable for long durations. Increase in iron loading up to 300 ppm increased selectivity. Sodium loading to catalysts increased activity and improved stability but caused much decrease in selectivity. Catalysts were shown to have high capability of regeneration. Expense of N_2O decreases industrialization probability of the method (Duma and Hönicke 2000).

Similarity of gold with silver and interesting properties of gold particles brought the idea of applying gold to propylene epoxidation reaction. In 1998, gold particles supported on titania are reported as a more selective catalyst for propylene epoxidation than silver catalysts. The achievement was great; above 99% selectivity

and 1% propylene conversion at relatively low temperatures and atmospheric pressure when H_2 is present in reaction media. Au or TiO_2 alone are not active or selective for propylene epoxidation whereas Au/TiO_2 catalyst leads to combustion without H_2 in reactant stream. Alteration in the catalytic activity was observed when Au loading and hence the particle size of Au changed. High catalytic activity of Au/TiO_2 was correlated with its similarity with monooxygenase enzymes which were reported to be highly selective for epoxidation reactions of alkenes. On the other hand, it was reported that the activity of the catalyst decreases in a very short time, after 20 minutes of operation. Au/TiO_2 catalyst's stability and sustained activity should be settled for further scale-up of this method (Hayashi, Tanaka et al. 1998).

Haruta's achievement inspired many researches about gold catalysts supported on titanium containing molecules for propylene epoxidation. Selectivity around 60-85% and activities of 2.5-6.5% achieved when Au/TS-1 catalysts were tested. Both activity and selectivity were dependent on Au composition which is between 0.06 and 0.074wt% and Ti/Si ratio is between 33 and 48. Catalysts with low doping of Au and Ti were reported as both more stable and more active (Yap, Andres et al. 2004).

Later, in order to understand propylene epoxidation reaction on gold, the mechanism is investigated on Au(111) with low oxygen coverage by means of periodic density functional theory study implemented on VASP code. Analysis revealed that extended Au(111) surface is nonselective towards PO due to lower activation energy barrier of hydrogen stripping which leads to allylic radical formation and further combustion. Referring to a previous work (Torres, Lopez et al. 2007), the authors stated that the reason is the high basicity of extended Au(111) (Roldan, Torres et al. 2009).

In 2005, Cu was proposed as a selective catalyst for propylene epoxidation. Cu/SiO_2 catalysts gave selectivity of propylene to PO comparable with those obtained from Au/TiO_2 catalysts in Haruta's study. Other reaction products are combustion

products CO, CO_2, and acrolein whose selectivity increases as the temperature increases from 225 ^oC to 325 ^oC and then decreases. Based on study of Rodriguez et al. (Rodriguez, Kim et al. 2003) in which metallic Cu is observed at temperatures below 250 ^oC, CuO after 350 ^oC and Cu_2O in between by XRD analysis, it is stated that metallic Cu catalyzes epoxidation reaction, Cu_2O favor acrolein production and CuO result in propylene combustion (Vaughan, Kyriakou et al. 2005).

Later, in 2007 DFT study has been performed on both metallic (111) surfaces of Cu and Ag with atomic oxygen in terms of propylene epoxidation and it is proposed that Cu facilitates PO formation while Ag favors combustion. Reaction mechanism studies on different adsorption configurations of propylene with respect to the surface resulted in different activation barriers meaning adsorption configuration has effect on selectivity. Their proposal for the reason of better catalytic performance of Cu over Ag is lower basicity of adsorbed oxygen on Cu (Torres, Lopez et al. 2007).

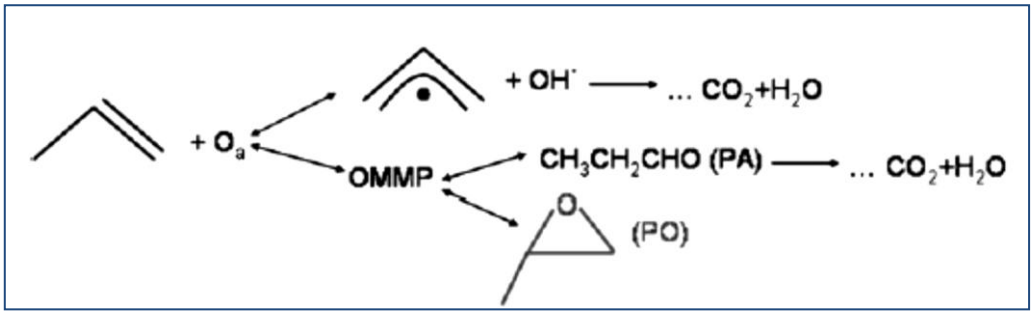

Figure 2.1 Propylene partial oxidation mechanism proposed for Ag(111) and Cu(111) (Torres, Lopez et al. 2007)

Copper catalysts modified with 1wt% of K^+ and supported on SBA-15 were used in an experimental study and moderate propylene conversions around 6% with an average selectivity of 18% towards PO were obtained. Modification of the catalyst with K^+ switches the catalytic activity from allylic oxidation to PO formation. Based on TEM and XRD measurements, copper and potassium particles were stated to be dispersed in mesoporous channels of the support material SBA-15. Increase in

partial pressure of O_2 in reaction environment did not reduce the selectivity towards PO which means oxidized phase of copper was the active phase rather than metallic copper (Wang, Chu et al. 2008).

NaCl modified $VCe_{1-x}Cu_x$ oxide catalysts implemented for propylene epoxidation were moderately selective (43%) increasing with the increase in copper content. However, the conversion of propylene is below 1%. Promotion with NaCl enhanced the selectivity and tuned the activity of catalyst towards PO rather than acrolein production. Pretreatment of catalyst with H_2 before reactant feed and H_2 in feed stream increased selectivity and protected catalyst stability. XPS analysis of H_2 pretreated catalysts revealed the presence of both Cu and Cu^+ species (Lu, Luo et al. 2002).

Another study about Cu/SiO_2 catalysts was performed in 2009 by Can Li's group. Catalysts were prepared by homogenous deposition precipitation method, after which the promoters, if exists, are impregnated to the calcined catalyst. UV-Vis spectra prove the presence of Cu, Cu_2O and CuO species. Propylene was proposed to be adsorbed on Cu and Cu^+ sites after IR studies. The best performance for propylene epoxidation is achieved with 40% selectivity and 1% conversion. CuO and Cu^+ in Cu/SiO_2 were stated to be active for propylene epoxidation. (Su, Wang et al. 2009).

Recently, a combination of gold and copper catalysts supported on SiO_2 was utilized experimentally. Very large group of gold species were observed XRD and TEM suppressing the observation of copper species. Visible spectroscopy suggests the low interaction between Au and Cu species. Pretreatment with H_2 reduced the catalyst and led the formation of copper-gold alloy, in which the interaction between the metals is higher. XPS analysis of subsequently calcined samples suggested the presence of Cu_2O species, and metallic gold. Catalysts performance to propylene epoxidation was affected so much by composition and pre-treatments, conversion was generally <1% while propylene oxide selectivity was up to 70% (Bracey, Carley et al. 2011). Similarly; catalytic properties of silver, copper,

manganese and bimetallic systems prepared with these metals were investigated via high throughput catalyst preparation and screening tools for propylene oxide production. Cu is claimed as the most favorable unimetallic catalyst for propylene oxide whereas Ag-Cu and Cu-Mn were promising bimetallic systems (Onal, Düzenli et al. 2010).

Under epoxidation conditions where the atmosphere contains oxygen, Cu was proposed to be present as the oxide Cu_2O phase based on the analysis by low-angle XRD and XPS (Monnier and Hartley 2001). In another experimental study, Cu(I) was proposed to be the active copper phase for propylene epoxidation under highly oxidizing atmosphere in studies with catalysts prepared by sol-gel method. Testing resulted in 20-33% selectivity with 2.3-6.5% conversion. Several different pretreatments were applied to the catalysts and those leading to Cu(I) formation performed best in reaction. PO formation rate was 10 times higher than those whose dominant phase was Cu(0) (Zhu, Zhang et al. 2008).

Phase transition properties of Cu_2O were also investigated experimentally and researchers did not observe any phase transformation until the pressure was increased to 10 GPa in their experiments in which maximum pressure was 24 GPa. Within the experimental pressure range, transition of Cu_2O to Cu or CuO was not observed. Around 18 GPa cubic structure was modified to a $CdCl_2$-type geometry, and before that at 10 GPa the structure moved to a phase between $CdCl_2$-type and cuprite type structure. (Werner and Hochheimer 1982).

Implementation of XPS, UPS and LEED in analysis of geometric, electronic and oxygen adsorption properties of copper oxide surfaces after oxidation of metallic copper revealed the structure of ideal $Cu_2O(111)$ and $Cu_2O(100)$ surfaces. UPS analyses resulted in the proposal of dissociative adsorption of molecular oxygen on the surfaces therefore the proposal of a structure as ideal oxygen terminated (100) surface. Furthermore, copper terminated surface experienced a reconstruction in terms of single coordinated copper species at the top of the surface. XPS analyses were performed to determine Cu-to-O ratios after annealing of samples at different temperatures. No significant decrease in ratios was observed and there was no

transition to Cu^{2+} or Cu^{0} species up to annealing temperatures of 900 K. (Schulz and Cox 1991). First principle study by ab-initio thermodynamics approach was performed for $Cu_2O(100)$ surface and its interaction with gas phase O_2. $Cu_2O(100)$ surface whose upper-most layer is oxygen was named as O-terminated $Cu_2O(100)$ and it was proposed to be more stable than Cu-terminated surface whose upper-most layer is copper. Cu-terminated surface was said to undergo surface reconstruction and only stable in the reduction range of oxide copper to metal. In the same study, reactivity of the stable O-terminated $Cu_2O(100)$ surface is analyzed by means of CO oxidation to CO_2 by means of DFT study using VASP code. CO is found to diffuse spontaneously to the bridge oxygen between two Cu atoms on the surface where spontaneous reaction to CO_2 occurs. After desorption of CO_2 oxygen vacancies on O-terminated Cu_2O surface could be healed with the dissociative adsorption of gas phase O_2 (Le, Stolbov et al. 2009).

Besides copper, various metals and combinations of them has been tested for propylene epoxidation by high throughput screening methods (Kahn, Seubsai et al. 2010). The analysis revealed that multi-metallic systems and more importantly, trimetal catalyst containing Ru, Cu and Na (RuO_2-CuO_x-$NaCl/SiO_2$) was promising for propylene epoxidation with 40-50% selectivity and 10-20% conversion. Further analysis in different reaction conditions were stated to prove their industrial applicability. NaCl effect on propylene oxide mechanism in this case was stated to be chlorine's altering of the surface electronically due to its high electronegativity (Seubsai, Kahn et al. 2011). Basing on the results of this research, propylene epoxidation studies on chlorinated RuO_2 are included in this research.

$RuO_2(110)$ surface was investigated in this study for propylene epoxidation reaction since $RuO_2(110)$ was proposed to be spontaneously formed after high doses O_2 deposition on single crystal Ru(0001) surface. $RuO_2(110)$ was observed by LEED and STM analysis. Additionally, they have implemented a DFT research on the structural parameters of $RuO_2(110)$ surface and their calculated values were said to be in consisted with experimental founding (Over, Kim et al. 2000).

Ammonia oxidation to NO is investigated on $RuO_2(110)$ surface by both DFT calculations and high resolution core level shift spectroscopy (HRCLS)

experiments. RuO_2(110) has claimed to have two active sites for that reaction: under coordinated Ru atoms and under coordinated bridge oxygen atoms. Both of them play role in adsorption and activation of NH_3. Another possible site is the on-top oxygens bonded on Ru-cus atoms in case there is excess oxygen in the environment. Those on-top oxygens which are more active than bridge oxygens have the same role with bridge oxygens on stoichiometric surface (Seitsonen, Crihan et al. 2009).

However, on-top oxygens' adsorption activity was found too much a for partial oxidation reaction in a study where ethylene adsorption and interaction was investigated on stoichiometric and oxygen-rich RuO_2(110) surface with the aid of thermal desorption spectroscopy (TDS) and vibrational signals obtained by high-resolution electron energy-loss spectroscopy (HREELS). On stoichiometric RuO_2(110) surface, adsorption and desorption of ethylene is found to be molecular. At 320 K, C-H bond weakens but C_2H_4 is still molecularly adsorbed (Paulus, Wang et al. 2004).

CHAPTER 3

SURFACE MODELS and COMPUTATIONAL METHODOLOGY

Prior to the analysis of catalytic activity, the surfaces of the materials that will be used are constructed. Development of the catalytic surfaces start with the bulk phase construction and optimization of the material. Afterwards, selected surfaces to be used in the catalytic activity analysis are cleaved from the bulk structure and geometry optimization studies are performed. In this study, chlorinated $Cu_2O(001)$ and chlorinated $RuO_2(110)$ surfaces are investigated. Surface models and the procedure how catalytic activity analysis is performed are demonstrated in the following sections.

3.1. Surface Models of Copper Oxide and Ruthenium Oxide

3.1.1. Copper Oxide $Cu_2O(001)$ surface

Cu_2O has a cubic Bravais lattice with six atoms in the unit cell. The structure is body centered cubic (bcc) with respect to oxygen atoms which are at the corner and at the center of each unit cell and face centered cubic (fcc) with respect to copper atoms. Each oxygen atom in bulk is surrounded by a tetrahedron of copper atoms while each copper atom is linearly coordinated with two oxygen atoms. High pressure energy dispersive X-ray diffraction technique was utilized in order to

determine the cubic structure of Cu_2O produced by grain-growth of crystalline copper (Werner and Hochheimer 1982).

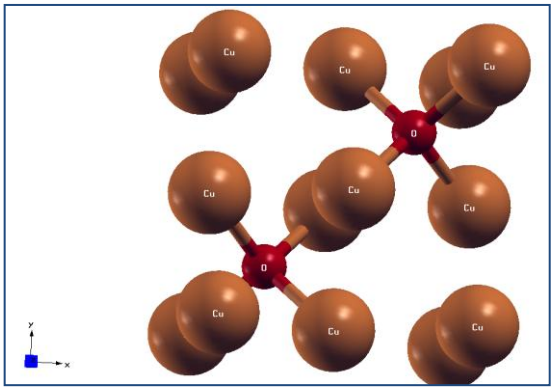

Figure 3.1 Bulk structure of Cu_2O (Cu: gray,big ones; O: black, small)

Cu_2O can be produced by several routes but care should be taken since Cu_2O is instable to oxidation reaction and can produce CuO in moist air while it is stable in dry air. Cu_2O production can be produced by either pyrometallurgical methods, i.e. heating of copper to temperatures between 750^oC and 1000^oC depending on the method and in an oxidizing environment and further isolation to prevent further oxidation to CuO, or hydrometallurgical methods which depends on extraction of Cu_2O from copper containing compounds (Richardson 2000).

$Cu_2O(001)$ is selected in this study to investigate the catalytic properties of Cu_2O for propylene partial oxidation reaction. Ideal $Cu_2O(001)$ has a bulk structure arrangement of alternating copper and oxygen layers which are perpendicular to (001) direction. $Cu_2O(001)$ surfaces may possess one of the two surface forms possible for Cu_2O; O-terminated surface where atoms at the top are oxygen atoms forming a bridge structure with copper atoms below and Cu-terminated surface where upper layer is copper. Top view and side view of O-terminated $Cu_2O(001)$ surface are given in Figure 3.2.

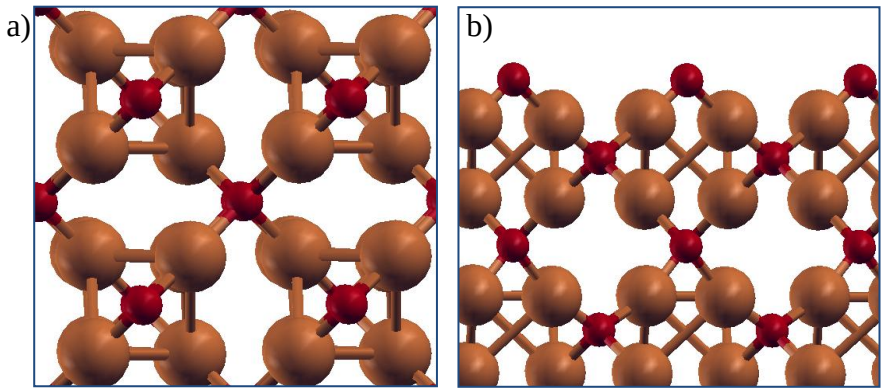

Figure 3.2 a) Top view and b) Side view of O-terminated $Cu_2O(001)$ structure (Cu: gray,big ones; O: black, small)

First principle study has been done using ab-initio thermodynamics approach in order to identify the interaction of $Cu_2O(100)$ surface mentioned above with gas phase O_2. Two types of surface structure are considered; oxygen terminated $Cu_2O(100)$ where the topmost layer on the surface is composed of oxygen and copper terminated $Cu_2O(100)$ where copper atoms are present at the top of the surface. Oxygen terminated $Cu_2O(100)$ (O-terminated $Cu_2O(100)$) surface is proposed to be more stable than copper terminated $Cu_2O(100)$ (Cu-terminated $Cu_2O(100)$) surface in which surface cannot keep its original shape and reconstruct. Cu-terminated $Cu_2O(100)$ is proposed to be only stable in the reduction range of copper oxide to metal (Le, Stolbov et al. 2009). Therefore, in this study O-terminated $Cu_2O(001)$ surface is employed to generate chlorinated surfaces for the calculations in this study.

In order to construct chlorinated $Cu_2O(001)$, chlorine atom is introduced on a bridge site of O-terminated $Cu_2O(001)$ surface on an oxygen vacancy. It is introduced to a place where the chlorine and the oxygen of the reaction site are on the same diagonal of supercell. Furthermore, bridge site of chlorine occupation and the bridge site where the reactions take place are at two sides of a tetragon formed by a subsurface oxygen atom on $Cu_2O(001)$-Cl-1 surface. Chlorine occupies one of the four bridge positions on the unit cell hence; surface chlorine coverage is 0.25 ML. This surface will be referred as $Cu_2O(001)$-Cl-1 hereafter. The details of the structure can be seen in Figure 3.3 where top and side views of the surface are displayed.

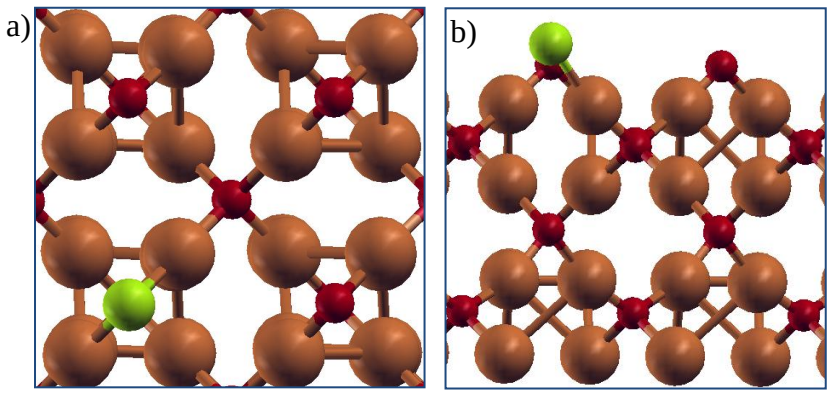

Figure 3.3 a) Top view and b) Side view of $Cu_2O(001)$-Cl-1 surface (Cu: dark gray, big ones; O: black, small; Cl: light gray)

In addition to $Cu_2O(001)$-Cl-1 surface, one more chlorine substituted surface of $Cu_2O(001)$ is prepared. In order to determine the effect of position of the chlorine atom relative to the reaction site, chlorine is substituted to a place where it is in the same row with oxygen at reaction site in $Cu_2O(001)$-Cl-2 structure. Chlorine and the employed oxygen exist alternatingly on the bridge structure of the same row. The distance between the chlorine and the bridge oxygen at reaction site is lower than the corresponding distance in $Cu_2O(001)$-Cl-1 structure where the chlorine and the oxygen at reaction site are placed alternatingly on the same diagonal. However, chlorine site and the reaction site do not have a common atom like subsurface atom in $Cu_2O(001)$-Cl-1 structure. The surface coverage of $Cu_2O(001)$-Cl-2 and $Cu_2O(001)$-Cl-1 are the same, 0.25ML. Top and side views of the surface $Cu_2O(001)$-Cl-2 are given in Figure 3.4.

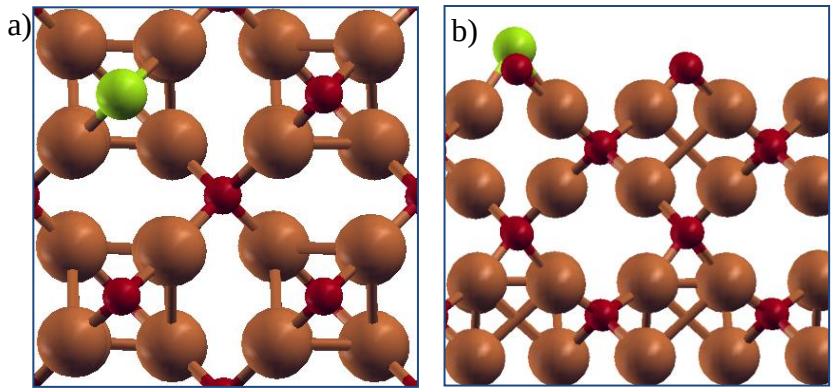

Figure 3.4 a) Top view and b) Side view of $Cu_2O(001)$-Cl-2 surface (Cu: dark gray, big ones; O: black, small; Cl: light gray)

3.1.2. Ruthenium Oxide RuO_2(110) surface

RuO_2 has a primitive tetragonal rutile lattice with six atoms in the unit cell. Ruthenium is coordinated to six oxygens. Around ruthenium atom, an octahedron is formed by six oxygens and each oxygen is connected to three ruthenium atoms nearby. The unit cell has a body centered cubic (bcc) structure with respect to ruthenium atoms. Structure of the RuO_2 is determined with the analysis by LEED previously (Over, Kim et al. 2000). The structure is demonstrated in Figure 3.5.

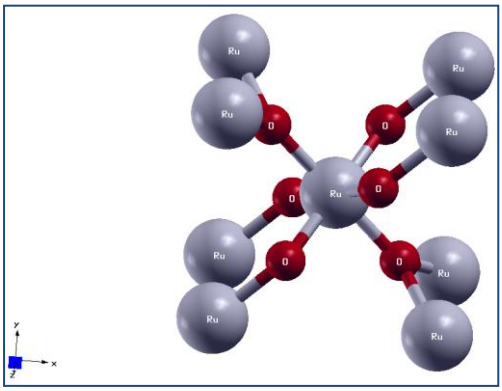

Figure 3.5 Bulk structure of RuO_2
(Ru: gray, big ones; O: black, small)

Due to the fact that RuO_2(110) is the most stable surface of RuO_2, it is utilized as the representative surface to generate chlorinated RuO_2 to be utilized propylene partial epoxidation reaction. Experimentally, RuO_2(110) surface was generated by high doses O_2 treatment of well-defined, single crystal Ru(0001) surface. Oxygen uptake to metal surface was around 10 ML. Subsequent LEED and STM analysis demonstrated the formation of bulk phase RuO_2(110) over Ru(0001) surface (Over, Kim et al. 2000). Before formation of RuO_2(110), chemisorbed oxygens are claimed to be able to present on Ru(0001) up to 2-3 monolayers. Higher coverages led to epitaxial growth of RuO_2(110) on Ru(0001) surface (Kim, Seitsonen et al. 2001). Ideal RuO_2(110) has a structure that can be considered as alternating sequence of rutile O-(RuO)-O trilayers both in the parallel and perpendicular to (110) direction. Top view and side view of RuO_2(110) surface is represented in Figure 3.6.

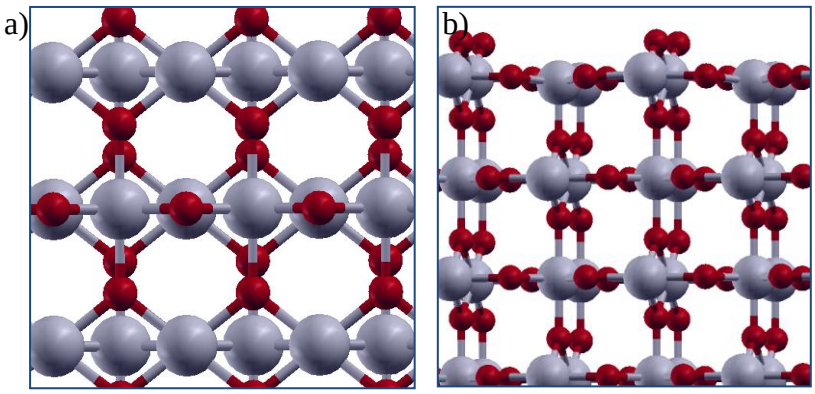

Figure 3.6 a) Top view and b) Side view of RuO_2(110) surface
(Ru: gray, big ones; O: black, small)

In order to generate chlorinated RuO_2 surface, chlorine atom is substituted on the bridge site of the RuO_2(110) on a bridge oxygen vacancy. Chlorinated surface is named and will be referred as RuO_2(110)-Cl hereafter. Chlorine and the oxygen employed for catalytic reactions on the RuO_2(110)-Cl are on the same row generating at the alternating bridge positions. Furthermore, they share electrons of a ruthenium atom coordinated by four oxygen atoms other than the chlorine and the employed oxygen. The exact position of the chlorine can be seen on Figure 3.7 from top view and side view.

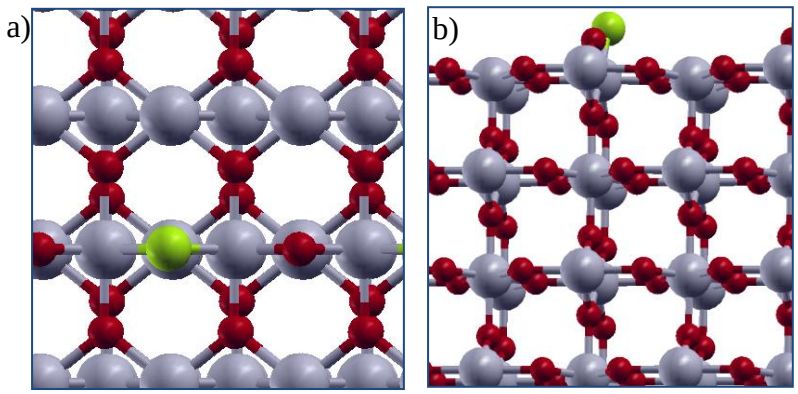

Figure 3.7 a) Top view and b) Side view of RuO_2(110)-Cl surface
(Ru: dark gray, big ones; O: black, small; Cl: light gray)

3.2. Computational Methodology for Calculations

3.2.1. Vienna Ab Initio Simulation Package

Quantum mechanical calculations were performed using the Vienna Ab initio Simulation Package (VASP) (Kresse and Hafner 1994; Kresse and Furthmuller 1996) which was developed by Georg Kresse, Jurgen Furthmuller and their collaborators in the University of Vienna. The code implements density functional theory in a periodic manner in which an artificial periodicity is implemented by repeating the unit cell finite number combined with periodic boundary conditions. Specifically, the code is developed for solid systems having periodic boundary conditions. VASP uses plane wave basis sets and pseudopotentials. There are two major loops in the VASP code. The first one; the inner loop is constructed to solve Kohn-Sham equations. In the inner loop, energies and forces are also calculated. The second loop is the outer loop and ionic movement is considered in the outer loop which is useful in geometry optimizations.

In this study**,** VASP is implemented within the supercell approach by using projector augmented-wave (PAW) method (Blöchl 1994; Kresse and Joubert 1999) for electron ion interactions and generalized gradient approximations (GGA) (Perdew, Chevary et al. 1992) method to take exchange and correlation energy into account. Homogenously distributed (4x4x1) k-points by Monkhorst-Pack mesh are utilized in order to define the integration points of the supercells (Monkhorst and Pack 1976). Optimizations of the structures were carried out until the net force acting on the atoms is smaller than 0.025 eV/Å. The energy cut-off value in calculations was 500 eV.

3.2.2. Computational Strategy

3.2.2.1. Structure Analysis

Investigations start by the construction of bulk structures of Cu_2O and RuO_2 according to the structure that are explained in detail in Section 3.1. Bulk structures are optimized in terms of the criteria discussed in the previous paragraph to obtain lattice parameters of the unit cell which is the smallest repeating structure of a

crystal structure. Selected $Cu_2O(001)$ and $RuO_2(110)$ surfaces are generated as 8 atomic layers from their corresponding bulk structures in accordance with previous studies (Özbek, Önal et al. 2011). Throughout the calculations, two layers at the bottom are kept frozen so that they represent the bulk phase under the surface. Other than the bottom two layers, all of the atoms in the structure are relaxed in all degrees of freedom. Above the top layer of the surface a vacuum layer is introduced to a distance of 15Å. Subsequent to surface optimization of $Cu_2O(001)$ and $RuO_2(110)$ slabs, chlorine atoms are substituted to the pre-determined positions on the surfaces. $Cu_2O(001)$-Cl-1 and $RuO_2(110)$-Cl, chlorinated surfaces of $Cu_2O(001)$ and $RuO_2(110)$, are optimized afterwards.

3.2.2.2. Energy Analysis

Following determination of structural parameters of the surfaces utilized as catalysts, energetic properties of them are studied towards propylene and the products of partial oxidation reaction of propylene which are demonstrated in Figure 3.8. Adsorption of raw material propylene and products propylene oxide, propionaldehyde, acetone and allyl-radical are investigated on the surfaces $Cu_2O(001)$-Cl-1 and $RuO_2(110)$-Cl. Either chemisorption or physisorption occurs on the surface based on the interaction between the adsorbates and the adsorbent surface. If the adsorbates are distant from the surface and they are weekly held over the surface, they are physisorbed on the surface and the adsorption energy is small. On the other hand, if they are close to the surface and they alter the surface structure, the adsorption energy is relatively high and the phenomenon is chemisorption. Adsorption energy is calculated according to the following formula:

$$E_{adsorption} = E_{\substack{adsorbate \\ on\ the\ surface}} - (E_{adsorbate} + E_{surface}) \quad (3.1)$$

where $E_{adsorption}$ is the adsorption energy of the considered adsorbate; $E_{\substack{adsorbate \\ on\ the\ surface}}$ is the energy of the optimized system in which the considered compound is adsorbed on corresponding surface; $E_{adsorbate}$ is the energy of the gas phase adsorbate; and finally $E_{surface}$ is the energy of the optimized structure of the utilized surface, $Cu_2O(001)$-Cl-1 or $RuO_2(110)$-Cl in this case. The total

energies of gas phase molecules were calculated using (1x1x1) k-point and the periodic molecules were separated with at least 10 Å vacuum distances. As reactions are considered in this study, heat of reaction is an important parameter that determines whether the system requires energy, endothermic, or releases energy to the surroundings, exothermic. It is calculated as the difference between the total energy of the final state of a reaction, energy of products, and total energy of the initial state of the reaction, energy of reactants.

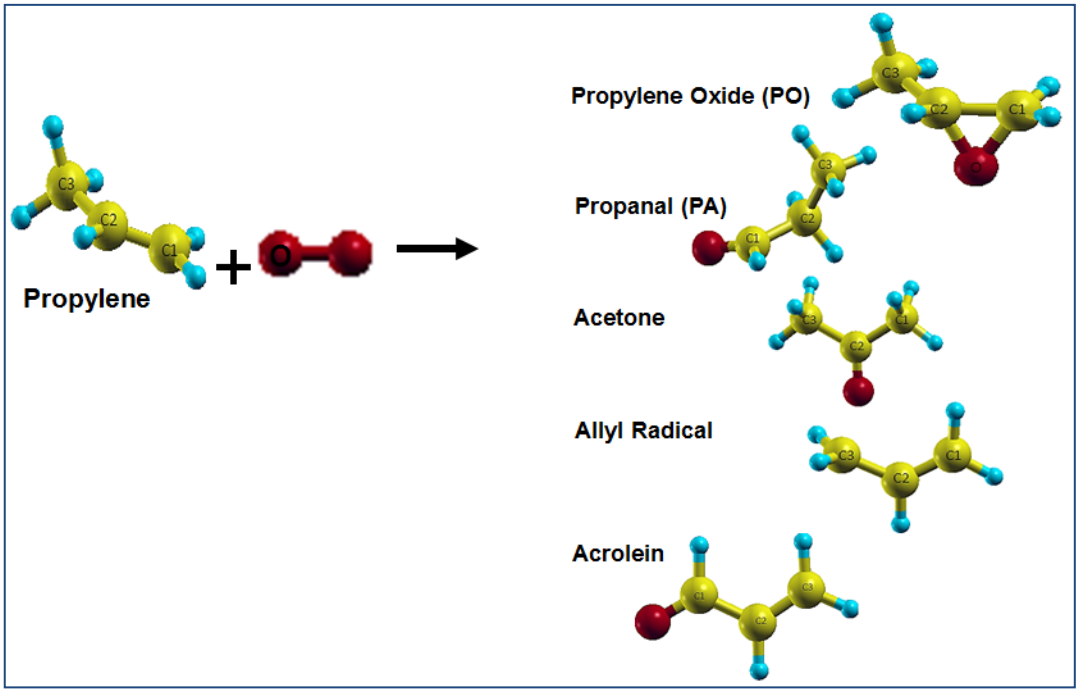

Figure 3.8 Partial oxidation reaction products of propylene
(C: light gray, big ones; O: black, small; H: light gray)

Initial and final states of a reaction are used to get the minimum energy path (MEP) of the reaction. Minimum energy path is the easiest route, in terms of the required energy, that reactants can go through to generate products. Climbing image nudged elastic band method (Henkelman and Jónsson 2000) is a technique to determine the MEP on the potential energy surface of the reaction. It is adjusted version of the nudged elastic band (NEB) method. N numbers of images are created between the initial and final state of the reaction. Those images are also bonded to each other

and to the potential energy surface between reactants and products. Each image is optimized separately according to the criteria discussed previously. The difference of CI-NEB method from standard NEB arises at this point. Standard NEB method does not allow images to alter their positions on the potential energy surface whereas they can move and exactly locate on the highest energy when calculations are performed using CI-NEB method. This freedom of location along potential energy surface makes determination of transition state structures easier. Transition state structure is at the highest energy and can be directly obtained by just CI-NEB method. Energy of the transition state is used to determine the activation barrier of the corresponding reaction.

Transition state structures are analyzed by frequency calculations. Frequency analysis is based on Hessian matrix calculations within finite difference approach. Step size in finite difference calculations is determined as 0.02 Å for the movement of the atoms along each direction.

3.2.2.3. SO_2 adsorption as Lewis acid probe

The understanding of the underlying reason for the material's catalytic activity is very important. As catalytic activity in propylene epoxidation reaction is dependent on the characteristics of oxygen molecule on the surface, probe molecules have been utilized in order to determine the characteristics of the surface oxygen and correlate catalytic activity to properties of the oxygen (Pacchioni, Ricart et al. 1994; Torres, Lopez et al. 2007; Kizilkaya, Senkan et al. 2010). For this purpose, SO_2, a Lewis acid probe is adsorbed to the surface to form SO_3 with surface oxygen. Binding energy of SO_2 gives information about the character of the oxygen in structure.

CHAPTER 4

RESULTS and DISSCUSSION

4.1. Propylene Partial Oxidation Mechanism on $Cu_2O(001)$-Cl-1

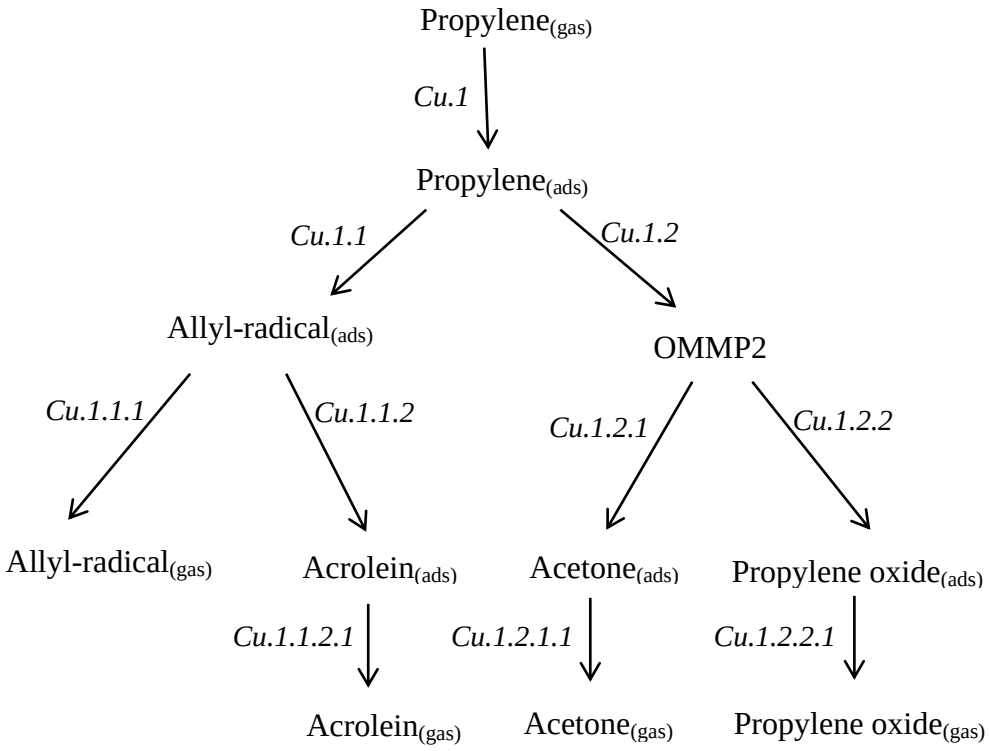

Scheme 4.1 Reaction scheme for propylene partial oxidation reaction on $Cu_2O(001)$-Cl-1

Above, reaction steps are proposed for the reaction mechanism of propylene partial oxidation on $Cu_2O(001)$-Cl-1 in Scheme 4.1.

4.1.1. Adsorption of Oxygen, Chlorine, and Propylene

After surface optimization of $Cu_2O(001)$-Cl-1, atomic oxygen and chlorine adsorption on a vacant site is investigated. Oxygen atom is substituted on most favorable adsorption site, vacant 2-fold bridge sites that two metal atoms form (Wang, Deo et al. 1999). Subsurface oxygen in tetragonal orientation makes the bridge site favorable for adsorption. Surface oxygen in bridge positions has low coordination number than 3-fold or 4-fold oxygens on metallic surfaces (Torres, Lopez et al. 2007) suggesting high reactivity towards epoxidation due to weak binding energy. Chlorine atom is also substituted on a vacant 2-fold bridge site similar to surface oxygen.

Adsorption energy calculations are performed as dissociative adsorption energies of the gas phase oxygen according to the following equation:

$$\mathrm{E}_{\substack{\text{oxygen}\\\text{adsorption}}} = \mathrm{E}_{\text{system}} - \left(\frac{1}{2}\,\mathrm{E}_{\mathrm{O}_2} + \mathrm{E}_{\text{surface}}\right) \qquad (4.1)$$

where $E_{\substack{oxygen\\adsorption}}$ is the adsorption energy of propylene; E_{system} is the energy of the optimized system in which oxygen is adsorbed on corresponding surface; E_{O_2} is the energy of the gas phase molecular oxygen; and finally $E_{surface}$ is the energy of the optimized structure of the utilized surface for dissociative oxygen adsorption. Chlorine adsorption investigations are accomplished similar with oxygen adsorption studies. Adsorption energies of oxygen and chlorine are both -60kcal/mol. That means, chlorine atoms have the same probability in the competititon to adsorb on a vacancy on the bridge site of the $Cu_2O(001)$ surface. Furthermore, chlorinated copper oxide $Cu_2O(001)$-Cl-1 surface will transfer one of its bridge oxygen at the reaction site to propylene in partial oxidation reaction of propylene and have one vacant bridge oxygen site at the end of the reaction. Oxygen adsorption to that

vacant site in the presence of chlorine at the neighboring site creates 40kcal/mol of energy, that means it is harder than adsorption to a vacant site.

Charges of O_s and Cu in the bridge structure and average distances together with measure of the angle that the bridge structure forms are given in Table 4.1. The average Cu-O distances calculated are in reasonable agreement with the values 1.762, 1.862Å theoretically (Le, Stolbov et al. 2009) and 1.84Å experimentally (Ghijsen, Tjeng et al. 1988) obtained in literature. The angle of the bridge structure Cu-O-Cu decreases upon chlorine addition to the surface. The average bond lengths increase when chlorine is inserted to the oxide surface.

Table 4.1 Selected distances, angles and charge values on $Cu_2O(001)$[a] and $Cu_2O(001)$-Cl-1 surface

		$Cu_2O(001)$[a]	$Cu_2O(001)$-Cl-1
Distances (Å)	Cu-Os[b]	1.759	1.768
	Cu-Cl	-	2.141
	Cu(O)-Cu(O)	3.219	3.235
	Cu(O)-Cu(Cl)	-	3.17
Angles (degree)	Cu-Os-Cu	109.1	107.2
	Cu-Cl-Cu	-	88.4
	Cu(O)-Oss[b]-Cu(O)	119.2	119.9
	Cu(O)-Oss-Cu(Cl)	-	114.8
Charges[c]	O	-0.9	-0.88
	Cl	-	-0.5
	Cu	2.6	2.3

[a] Investigations on $Cu_2O(001)$ surface without chlorine has been conducted by Deniz Onay (Onay; expected January 2012)

[b] Os and Oss denote surface oxygen and subsurface oxygen, respectively.

[c] Charges are calculated by Bader charge analysis method (Tang and et al. 2009). Reported oxygen charges are the charge of oxygen employed for reactions. The charges of copper are the average charge of copper atoms that form the bridge structure with the employed oxygen.

Consequent to oxygen and chlorine adsorption, propylene adsorption is investigated. Propylene is adsorbed on a site predicted to be close to its final position on the surface. It is adsorbed nearly parallel to the surface over a copper atom near the bridge oxygen. The following mechanism as indicated as Step Cu.1 in Scheme 4.1 is proposed for propylene adsorption on $Cu_2O(001)$-Cl-1:

$$C_3H_{6(gas)} \rightarrow [CH_2CHCH_3]_{surface} \qquad (4.2)$$

Stable structure conformation of the adsorption site is presented in Figure 4.1. Carbon atoms are labeled as follows; carbon atom at the edge of the double bond having two hydrogens is C1, the middle carbon is C2 and lastly, allyl hydrogen containing carbon is C3.

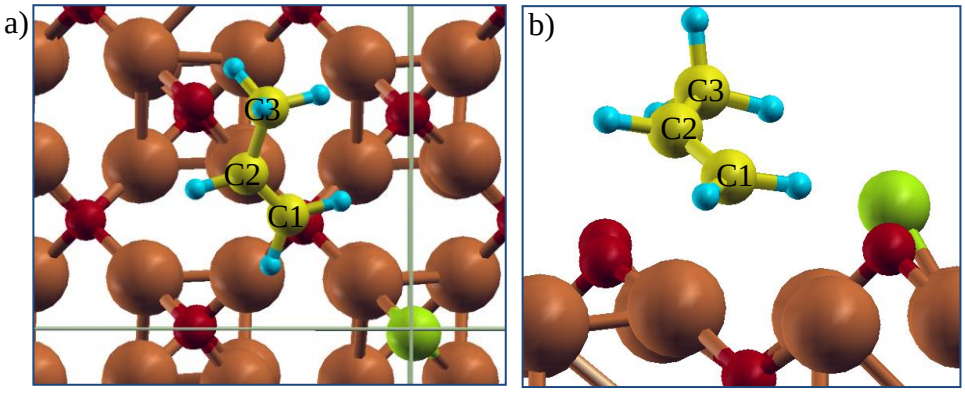

Figure 4.1 a) Top view and b) Side view of optimized adsorbed propylene on $Cu_2O(001)$-Cl-1 (Cu: dark gray, big ones; O: black, small; Cl: light gray, bigger; C: light gray, smaller; H: gray, small)

4.1.2. Allylic Hydrogen Stripping Reaction

Allylic hydrogen stripping (AHS) reaction as indicated Step Cu.1.1 in Scheme 4.1 is investigated subsequent to propylene adsorption. The reaction takes place upon C-H bond activation and as a result one of the allylic hydrogens is stripped to the surface. Although ally radical is adsorbed on the metal species in previous theoretical studies (Roldan, Torres et al. 2009; Kizilkaya, Senkan et al. 2010) where metal catalysts are examined under low oxygen regimes, in this study adsorption on a bridge oxygen atom on the oxide surface is computed to be more favorable. The structure of final geometry of allyl-radical is presented in Figure 4.2.

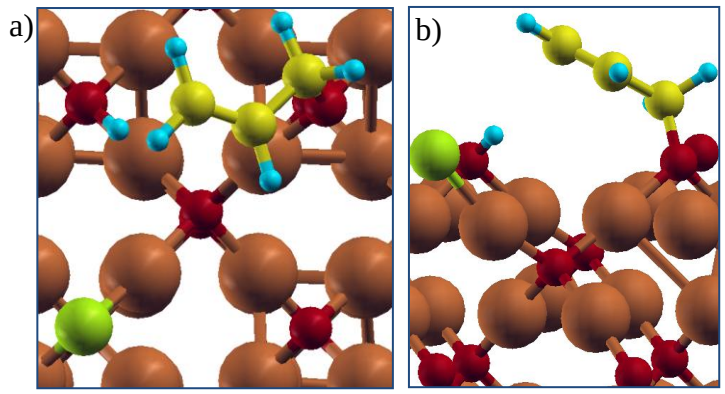

Figure 4.2 a) Top view and b) Side view of optimized allyl-radical on $Cu_2O(001)$-Cl-1 (Cu: dark gray, big ones; O: black, small; Cl: light gray, bigger; C: light gray, smaller; H: gray, small)

In the approximate minimum energy path of AHS reaction, allylic hydrogen is transferred to bridge oxygen to make an O-H bond of 0.978Å after C-H bond activation is accomplished. Subsequently, allyl-radical is adsorbed on the surface to make C1-O bond of 1.448Å with other bridge oxygen. At final state surface will be covered by 0.25 ML hydrogen on bridge oxygen.

Allylic hydrogen stripping step can be followed by either desorption of the allyl-radical from the site, indicated Step Cu.1.1.1, or further reaction of it on the surface to form acrolein which will be discussed in the following section. Based on the analysis on allylic hydrogen stripping, the following reaction steps are proposed for allylic hydrogen stripping and desorption of allyl-radical, respectively:

$$[CH_2CHCH_3]_{surface} + 2[O]_{surface} \rightarrow [H_{(O)}]_{surface} + [C_{(O)}H_2CHCH_2\bullet]_{surface} \quad (4.3)$$

$$[C_{(O)}H_2CHCH_2\bullet]_{surface} \rightarrow [O]_{surface} + CH_2CHCH_2\bullet_{(gas)} \quad (4.4)$$

4.1.3. Acrolein Formation Reaction through Adsorbed Allyl-radical

Acrolein generation on $Cu_2O(001)$-Cl-1 is accomplished by a reaction, labeled as Cu.1.1.2 in Scheme 4.1, whose initial state is the adsorbed allyl-radical on surface which is the final state of the elementary reaction of allylic hydrogen stripping. Previously bonded hydrogen on neighboring bridge oxygen species is also included

in the initial state. As acrolein generation also creates a surface bonded hydrogen species; at the end of acrolein formation, reaction surface will be covered by 0.5ML hydrogen. Final state of acrolein generation reaction is presented in Figure 4.3.

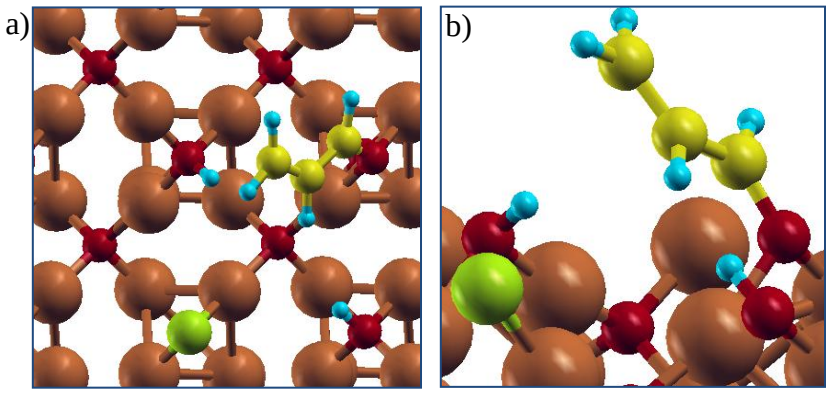

Figure 4.3 a) Top view and b) Side view of final state of optimized acrolein on $Cu_2O(001)$-Cl-1 (Cu: dark gray, big ones; O: black, small; Cl: light gray, bigger; C: light gray, smaller; H: gray, small)

In the approximate minimum energy path of acrolein formation reaction by CI-NEB method, one of the hydrogens of adsorbed allyl-radical species which is bonded to C1 is separated from the radical and transferred to neighboring surface oxygen. Simultaneously, C1-O bond decreases to 1.333Å and the oxygen will become more integrated with C1 forming acrolein structure. The angle of the bridge structure also decreases to 95.21^{o} as bridge oxygen moves upward moving acrolein to a position almost perpendicular to the surface.

After it is formed on the surface, acrolein should be desorbed from the surface to gas phase which is indicated as step Cu.1.1.2.1. The following reaction steps are proposed for the formation of acrolein on the surface and desorption of it to gas phase, respectively.

$$[C_{(O)}H_2CHCH_2\bullet]_{surface} + [O]_{surface} \rightarrow [H_{(O)}]_{surface} + [CO_{(Cu)}HCHCH_2] \quad (4.5)$$

$$[CO_{(Cu)}HCHCH_2] \rightarrow [Cu]_{surface} + COHCHCH_{2(gas)} \quad (4.6)$$

4.1.4. Surface Intermediate OMMP formation Reaction

Stable surface intermediate formation in propylene partial oxidation has been proposed in previous studies (Medlin, Mavrikakis et al. 1999; Torres, Lopez et al. 2007; Roldan, Torres et al. 2009). Formation of a surface intermediate can be considered as an elementary reaction. Surface intermediates are also called oxametallacycle or OMMP. The name OMMP is derived from first letters of the ring type of surface structure formed on low oxygenated metallic surfaces as oxygen-metal-metal-propylene. In this study, two types of OMMP are considered in accordance with the literature. OMMP1 is generated when C1 is bonded to bridge oxygen and C2 binds to the copper atom on the bridge structure. In OMMP2 geometry, C1 has a bond with copper atom and C2 has a bond with the bridge oxygen. Previous studies on metal surfaces with low oxygen regimes resulted in the proposal of OMMP1 being more stable having smaller activation barrier (Torres, Lopez et al. 2007; Roldan, Torres et al. 2009). Moreover, in another study, OMMP1 was claimed to be less stable than OMMP2 but OMMP2 was stated to occur in decomposition of propylene oxide (Medlin, Mavrikakis et al. 1999). In this study OMMP1 formation seems improbable based on calculations. In OMMP1 formation computations, stripping of allylic hydrogen is observed rather than stable OMMP1 structure. It can be said that allylic hydrogen stripping reaction is more favorable than OMMP1 formation reaction on bridge oxygen species as inclined position of OMMP1 on the surface decreases the distance between surface oxygen and one of the allylic hydrogen species. OMMP2 formation is possible, step Cu.1.2 in Scheme 4.1, and optimized OMMP2 structure is presented in Figure 4.4.

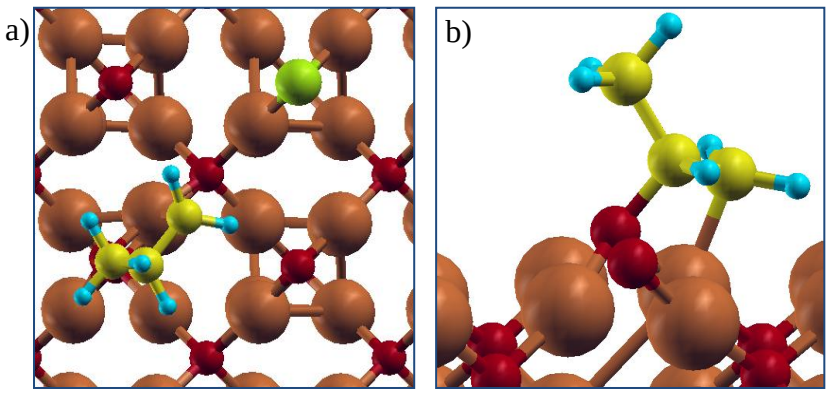

Figure 4.4 a) Top view and b) Side view of optimized OMMP2 structure on $Cu_2O(001)$-Cl-1 (Cu: dark gray, big ones; O: black, small; Cl: light gray, bigger; C: light gray, smaller; H: gray, small)

In the minimum energy route of OMMP2 formation, first C1 is bonded to copper atom with a bond length of 2.017Å. Then, C2 is connected to the bridge oxygen completing the structure. The angle of the bridge structure decreases from 120 degree to 106 degree throughout the reaction and the distance between C2 and bridge oxygen also decreases from 2.689Å to 1.489Å with an upward movement of bridge oxygen. As allyl hydrogen containing carbon C3 is inclined upwards in OMMP2 structure, allylic hydrogens are not transferred to the surface.

OMMP2 surface intermediate can further react on the surface to generate either acetone or PO which will be discussed in sections 4.1.5 and 4.1.6, respectively. The following reaction step is proposed for the generation of OMMP2 on the surface.

$$[CH_2CHCH_3]_{surface} + [Cu]_{surface} + [O]_{surface} \rightarrow [C_{(Cu)}H_2C_{(O)}HCH_3]_{surface} \quad (4.7)$$

4.1.5. Acetone Formation Reaction through OMMP2

Propionaldehyde (propanal) and acetone are also products of propylene partial oxidation reaction. Propionaldehyde is an unwanted product as it leads to total combustion (Torres, Lopez et al. 2007). Its formation mechanism was proposed through OMMP1 surface intermediate; therefore propionaldehyde formation reaction has not been investigated in this study since formation of OMMP1

structure does not occur on $Cu_2O(001)$-Cl-1 surface according to VASP calculations.

Acetone formation path is investigated according to the previously proposed mechanism (Medlin, Mavrikakis et al. 1999). The initial state of the elementary reaction of acetone formation is the OMMP2 structure as indicated by step Cu.1.2.1 in Scheme 4.1. Acetone is formed by the activation of OMMP2. Stable structure of the final state of the reaction, acetone can be observed in Figure 4.5.

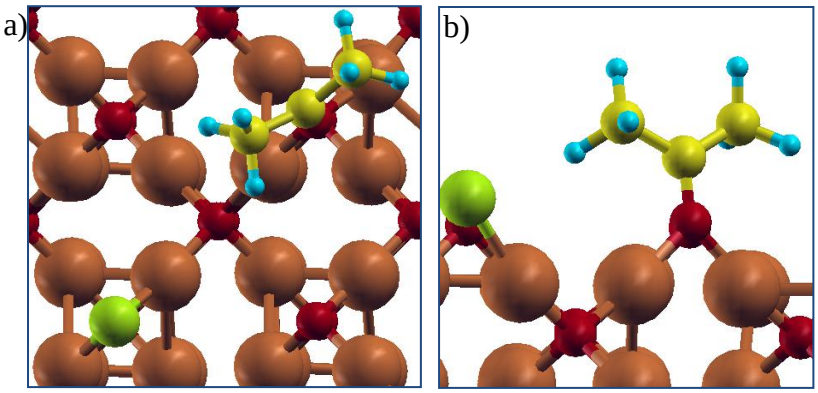

Figure 4.5 a) Top view and b) Side view of optimized acetone on $Cu_2O(001)$-Cl-1 (Cu: dark gray, big ones; O: black, small; Cl: light gray, bigger; C: light gray, smaller; H: gray, small)

The elementary reaction includes proton transfer from C2 to C1 and bond breaking of C1-Cu. In the approximate minimum energy path, first C1-Cu distance increases to 3.198Å by breaking OMMP2 structure and then the proton on C2 is transferred to C1 with the decrease in C2-O bond length from 1.49 Å to 1.273Å. Angle of the bridge structure Cu-O-Cu decreases to 98.8 degree with an upward movement of bridge oxygen.

In order to get acetone as a product, it should be desorbed from the surface which is indicated as step Cu.1.2.1.1. The following mechanism is proposed for acetone formation reaction and desorption of acetone from the surface, respectively:

$$[C_{(Cu)}H_2C_{(O)}HCH_3]_{surface} \rightarrow [CH_3CO_{(Cu)}CH_3]_{surface} \quad (4.8)$$

$$[CH_3CO_{(Cu)}CH_3]_{surface} \rightarrow [Cu]_{surface} + CH_3COCH_{3(gas)} \quad (4.9)$$

4.1.6. Propylene Oxide Formation Reaction

Propylene oxide can be generated by two mechanisms on $Cu_2O(001)$-Cl-1 surface. The first path is the PO formation via stable surface intermediate and the second path is the direct epoxidation of propylene to PO without formation of any stable surface structures. Adsorbed propylene structure on the surface is presented in Figure 4.6.

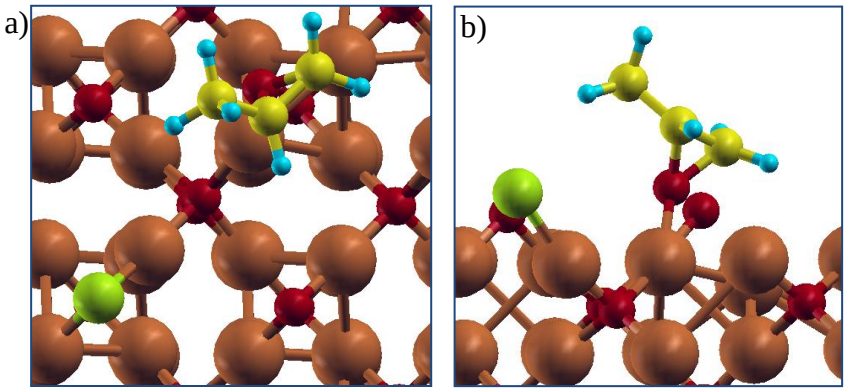

Figure 4.6 a) Top view and b) Side view of optimized propylene oxide adsorbed on $Cu_2O(001)$-Cl-1 (Cu: dark gray, big ones; O: black, small; Cl: light gray, bigger; C: light gray, smaller; H: gray, small)

PO generation via surface intermediate can be accomplished by activation of OMMP2 on the surface to obtain PO. In this elementary reaction, OMMP2 is considered as an initial state and adsorbed PO is the final state as labeled by step Cu.1.2.2 in Scheme 4.1.

In the minimum energy path of PO generation from OMMP2, first C1-Cu bond is broken and then C1 travels to bridge oxygen to close the ring structure of PO. C1-O distance decreases to 1.491Å with a TS value of 1.711Å whereas C1-Cu distance increases to 3.050Å passing through 2.398Å TS value. The bond length of C2-O does not change during the reaction. Thereafter, the angle of the bridge structure decreases to 81.9 degree and the structure is broken by the upward movement of PO. Selected bond lengths are tabulated in Table 4.2 below.

Table 4.2 Selected bond lengths of propylene oxide species on $Cu_2O(001)$-Cl-1 surface

		TS	Optimized Final state
Distances (Å)	C1-O	1.711	1.489
	C2-O	1.481	1.499
	C1-Cu	2.398	2.941
Angle (degree)	Cu-O-Cu	86.7	70.5

Subsequent to formation, PO should be separated from the surface by desorption to gas phase which is shown as Cu.1.2.2.1. For the formation of PO via OMMP2 and desorption of it from the surface, the reaction steps below are suggested:

$$[C_{(Cu)}H_2C_{(O)}HCH_3]_{surface} \rightarrow [C_3H_6O_{(Cu)}]_{surface} \quad (4.10)$$

$$[C_3H_6O_{(Cu)}]_{surface} \rightarrow [Cu]_{surface} + C_3H_6O_{(gas)} \quad (4.11)$$

Second path is PO formation from the adsorbed gas phase propylene directly, without formation of any stable surface intermediates as analogous to recently proposed direct ethylene oxide formation without OMME formation on Ag_2O (Özbek, Önal et al. 2011). However, minimum energy path search by CI-NEB analysis of second path namely direct epoxidation of propylene to PO resulted in spontaneous formation of OMMP2 structure along with the observation of a drop in the energy of the system. The energy profile in attempts to generate PO directly can be seen in Figure 4.7. It can be observed that there are two different maxima in the plot which suggests the existence of two elementary reactions each having an activation barrier. The final state of the first elementary reaction is the initial state of the second. It can be observed that the stable structure that creates two elementary reactions looks like OMMP2 which is discussed in section 4.1.4. Therefore, the second path does not have much probability of occurrence and the first path through stable surface intermediate OMMP2 is proposed for propylene epoxidation.

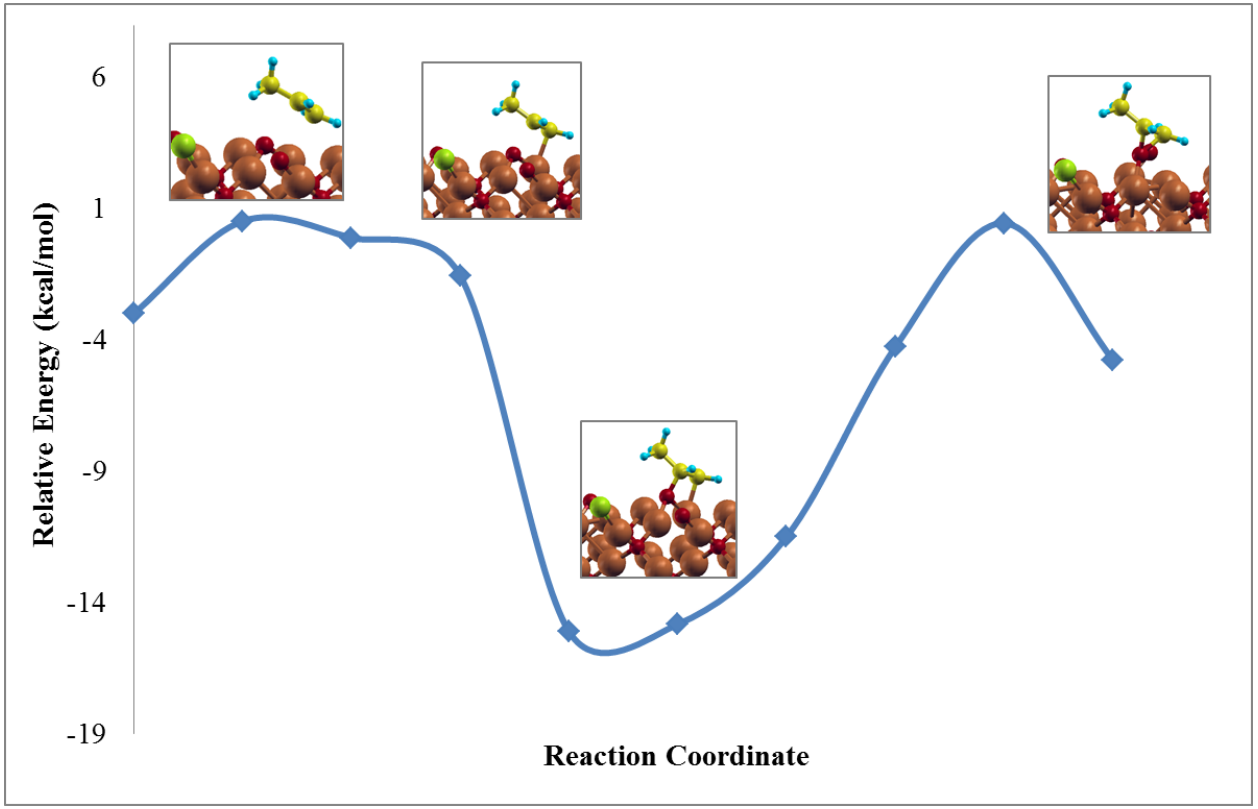

Figure 4.7 Energy profile obtained in CI-NEB analysis of direct PO formation on $Cu_2O(001)$-Cl-1 surface

The analysis of each elementary reaction in detail, results in the formation of overall reaction mechanism on $Cu_2O(001)$-Cl-1. It is presented step by step in the following lines.

Step Cu.1, Adsorption of propylene

$$C_3H_{6(gas)} \rightarrow [CH_2CHCH_3]_{surface} \quad (4.2)$$

Step Cu.1.1, Allylic hydrogen stripping reaction

$$[CH_2CHCH_3]_{surface} + 2[O]_{surface} \rightarrow [H_{(O)}]_{surface} + [C_{(O)}H_2CHCH_2\bullet]_{surface} \quad (4.3)$$

Step Cu.1.1.1, Desorption of allyl-radical

$$[C_{(O)}H_2CHCH_2\bullet]_{surface} \rightarrow [O]_{surface} + CH_2CHCH_2\bullet_{(gas)} \quad (4.4)$$

Step Cu.1.1.2, Acrolein generation through adsorbed allyl-radical

$$[C_{(O)}H_2CHCH_2\bullet]_{surface} + [O]_{surface} \rightarrow [H_{(O)}]_{surface} + [CO_{(Cu)}HCHCH_2] \quad (4.5)$$

Step Cu.1.1.2.1, Desorption of acrolein

$$[CO_{(Cu)}HCHCH_2] \rightarrow [Cu]_{surface} + COHCHCH_{2(gas)} \quad (4.6)$$

Step Cu.1.2, OMMP2 formation

$$[CH_2CHCH_3]_{surface} + [Cu]_{surface} + [O]_{surface} \rightarrow [C_{(Cu)}H_2C_{(O)}HCH_3]_{surface} \quad (4.7)$$

Step Cu.1.2.1, Acetone generation through OMMP2

$$[C_{(Cu)}H_2C_{(O)}HCH_3]_{surface} \rightarrow [CH_3CO_{(Cu)}CH_3]_{surface} \quad (4.8)$$

Step Cu.1.2.1.1, Desorption of acetone

$$[CH_3CO_{(Cu)}CH_3]_{surface} \rightarrow [Cu]_{surface} + CH_3COCH_{3(gas)} \quad (4.9)$$

Step Cu.1.2.2, PO formation through OMMP2

$[C_{(Cu)}H_2C_{(O)}HCH_3]_{surface} \rightarrow [C_3H_6O_{(Cu)}]_{surface}$ (4.10)

Step Cu.1.2.2.1, Desorption of PO

$[C_3H_6O_{(Cu)}]_{surface} \rightarrow [Cu]_{surface} + C_3H_6O_{(gas)}$ (4.11)

4.2. Propylene Partial Oxidation Mechanism on RuO_2(110)-Cl

The following reaction scheme (Scheme 4.2) shows the possible paths of propylene partial oxidation reaction on RuO_2(110)-Cl surface.

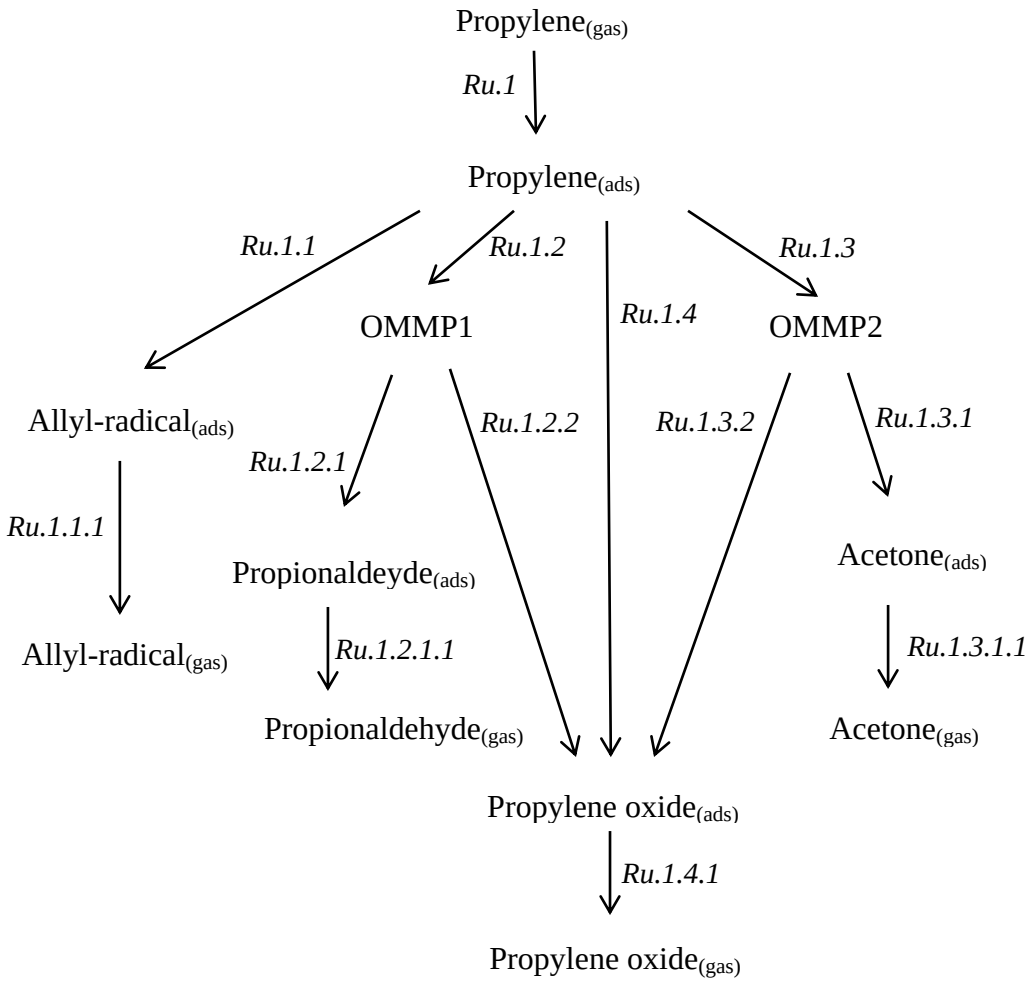

Scheme 4.2 Reaction scheme for propylene partial oxidation reaction on RuO_2(110)-Cl

4.2.1. Adsorption of Oxygen, Chlorine and Propylene

Adsorption properties of RuO_2(110)-Cl surface have been investigated similar to the adsorption study on Cu_2O(001)-Cl-1. Atomic oxygen species are substituted on vacant 2-fold bridge sites (Wang, Deo et al. 1999). Surface oxygens in bridge positions has lower coordination number than 3-fold oxygens on the same surface and all of the 3-fold or 4-fold oxygen species on metallic surfaces (Torres, Lopez et al. 2007). As analogous to Cu_2O(001)-Cl-1 surface, chlorine atom is also inserted on a vacant 2-fold bridge site. At this case, chlorine atom and the bridge oxygen atom utilized for the partial oxygen reaction share the electrons of the same ruthenium atom. Adsorption energy of oxygen is -57kcal/mol whereas adsorption energy of chlorine on the same vacant site is -59kcal/mol, calculated according to Equation 4.1. in Section 4.1.1. In case both oxygen and chlorine is present in the feed stream, they compete to adsorb on vacant sides and it seems that they have almost the same tendency to be adsorbed on the site. Partial oxidation reactions on the surface will take the bridge oxygen at the reaction site and at the end the surface will have a vacant oxygen site in the presence of chlorine on the surface. Adsorption energy of oxygen to that site is calculated as -58kcal/mol almost the same energy when it adsorbs to a vacant site of non-chlorinated surface. Therefore it is not harder to adsorb an oxygen to a vacant site on RuO_2(110)-Cl as it is on Cu_2O(110)-Cl-1 surface.

Average distances together with measure of the angle that the bridge structure forms on the fully oxidized surface RuO_2(110) and chlorine adsorbed surface RuO_2(110)-Cl are given in Table 4.3. The angle of the bridge structure Ru-O-Ru increases upon chlorine addition to the surface. The average bond lengths decrease when chlorine is inserted on oxide surface.

Table 4.3 Selected distances and angles on $RuO_2(110)$[a] and $RuO_2(110)$-Cl surface

		$RuO_2(110)$[a]	$RuO_2(110)$-Cl
Distances (Å)	Ru-O_s[b]	1.914	1.891
	Ru-Cl	-	2.411
	Ru-Ru	3.137	3.122
Angles (degree)	Ru-O_s-Ru	110.1	111.3
	Ru-Cl-Ru	-	81.6
	Ru(O)-O_{ss}[b]-Ru(O)	99.6	100.4
	Ru(Cl)-O_{ss}-Ru(Cl)	-	110.2

[a] Investigations on $RuO_2(110)$ surface without chlorine has been conducted by Deniz Onay (Onay; expected January 2012).

[b] O_s is the surface oxygen at bridge position and O_{ss} is the subsurface oxygen that connects the bridge structure to the bulk.

Propylene adsorption studies has been conducted on two different adsorption sites on $RuO_2(110)$-Cl. Propylene is adsorbed over the bridge oxygen which is a coordinatively unsaturated atom on the first adsorption site named Site-1, as can be observed in Figure 4.8. Propylene is adsorbed above coordinatively unsaturated ruthenium atom on the second area of adsorption also named as Site-2. The orientation can be seen in Figure 4.9. Analysis of these different sites revealed that adsorption is endothermic on Site-2 hence not favorable while propylene is adsorbed exothermically on Site-1 which is more favorable. For that reason, further analyses are dependent on adsorption of propylene on Site-1 on this surface and it is labeled as step Ru.1 in Scheme 4.2. The following reaction step is proposed for propylene adsorption on $RuO_2(110)$-Cl surface:

$$C_3H_{6\,(gas)} \rightarrow [CH_2CHCH_3]_{surface} \qquad (4.12)$$

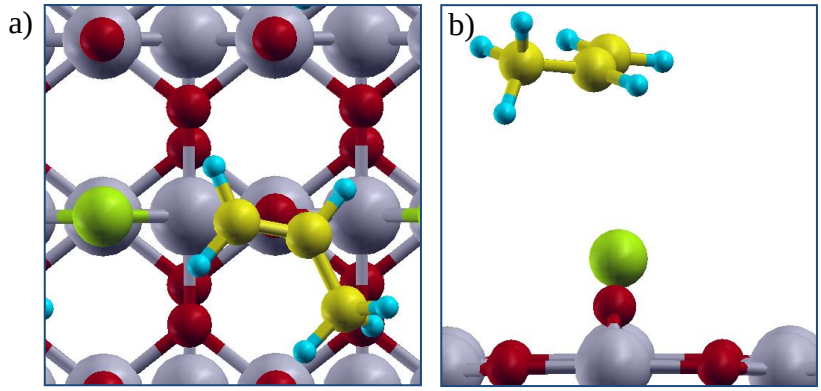

Figure 4.8 a) Top view and b) Side view of adsorption Site-1 on RuO_2(110)-Cl (Ru: gray, big ones; O: black, small; Cl: light gray, bigger; C: light gray, smaller; H: gray, small)

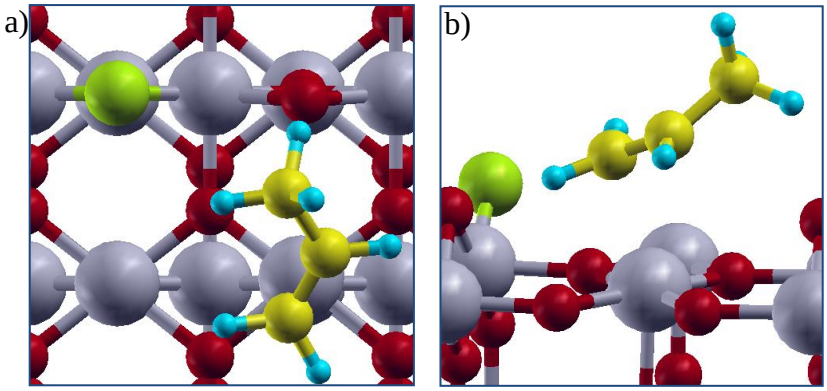

Figure 4.9 a) Top view and b) Side view of adsorption Site-2 on RuO_2(110)-Cl (Ru: gray, big ones; O: black, small; Cl: light gray, bigger; C: light gray, smaller; H: gray, small)

4.2.2. Allyl Hydrogen Stripping Reaction

Allylic hydrogen stripping reaction which is indicated as step Ru.1.1 in Scheme 4.2 is investigated subsequent to propylene adsorption. Different than the situation on Cu_2O(001)-Cl-1 case, allyl radical species is adsorbed on an under-coordinated ruthenium atom on the surface in accordance with previous theoretical studies of metal catalysts under scarce oxygen (Roldan, Torres et al. 2009; Kizilkaya, Senkan et al. 2010). The structure of the allyl radical species on RuO_2(110)-Cl can be seen in Figure 4.10.

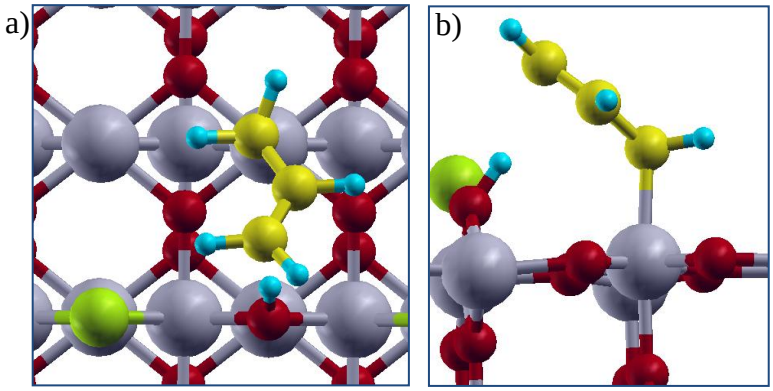

Figure 4.10 a) Top view and b) Side view of optimized adsorbed allyl radical species on RuO_2(110)-Cl (Ru: gray, big ones; O: black, small; Cl: light gray, bigger; C: light gray, smaller; H: gray, small)

In the minimum energy path of AHS, allylic hydrogen is transferred to a bridge oxygen to make an O-H bond of 0.993Å simultaneous to formation of C1-Ru bond of 2.164Å with under-coordinated ruthenium atom. The angle of bridge structure decreases to 101.5^{o} as hydrogen species is bonded to the oxygen in the structure. Subsequent to formation of allyl radical on the surface, it may desorb to gas phase as labeled as Ru.1.1.1. The following reaction steps are proposed for the generation of allyl-radical by allylic hydrogen stripping elementary reaction and desorption of allyl-radical:

$$[CH_2CHCH_3]_{surface}+[Ru]_{surface}+[O]_{surface}\rightarrow[H_{(O)}]_{surface}+[C_{(Ru)}H_2CHCH_2\bullet]_{surface} \quad (4.13)$$

$$[C_{(Ru)}H_2CHCH_2\bullet]_{surface} \rightarrow [Ru]_{surface} + CH_2CHCH_2\bullet_{(gas)} \quad (4.14)$$

4.2.3. Surface Intermediate OMMP Formation Reaction

Surface intermediate formation on RuO_2(110)-Cl surface has been investigated in accordance with Cu_2O(001)-Cl-1 surface research and previous studies (Medlin, Mavrikakis et al. 1999; Torres, Lopez et al. 2007; Roldan, Torres et al. 2009). On RuO_2(110)-Cl surface both types of OMMP; OMMP1 indicated as step Ru.1.2 in Scheme 4.2 and OMMP2 indicated as Ru.1.3 resulted in stable formation.

Optimized OMMP1 and OMMP2 structures are presented in Figure 4.11 and Figure 4.12, respectively.

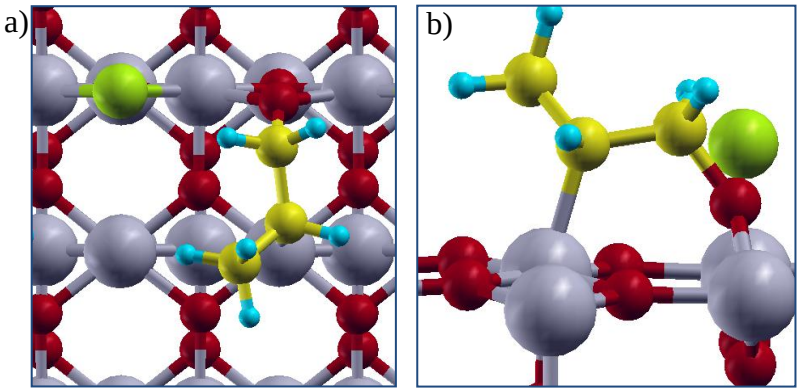

Figure 4.11 a) Top view and b) Side view of optimized OMMP1 structure on RuO_2(110)-Cl (Ru: gray, big ones; O: black, small; Cl: light gray, bigger; C: light gray, smaller; H: gray, small)

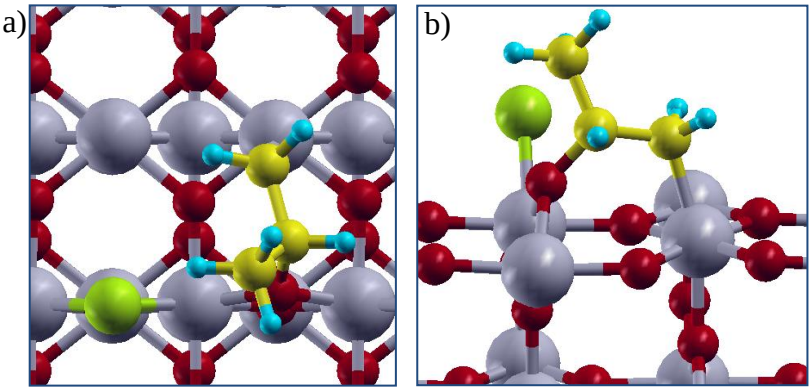

Figure 4.12 a) Top view and b) Side view of optimized OMMP2 structure on RuO_2(110)-Cl (Ru: gray, big ones; O: black, small; Cl: light gray, bigger; C: light gray, smaller; H: gray, small)

Critical bond lengths of OMMP structures are tabulated in Table 4.4. Bond lengths of carbon-oxygen and carbon-metal do not differ significantly although C1 is bonded to oxygen in OMMP1 and C2 is bonded in OMMP2 formation.

Table 4.4 Critical bond lengths of OMMP structures on RuO_2(110)-Cl

	OMMP1		OMMP2	
	C1-O	C2-Metal	C2-O	C1-Metal
TS	1.567	4.056	2.908	2.592
Optimized Final State	1.454	2.132	1.482	2.116

OMMP1 is activated to form either propionaldehyde or propylene oxide on the surface. Corresponding elementary reactions will be discussed in section 4.2.4 and 4.2.6, respectively. For the formation of OMMP1 from adsorbed propylene, the following reaction step is suggested according to the results of investigations:

$$[CH_2CHCH_3]_{surface}\ [Ru]_{surface} + [O]_{surface} \rightarrow [C_{(O)}H_2C_{(Ru)}HCH_3]_{surface} \quad (4.15)$$

OMMP2 is the surface precursor of either acetone or propylene oxide whose formation reactions will be discussed in sections 4.2.5 or 4.2.6. Similar to OMMP1 formation, a mechanism is proposed for OMMP2 formation:

$$[CH_2CHCH_3]_{surface} + [Ru]_{surface} + [O]_{surface} \rightarrow [C_{(Ru)}H_2C_{(O)}HCH_3]_{surface} \quad (4.16)$$

4.2.4. Propionaldehyde Formation Reaction

Propionaldehyde is an unwanted reaction product as it was proposed to further reacts on surface to give total combustion products carbon dioxide and water (Torres, Lopez et al. 2007). It is generated through the surface intermediate OMMP1 shown as step Ru.1.2.1 in Scheme 4.2. The structure of adsorbed propionaldehyde on surface is represented in Figure 4.13.

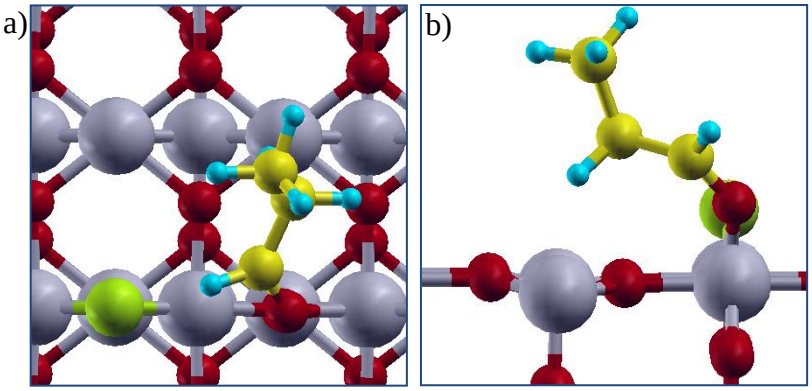

Figure 4.13 a) Top view and b) Side view of optimized adsorbed propionaldehyde on RuO_2(110)-Cl (Ru: gray, big ones; O: black, small; Cl: light gray, bigger; C: light gray, smaller; H: gray, small)

First OMMP1 structure is broken down as the distance between C2 and Cu increases and the bond is broken in the approximate minimum energy path computed by CI-NEB analysis. Afterwards, a proton is transferred from C1 to C2 and propionaldehyde is generated. Subsequent to the formation of propionaldehyde on the surface, it may desorb to the gas phase which can be observed as step Ru.1.2.1.1. The first equation below is the proposed elementary reaction mechanism to generate propionaldehyde from OMMP1 and the second is for desorption of propionaldehyde to the gas phase:

$$[C_{(O)}H_2C_{(Ru)}HCH_2]_{surface} \rightarrow [CHO_{(Ru)}CH_2CH_3]_{surface} \quad (4.17)$$

$$[CHO_{(Ru)}CH_2CH_3]_{surface} \rightarrow [Ru]_{surface} + CHOCH_2CH_{3(gas)} \quad (4.18)$$

4.2.5. Acetone Formation Reaction

Acetone formation is accomplished via OMMP2 surface intermediate, shown in step Ru.1.3.1 in Scheme 4.2, on RuO_2(110)-Cl surface, the same mechanism with acetone formation reaction on Cu_2O(001)-Cl-1. Acetone structure on RuO_2(110)-Cl can be observed in Figure 4.14. Relevant bond energies of acetone structure on RuO_2(110)-Cl are presented in Table 4.5.

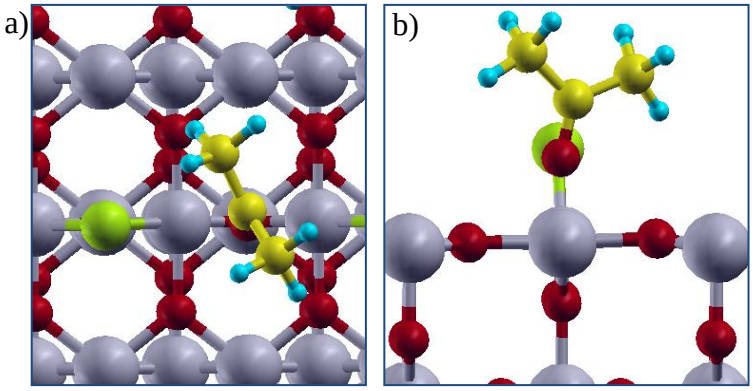

Figure 4.14 a) Top view and b) Side view of optimized adsorbed acetone on RuO_2(110)-Cl (Ru: gray, big ones; O: black, small; Cl: light gray, bigger; C: light gray, smaller; H: gray, small)

In the minimum energy path of acetone generation through OMMP2, first C1-Ru bond of OMMP2 breaks and then the proton on C2 is transferred to C1 with the decrease in C2-O bond length from 1.466 Å to 1.250 Å to form the final structure. Energy profile of acetone formation is obtained by CI-NEB method and it is shown in Figure 4.15. Adsorbed acetone should pass to the gas phase to be separated and isolated from the catalyst surface which is indicated as Ru.1.3.1.1. For the generation step of acetone through OMMP2, the first reaction below is proposed. And the second is suggested for the desorption step:

$$[C_{(Ru)}H_2C_{(O)}HCH_3]_{surface} \rightarrow [CH_3CO_{(Ru)}CH_3]_{surface} \quad (4.19)$$

$$[CH_3CO_{(Ru)}CH_3]_{surface} \rightarrow [Ru]_{surface} + CH_3COCH_{3(gas)} \quad (4.20)$$

Table 4.5 Selected bond lengths of adsorbed acetone species on RuO_2(110)-Cl surface

		TS	Optimized Final state
Distances (Å)	C2-H	1.234	2.132
	C1-H	1.603	1.103
	C1-Ru	3.389	4.060
Angle (degree)	Ru-O-Ru	95.7	82.0

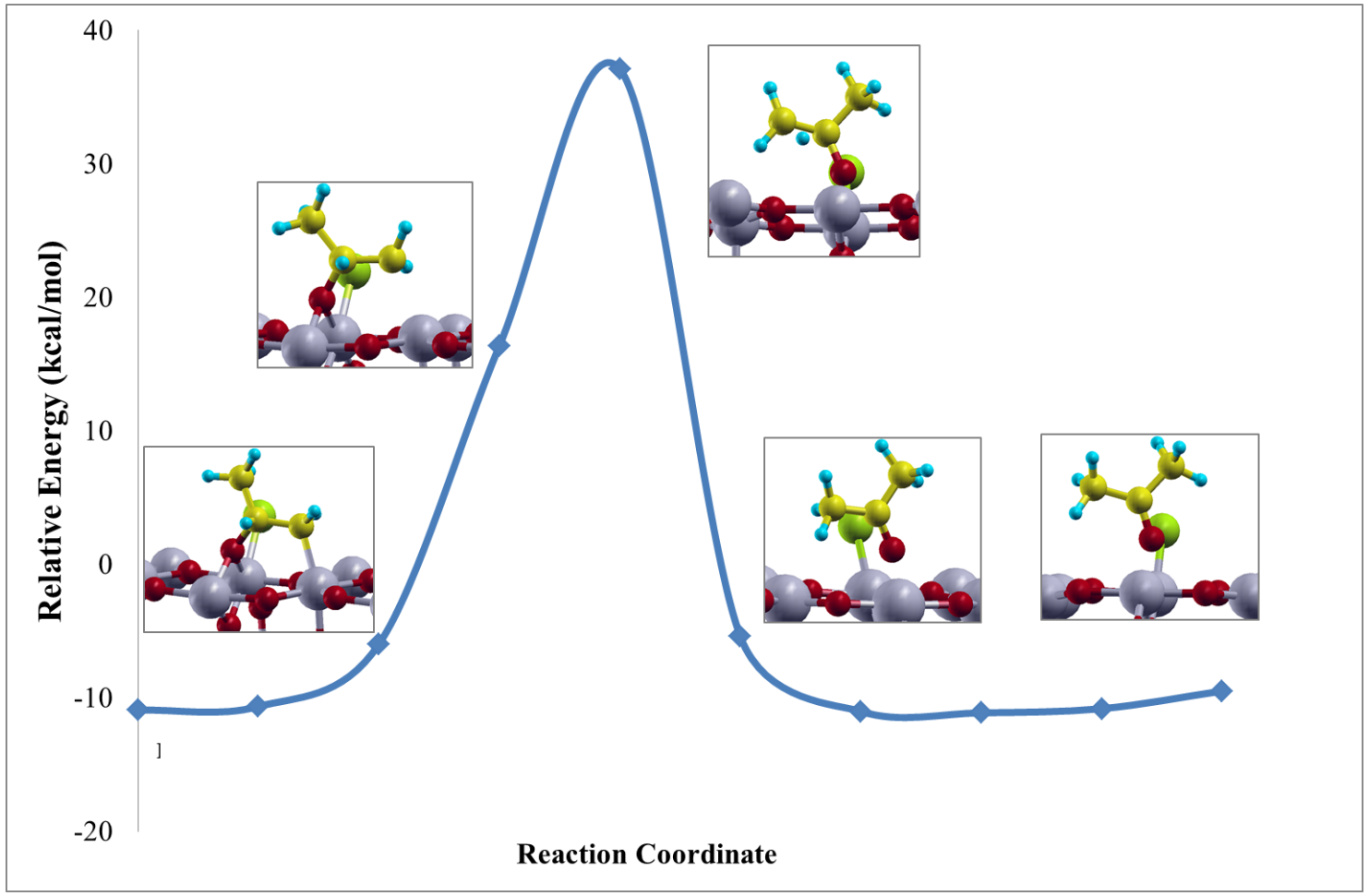

Figure 4.15 Energy profile obtained in CI-NEB analysis of acetone formation on RuO_2(110)-Cl

4.2.6. Propylene Oxide Formation Reaction

There are three PO generation mechanism on this surface as both surface intermediates OMMP1 and OMMP2 are obtained as stable structures; PO formation by OMMP1, PO formation by OMMP2 and direct PO generation. Propylene oxide structure as adsorbed on the surface is presented in Figure 4.16.

The first mechanism, elementary reaction of PO formation through OMMP1, can be observed as step Ru.1.2.2 in Scheme 4.2, starts with the activation of OMMP1 structure. C2 atom starts to move in upwards direction and C2-Ru bond is broken. Simultaneously, the distance between C2 and the bridge oxygen that C1 is bonded decreases with a TS value of C2-O distance of 2.387Å. Finally, epoxide ring is constructed as the bridge structure is destroyed and bridge oxygen moves upwards to join epoxide ring. The following reaction step is suggested for this elementary reaction on RuO_2-Cl surface:

$$[C_{(O)}H_2C_{(Ru)}HCH_3]_{surface} \rightarrow [C_3H_6O_{(Ru)}]_{surface} \quad (4.21)$$

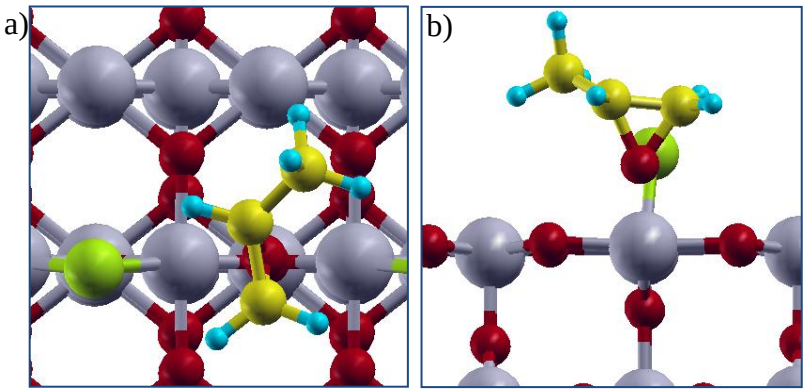

Figure 4.16 a) Top view and b) Side view of optimized adsorbed propylene oxide on RuO_2(110)-Cl (Ru: gray, big ones; O: black, small; Cl: light gray, bigger; C: light gray, smaller; H: gray, small)

The position of adsorbed propylene oxide is slightly different than Cu_2O(001)-Cl-1. Propylene oxide backbone constructed by carbon atoms are nearly parallel on chlorinated RuO_2(110) whereas the skeleton is slightly inclined on chlorinated Cu_2O(001).

The second mechanism is PO production via OMMP2 which destroys OMMP2 and produces PO by initially breaking C1-Ru bond and the formation of C1-O bond in the form of epoxide ring. Reaction is shown as step Ru.1.3.2 and the mechanism proposed for this reaction is as follows:

$$[C_{(Ru)}H_2C_{(O)}HCH_3]_{surface} \rightarrow [C_3H_6O_{(Ru)}]_{surface} \quad (4.22)$$

Third mechanism of PO formation is the direct generation from adsorbed propylene as indicated by step Ru.1.4 in Scheme 4.2, without formation of any stable surface intermediates in accordance with a recent study on Ag_2O (Özbek, Önal et al. 2011). In the minimum energy path (MEP) of direct PO formation, after propylene getting closer to the surface, first C2 is bonded to the bridge oxygen and then C1 approaches to close the ring structure. The angle of the bridge structure decreases throughout the path being 114.5 degree at the beginning passing through TS of 102.5 degree angle to reach the minimum of 85.4 degree at the end when propylene oxide is formed as adsorbed on the surface. Simultaneously, the distance between C2 and bridge oxygen decreases from 2.262Å to 1.497Å. Transition state (TS) is characterized also by vibrational frequency analysis having only one imaginary mode. TS structure can be seen in Figure 4.17. The proposed mechanism for direct PO formation is presented in equation (4.22) below:

$$[CH_2CHCH_3]_{surface} + [Ru]_{surface} \rightarrow [C_3H_6O_{(Ru)}]_{surface} \quad (4.23)$$

After the formation of PO by either of the three discussed PO generation elementary reactions, PO requires transferring to the gas phase as indicated by step Ru.1.4.1 whose mechanism is suggested as follows:

$$[C_3H_6O_{(Ru)}]_{surface} \rightarrow [Ru]_{surface} + C_3H_6O_{(gas)} \quad (4.24)$$

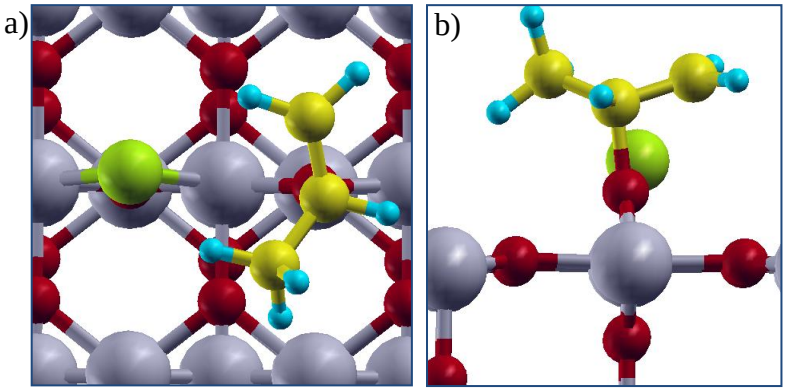

Figure 4.17 a) Top view and b) Side view of TS for direct PO formation on RuO_2(110)-Cl (Ru: gray, big ones; O: black, small; Cl: light gray, bigger; C: light gray, smaller; H: gray, small)

The analysis of each elementary reaction possible on the surface resulted in the formation of the general reaction mechanism for propylene partial oxidation on RuO_2(110)-Cl.

Step Ru.1, Adsorption of propylene

$$C_3H_{6\,(gas)} \rightarrow [CH_2CHCH_3]_{surface} \quad (4.12)$$

Step Ru.1.1, Allylic hydrogen stripping reaction

$$[CH_2CHCH_3]_{surface}+[Ru]_{surface}+[O]_{surface}\rightarrow[H_{(O)}]_{surface}+[C_{(Ru)}H_2CHCH_2\bullet]_{surface} \quad (4.13)$$

Step Ru.1.1.1, Desorption of allyl-radical

$$[C_{(Ru)}H_2CHCH_2\bullet]_{surface} \rightarrow [Ru]_{surface} + CH_2CHCH_2\bullet_{(gas)} \quad (4.14)$$

Step Ru.1.2, OMMP1 formation

$$[CH_2CHCH_3]_{surface}\ [Ru]_{surface}+ [O]_{surface} \rightarrow [C_{(O)}H_2C_{(Ru)}HCH_3]_{surface} \quad (4.15)$$

Step Ru.1.2.1, Propionaldehyde generation through OMMP1

$$[C_{(O)}H_2C_{(Ru)}HCH_2]_{surface} \rightarrow [CHO_{(Ru)}CH_2CH_3]_{surface} \quad (4.17)$$

Step Ru.1.2.1.1, Desorption of propionaldehyde

$[CHO_{(Ru)}CH_2CH_3]_{surface} \rightarrow [Ru]_{surface} + CHOCH_2CH_{3(gas)}$ (4.18)

Step Ru.1.2.2, PO generation through OMMP1

$[C_{(O)}H_2C_{(Ru)}HCH_3]_{surface} \rightarrow [C_3H_6O_{(Ru)}]_{surface}$ (4.21)

Step Ru.1.3, OMMP2 formation

$[CH_2CHCH_3]_{surface} + [Ru]_{surface} + [O]_{surface} \rightarrow [C_{(Ru)}H_2C_{(O)}HCH_3]_{surface}$ (4.16)

Step Ru.1.3.1, Acetone generation through OMMP2

$[C_{(Ru)}H_2C_{(O)}HCH_3]_{surface} \rightarrow [CH_3CO_{(Ru)}CH_3]_{surface}$ (4.19)

Step Ru.1.3.1.1, Desorption of acetone

$[CH_3CO_{(Ru)}CH_3]_{surface} \rightarrow [Ru]_{surface} + CH_3COCH_{3(gas)}$ (4.20)

Step Ru.1.3.2, PO generation through OMMP2

$[C_{(Ru)}H_2C_{(O)}HCH_3]_{surface} \rightarrow [C_3H_6O_{(Ru)}]_{surface}$ (4.22)

Step Ru.1.4, Direct PO generation without a surface intermediate

$[CH_2CHCH_3]_{surface} + [Ru]_{surface} \rightarrow [C_3H_6O_{(Ru)}]_{surface}$ (4.23)

Step Ru.1.4.1, Desorption of PO

$[C_3H_6O_{(Ru)}]_{surface} \rightarrow [Ru]_{surface} + C_3H_6O_{(gas)}$ (4.24)

4.3. Overall reaction profiles on $Cu_2O(001)$ and $RuO_2(110)$

Overall reaction profile for propylene partial oxidation reaction on $Cu_2O(001)$-Cl-1 is presented in Figure 4.18. Acetone formation (Step Cu.1, Step Cu.1.2, Step Cu.1.2.1, Step Cu.1.2.1.1) and PO formation (Step Cu.1, Step Cu.1.2, Step Cu.1.2.2, Step Cu.1.2.2.1) have been generated by the same precursor, surface intermediate OMMP2 whereas allyl-radical formation (Step Cu.1, Step Cu.1.1, Step Cu.1.1.1) and acrolein formation (Step Cu.1, Step Cu.1.1, Step Cu.1.1.2, Step Cu.1.1.2.1) reactions have the same precursor reaction, allylic hydrogen stripping.

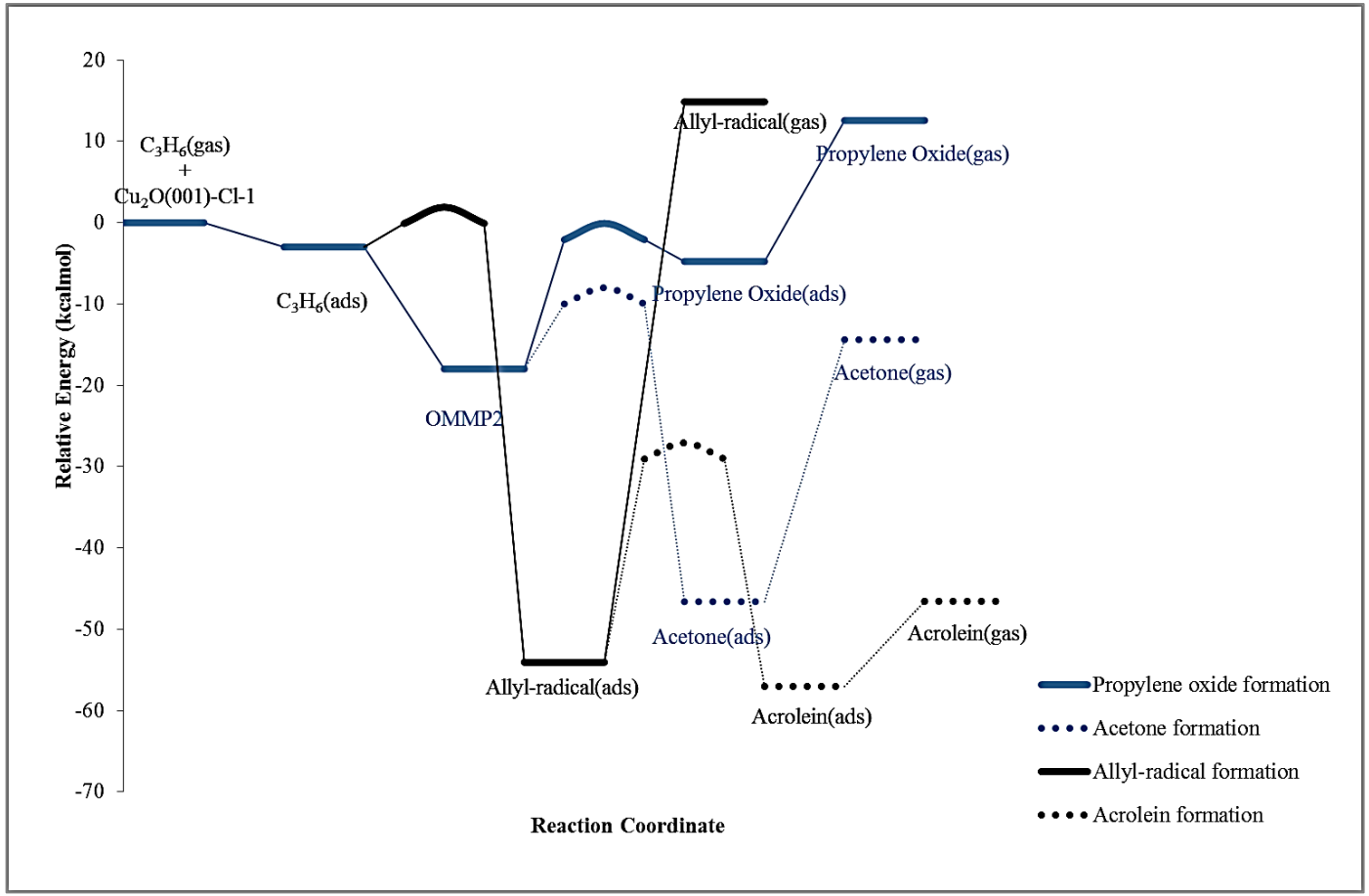

Figure 4.18 Energy profile for propylene epoxidation reaction on $Cu_2O(001)$-Cl-1 surface

Unwanted allyl-radical formation begins with propylene adsorption and then allylic hydrogen stripping reaction (Step Cu.1.1) which has a slight activation barrier of 4kcal/mol analyzed in the minimum energy path search. As desorption of allyl-radical (Step Cu.1.1.1) requires even more energy (69kcal/mol), the rate limiting step of allyl-radical formation seems to be desorption of allyl-radical from the surface. In case desorption does not occur due to high energy requirement, adsorbed allyl radical can further release a proton on an oxygen species on the surface to generate acrolein (Step Cu.1.1.2). The activation barrier of acrolein generation reaction appears to be 27kcal/mol. Energy requirement of acrolein desorption (Step Cu.1.1.2.1) from the surface is 11kcal/mol far less than ally-radical desorption. Therefore, acrolein formation is more favorable than gas phase ally-radical formation on $Cu_2O(001)$-Cl-1. After acrolein desorption, the surface is left covered with 0.5 ML of hydrogen each bonded on bridge oxygen on the surface.

Surface intermediate OMMP2 can be generated (Step Cu.1.2) as an alternative to allylic hydrogen stripping reaction. In fact, OMMP2 formation reaction is more favorable than allylic hydrogen stripping since it is a non-barriered reaction. Energy profile obtained in the minimum energy path analysis of two competing reaction routes that adsorbed propylene can follow on $Cu_2O(001)$-Cl-1 surface; allylic hydrogen stripping and OMMP2 formation reactions is presented in Figure 4.19. Both of the reactions are exothermic. Although allylic hydrogen stripping reaction is more exothermic than OMMP2 formation, reactants have to pass through a slight energy barrier to produce adsorbed allyl-radical. Being non-activated, less exothermic OMMP2 formation reaction is more favorable on $Cu_2O(001)$-Cl-1

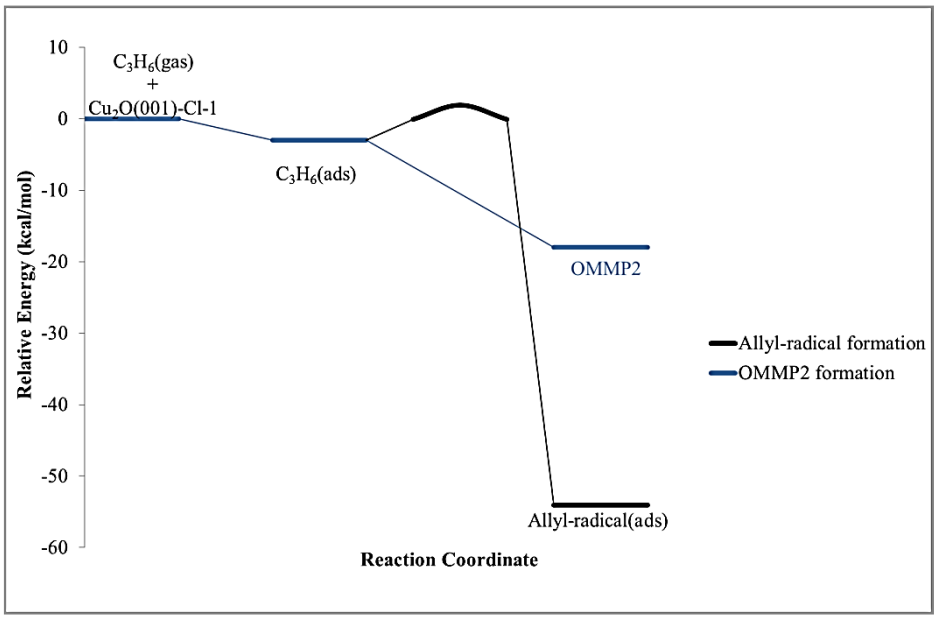

Figure 4.19 Competing reactions after propylene adsorption on $Cu_2O(001)$-Cl-1

OMMP2 activation can proceed to PO generation (Step Cu.1.2.2) by a reaction which has 18kcal/mol barrier. PO desorption (Step Cu.1.2.2.1) requires 17kcal/mol of energy. Therefore, the rate limiting step in PO production path is most probably PO generation through OMMP2 or PO desorption from the surface. As OMMP2 can also proceed another reaction of acetone generation (Step Cu.1.2.1), PO generation and acetone generation are competing reactions. Acetone generation through OMMP2 has 10kcal/mol activation barrier computed by CI-NEB, slightly higher than PO formation. Desorption energy of acetone (Step Cu.1.2.1.1) is 32kcal/mol which is nearly twice as much as PO desorption energy. More exothermic generation of acetone than PO by OMMP2 may have resulted in harder desorption of acetone than PO. Higher energy requirement in desorption step from surface makes this step the rate limiting step in acetone production on this surface.

Activation barriers of considered reactions on $Cu_2O(001)$-Cl-1 are tabulated in Table 4.6 in the following pages together with barrier values on non-chlorinated $Cu_2O(001)$ whose investigation is done by Deniz Onay in the scope of her Master of Science thesis studies (Onay; expected January 2012). When activation barrier values of chlorinated and nonchlorinated $Cu_2O(001)$ surfaces are compared; slight increase in barriers of allylic hydrogen stripping reaction and acrolein generation

reaction are observed when chlorine is introduced to surface. This might improve the selectivity of the catalyst towards products generated by OMMP2 mechanism; namely propylene oxide and acetone. Furthermore, a slight decrease in activation barrier of acetone generation is also observed.

Similar influence by chlorine addition is observed in an experimental propylene oxidation study on Cu/SiO_2 catalysts where incorporation of Cl^- containing species slightly improves the selectivity but cause a loss of activity (Su, Wang et al. 2009). However, researches could not agree on the underlying reason of chlorine's effect. In fact, underlying mechanism of halogens' promotion effect on epoxidation reactions is a controversial issue. There are two suggestions that researches could not agree on either, regarding the underlying reason of the chlorine promotion. One proposal is the geometric effect (Force and Bell 1976; Campbell and Koel 1985; Serafin, Liu et al. 1998; Özbek, Önal et al. 2011) namely, chlorine's blocking of the surface vacant sites which are necessary for combustion reaction since it demands more active sites rather than epoxides. Another theory is concerned with the electronic effect (Serafin, Liu et al. 1998; Lu, Luo et al. 2002; Lambert, Cropley et al. 2003) that occurs since electron affinity of chlorine is higher than the oxygen with which it competes for the electrons of the same metal atom. The strength of metal-oxygen bond weakens since metal donates more electrons to chlorine that makes the oxygen more electrophilic and more active for epoxidation reaction.

On RuO_2(110)-Cl surface, production of four different species are possible; allyl-radical formation (Step Ru.1, Step Ru.1.1, Step Ru.1.1.1), propionaldehyde formation (Step Ru.1, Step Ru.1.2, Step Ru.1.2.1, Step Ru.1.2.1.1), acetone formation (Step Ru.1, Step Ru.1.3, Step Ru.1.3.1, Step Ru.1.3.1.1) and PO formation. Moreover, PO can be produced by three different mechanisms; PO formation via OMMP1 (Step Ru.1, Step Ru.1.2, Step Ru.1.2.2, Step Ru.1.4.1), PO formation via OMMP2 (Step Ru.1, Step Ru.1.3, Step Ru.1.3.2, Step Ru.1.4.1) and direct PO formation (Step R1, Step R13, Step R8). Overall reaction profile of partial oxidation reactions of propylene on RuO_2(110)-Cl is presented in Figure 4.20.

On RuO_2(110)-Cl surface, allyl-radical can be produced as adsorbed to the surface after propylene adsorption by allylic hydrogen stripping reaction (Step Ru.1.1)

which is an exothermic reaction and it has 2.5kcal/mol activation barrier. As 45kcal/mol energy is needed to desorb allyl-radical from the surface (Step Ru.1.1.1), the rate limiting step of gas phase allyl-radical formation is desorption of allyl-radical from the surface.

Surface intermediate OMMP1 can be generated (Step Ru.1.2) on the surface as an alternative to allylic hydrogen stripping. OMMP1 generation from adsorbed propylene has an activation barrier of 21kcal/mol. OMMP1 may go under an endothermic reaction to produce an unwanted product propionaldehyde (Step Ru.1.2.1) but it should pass through a barrier of 42kcal/mol determined as the difference of transition state and initial state in minimum energy path computations. Furthermore, 13 kcal/mol energy is required for desorption of propionaldehyde (Step Ru.1.2.1.1) from surface which is far lower than formation of propionaldehyde from OMMP1 intermediate. This means, if propionaldehyde is formed on the surface, possibly it desorbs from the surface. The rate determining step in propionaldehyde production on this surface is the propionaldehyde generation step from OMMP1. Besides propionaldehyde generation, OMMP1 may result in PO generation by an endothermic reaction (Step Ru.1.2.2) if 32kcal/mol of activation barrier is overcome. Desorption energy of PO (Step Ru.1.4.1) is much lower, 10kcal/mol which makes PO generation by OMMP1 step the rate determining step in this option of PO generation. When OMMP1 is formed on the surface, it seems that probability of PA generation is lower than PO generation due to the fact that PO generation has lower barrier than PA generation.

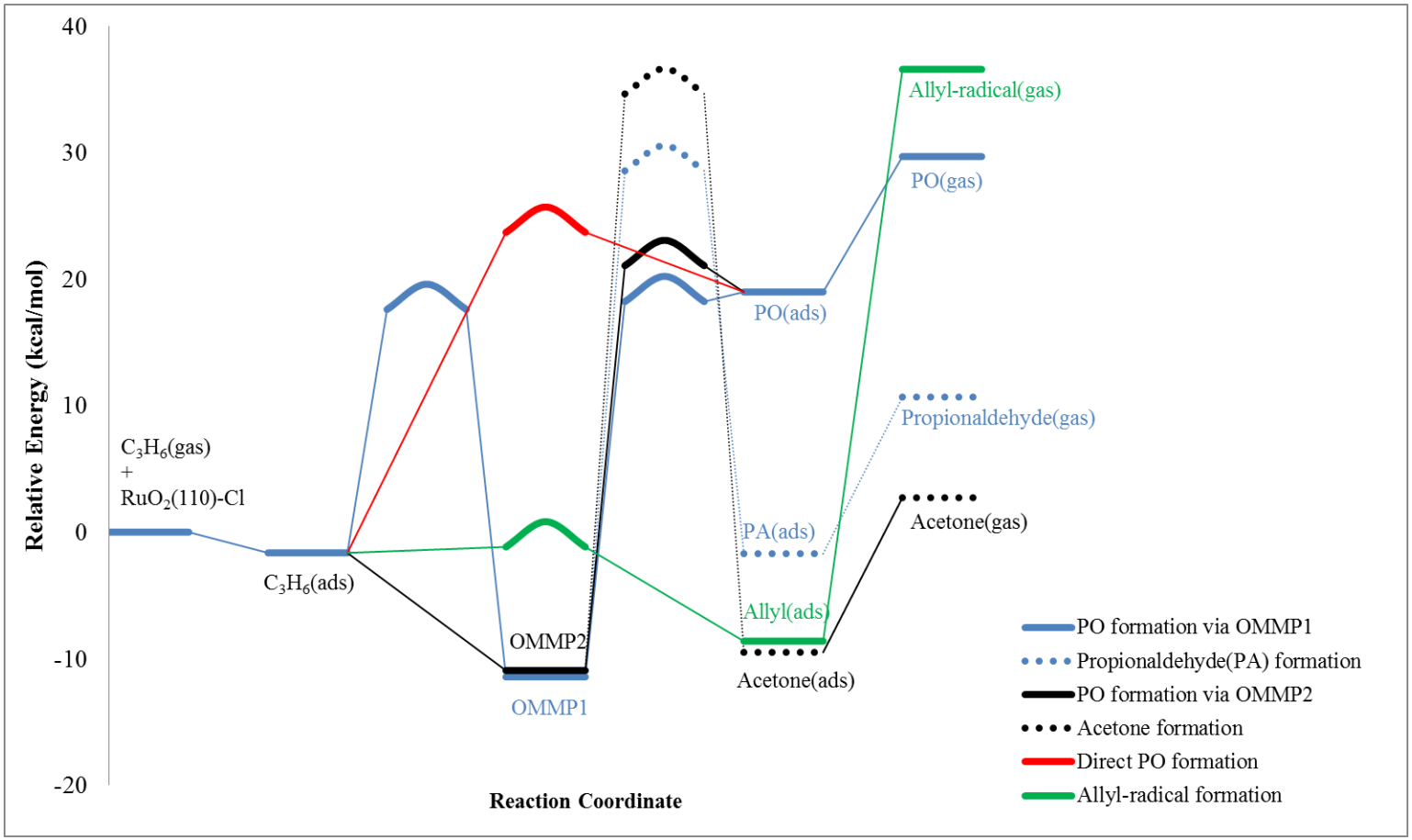

Figure 4.20 Energy profile for propylene epoxidation reaction on $RuO_2(110)$-Cl surface

Another surface intermediate, OMMP2 formation (Step Ru.1.3) is the second alternative reaction to allylic hydrogen stripping reaction. OMMP2 formation reaction is exothermic, and occurs without a barrier. When compared with OMMP1 formation, OMMP2 formation is more favorable as reactants should pass through a barrier to generate OMMP1, although the two surface intermediate formation reactions has almost the same heat of reactions, around 11kcal/mol. OMMP2 may result in acetone generation following the elementary reaction of acetone generation (Step Ru.1.3.1). It has an activation barrier of 48kcal/mol. Adsorbed acetone needs just 12kcal/mol energy to leave the surface therefore once it is formed, desorption of acetone (Step Ru.1.3.1.1) is more favorable than reverse reaction back to OMMP2. The rate limiting step of acetone production on RuO_2(110)-Cl is the formation of acetone from OMMP2 with relatively high activation barrier. Acetone generation reaction competes with PO generation reaction since there is a path to PO formation through OMMP2 (Step Ru.1.3.2). It seems to have an activation barrier of 34kcal/mol, less than acetone generation reaction. Therefore, PO formation via OMMP2 has more probability than acetone formation. Furthermore, this reaction is the second way to make PO on this surface it has more probability to produce PO when compared to the first way of PO production, via OMMP1.

The third alternative to allylic hydrogen stripping reaction and the third way to produce PO is direct PO generation reaction (Step Ru.1.4) without formation of any surface intermediate. The reaction has an activation barrier of 27kcal/mol, lower than the barriers of other methods to produce PO. Desorption (Step Ru.1.4.1) energy is lower than the barrier for formation therefore, the rate determining step is the formation reaction of PO in the third way of PO production on RuO_2(110).

Table 4.6 Activation barriers for reactions on $Cu_2O(001)$, $Cu_2O(001)$-Cl-1, $RuO_2(110)$ and $RuO_2(110)$-Cl

	$Cu_2O(001)$[a]	**$Cu_2O(001)$-Cl-1**	**$RuO_2(110)$[a]**	**$RuO_2(110)$-Cl**
AHS reaction	0.0	4.0	7.8	2.5
Acrolein generation	21.2	27.0	-	-
OMMP1 generation	-	-	14.1	21.2
PA generation	-	-	29.6	38.0
OMMP2 generation	0.0	0.0	4.4	0.0
Acetone generation	13.6	10.0	43.6	47.6
PO through OMMP1	-	-	33.9	32.0
PO through OMMP2	17.7	17.9	37.8	34.0
Direct PO	-	-	18.7	27.0

[a]Analysis of propylene partial oxidation reaction on non-chlorinated $Cu_2O(001)$ and non-chlorinated $RuO_2(110)$ have been performed by Deniz Onay (Onay; expected January 2012).

Activation barriers of considered reactions on $RuO_2(110)$-Cl are tabulated in Table 4.6 together with barrier values on non-chlorinated $RuO_2(110)$ whose investigation is done by Deniz Onay in the scope of her Master of Science thesis studies (Onay; expected January 2012). When activation barrier values of chlorinated and nonchlorinated $RuO_2(110)$ surfaces are compared; it is observed that chlorine addition to the surface decreases the barrier of unwanted allylic hydrogen stripping reaction and decreases

Competing reactions just after propylene is adsorbed on $RuO_2(110)$ is presented in Figure 4.20. Although reaction energies of OMMP1 and OMMP2 are similar, there exists a considerable difference between the activation barriers of these two surface intermediates. OMMP2 formation is far more favorable than OMMP1 formation on $RuO_2(110)$-Cl surface. Allylic hydrogen stripping reaction also seems to have high probability of occurrence together with OMMP2 formation. OMMP1 formation and direct PO formation have higher barriers therefore, they both are less favorable.

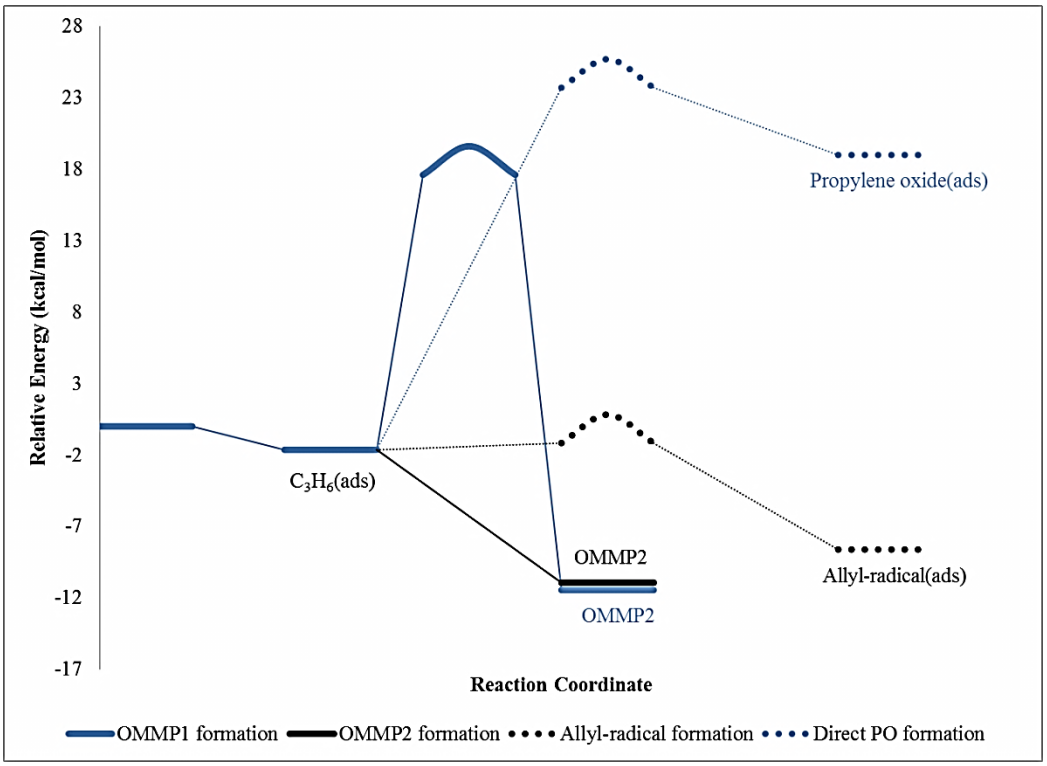

Figure 4.21 Competing reactions after propylene adsorption on RuO_2(110)-Cl

As mentioned before, there are three PO production methods on this surface; PO formation by surface intermediate OMMP1, PO formation by surface intermediate OMMP2 and direct PO formation. In Figure 4.22, energy profiles of all of the methods are shown. Although OMMP1 formation has higher barrier than OMMP2 formation, PO formation by OMMP1 seems the most favorable PO production method on RuO_2(110)-Cl.

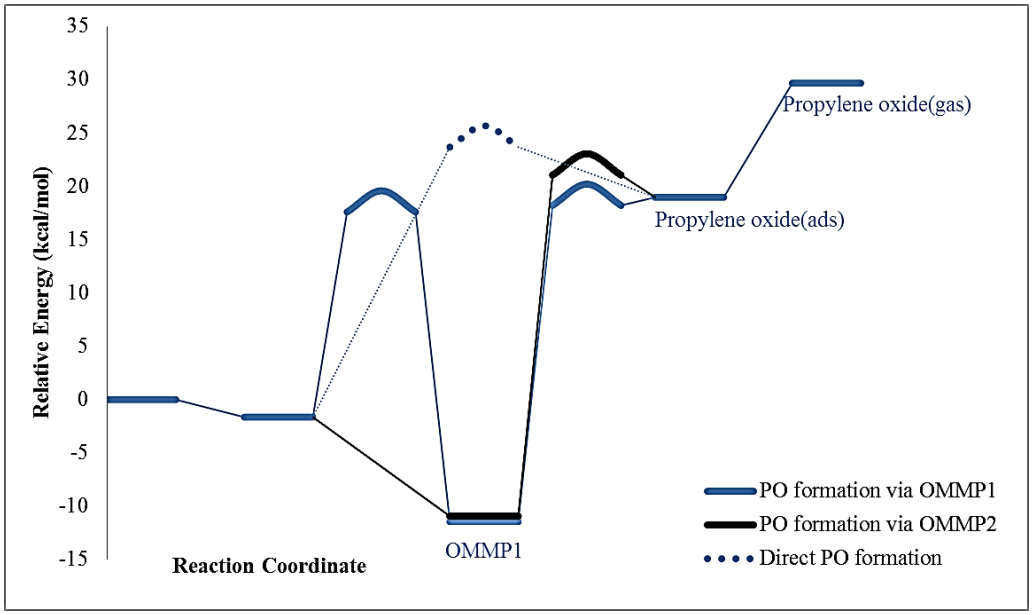

Figure 4.22: Energy profiles of all of the three PO production methods on RuO_2(110)-Cl

4.4. Variation of the Position of Chlorine on $Cu_2O(001)$

In order to see the effect of chlorine deeply and determine the underlying reasons of the influence, one more slab is constructed in addition to $Cu_2O(001)$-Cl-1. The new surface, named as $Cu_2O(001)$-Cl-2, has also the same surface chlorine coverage of 0.25 ML with $Cu_2O(001)$-Cl-1 on which the mechanism and energetics of partial oxidation of propylene are discussed in the previous sections. Though, the position of the chlorine on the surface with respect to bridge oxygen species utilized for the partial oxidation reaction is altered. The details of the surface structure of $Cu_2O(001)$-Cl-2 are explained in section 3.1.1.

Propylene adsorption site on $Cu_2O(001)$-Cl-2 and is the same as site investigated on $Cu_2O(001)$-Cl-1. Adsorption energies of propylene on both of the prepared surfaces are presented in Table 4.7 together with the charges of oxygen at bridge site and average charge of copper atoms that form the bridge site. Adsorption energies and charge values calculated by Bader charge analysis are almost the same on both of the surfaces.

Table 4.7 Adsorption energies of atomic oxygen, atomic chlorine and propylene on $Cu_2O(001)$-Cl-1 and $Cu_2O(001)$-Cl-2 with selected charges

	Adsorption Energy (kcal/mol)				Charge	
	Oxygen	Chlorine	Oxygen after reaction	Propylene	O	Cu
$Cu_2O(001)$-Cl-1	-60	-60	-40	3	-0.88	0.65
$Cu_2O(001)$-Cl-2	-60	-61	-43	2	-0.86	0.65

As the results of investigation on $Cu_2O(001)$-Cl-1 surface suggest, only reactions take place just after the adsorption of propylene is investigated on new generated surface $Cu_2O(001)$-Cl-2 rather than all partial oxidation mechanism.

4.4.1. Allylic Hydrogen Stripping (AHS) on Cu_2O-Cl-2

Allylic hydrogen stripping (AHS) reaction is investigated subsequent to propylene adsorption. Adsorption of ally-radical on a bridge oxygen atom rather than copper atom on Cu_2O(001)-Cl-2 surface is more favorable as it is on Cu_2O(001)-Cl-1. Details of the final state structure of allyl-radical can be seen in Figure 4.23.

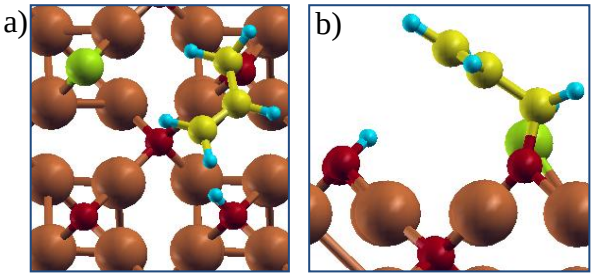

Figure 4.23 a) Top view and b) Side view of optimized adsorbed allyl-radical on Cu_2O(001)-Cl-2 (Cu: dark gray, big ones; O: black, small; Cl: light gray, bigger; C: light gray, smaller; H: gray, small)

The minimum energy path of allylic hydrogen stripping is slightly different on Cu_2O(001)-Cl-2 surface. When one of the allylic hydrogens leaves C3, C1 of allyl-radical is first binds to one of the coppers of the bridge structure. Then, ally-radical is transferred over bridge site oxygen and make a bond with bridge site oxygen having its final state with minimum energy.

Final states structures are somewhat different from each other. For instance, the angle of the bridge structure increases as the distance between chlorine and the oxygen at reaction site decrease. Relevant bond lengths and angle values are tabulated in Table 4.8.

Table 4.8 Comparison table for bond lengths and values of angles of allyl-radical on $Cu_2O(001)$-Cl-1 and $Cu_2O(001)$-Cl-2

	Distances(Å)		Angle (degree)
	C1-O	O-H	Cu-O-Cu
Cu_2O-Cl-1	1.448	0.978	102.5
Cu_2O-Cl-2	1.454	0.977	105.1

4.4.2. Surface Intermediate Formation on Cu_2O-Cl-2

Similar to the $Cu_2O(001)$-Cl-1 surface, only the surface intermediate OMMP2 formation is possible on $Cu_2O(001)$-Cl-2. Reaction mechanism is the same in both of the surfaces investigated. Relevant bond strengths of the final state structures of OMMP2 formation reaction on $Cu_2O(001)$-Cl-1 and $Cu_2O(001)$-Cl-2 can be observed in Table 4.9.

Table 4.9 Comparison table for bond lengths and values of angles of OMMP2 on $Cu_2O(001)$-Cl-1 and $Cu_2O(001)$-Cl-2

	Distances(Å)		Angle (degree)
	C1-Cu	C2-O	Cu-O-Cu
Cu_2O-Cl-1	2.017	1.489	106.5
Cu_2O-Cl-2	2.013	1.487	104.4

Although the mechanism of OMMP2 formation reaction is similar to that on Cu_2O-(001)-Cl-1, a little surface reconstruction of $Cu_2O(001)$-Cl-2 is observed by the connection of bridge oxygen and the copper bonded to chlorine atom as propylene gets closer to the surface. Upon binding of propylene to form OMMP2 structure, surface returned to its original state. The reason of the surface construction might be distance of chlorine and bridge oxygen being less than that on $Cu_2O(001)$-Cl-1.

Activation barrier values for Allylic hydrogen stripping (AHS) reaction and OMMP2 formation reaction on both of the investigated chlorinated $Cu_2O(001)$

surfaces are tabulated in Table 4.10. Although the adsorption properties of both of the surfaces are almost the same, activation barrier of allylic hydrogen stripping reaction is different. Allylic hydrogen stripping reaction seems harder to occur on $Cu_2O(001)$-Cl-2 surface than $Cu_2O(001)$-Cl-1. The first idea that comes to mind is the electronic effect since the distance of chlorine site and the reaction site is closer on $Cu_2O(001)$-Cl-2 surface than $Cu_2O(001)$-Cl-1. The charges of the bridge oxygens at reaction sites should be different to propose the electronic effect and only a slight difference occur in this case. The charges of the bridge oxygens are tabulated in Table 4.7 above.

Table 4.10 Comparison table for activation barriers and reaction energies of competing reactions on Cu_2O-Cl-1 and Cu_2O-Cl-2

	Allylic Hydrogen Stripping			OMMP2 Formation	
	Activation Barrier	Reaction Energy	Desorption Energy	Activation Barrier	Reaction Energy
	kcal/mol			kcal/mol	
$Cu_2O(001)$-Cl-1	4	-40	67	0	-15
$Cu_2O(001)$-Cl-2	18	-50	67	2.9	-11

4.5. Adsorption of SO_2 on Surfaces

Adsorption of SO_2 as an acidic surface probe on an oxygen atom on the surfaces aims to determine the basic character of oxygen species that it is adsorbed on. The technique was based on the idea that the hydrogen stripping tendency of adsorbed oxygen is related to its basic character. Tendency increases as basicity of oxygen atom increases. Therefore, adsorption of SO_2 to form SO_3 on the surface helps to determine the basic characteristics as adsorption energy of SO_2 gives information about electrons in valence band. The more the adsorption energy of SO_2 on the oxygen atom investigated on a surface, the more the surface has propensity for allylic hydrogen stripping reaction.

In the literature, SO_2 adsorption as a surface probe is employed for metallic surfaces to predict or confirm catalytic reactivity of the corresponding surface for propylene epoxidation reaction (Torres, Lopez et al. 2007; Kizilkaya, Senkan et al. 2010). In this study, SO_2 adsorption research has been performed according to a methodological publication for theoretical surface probes (Pacchioni, Ricart et al. 1994). The geometry of the adsorbed SO_2 on $Cu_2O(001)$-Cl-1 is presented as a sample in Figure 4.24. Furthermore, adsorption energy of SO_2 on each of the surfaces investigated throughout the study are shown in Table 4.12.

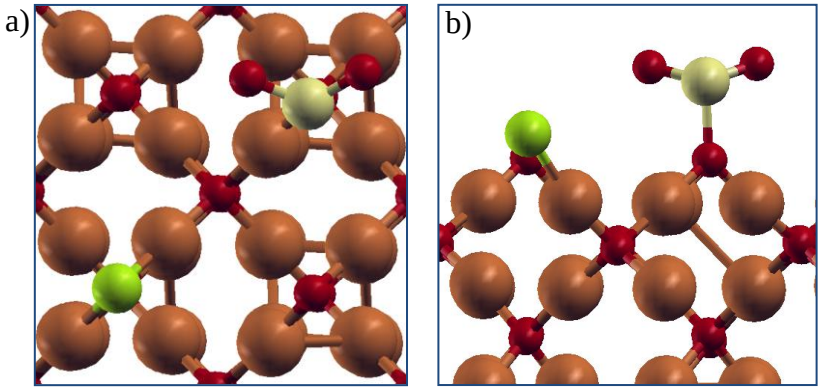

Figure 4.24 a) Top view and b) Side view of optimized adsorbed SO_2 on $Cu_2O(001)$-Cl-1 surface (Cu: dark gray, big ones; O: black, small; Cl: light gray, bigger; S: light gray, smaller)

Table 4.11 Adsorption energies of SO_2 probe on $Cu_2O(001)$-Cl-1, $Cu_2O(001)$-Cl-2 and chlorinated $RuO_2(110)$

	SO_2 Adsorption Energy (kcal/mol)
$Cu_2O(001)$-Cl-1	1.80
$Cu_2O(001)$-Cl-2	0.24
$RuO_2(110)$-Cl	0.14

The activity of $Cu_2O(001)$-Cl-2 is higher than $Cu_2O(001)$-Cl-1, and it is confirmed by SO_2 adsorption energy analysis. Expected activity of $RuO_2(110)$-Cl is highest according to results of SO_2 analysis since adsorption energy is lowest on that

surface. On the other hand, reaction analysis revealed that activity of RuO_2(110)-Cl surface is lower than the activity of Cu_2O(001)-Cl-1 surface. Therefore, SO_2 adsorption analyses are not consistent with the results of reaction analyses on the surfaces investigated. The reason of inconsistent results might be due to the effect of neighboring oxygen atoms on the oxygen at the reaction site.

CHAPTER 5

CONCLUSIONS

Propylene epoxidation reaction is investigated together with other partial oxidation reactions on metal oxide catalytic surfaces by the utilization of periodic Density Functional Theory calculations with generalized gradient approximation (GGA) method for the exchange and correlation energy.

In this study, (001) surface of copper(I)oxide, Cu_2O, and (110) surface of ruthenium(IV)oxide, RuO_2, are used as catalytic surfaces. Firstly, atomic oxygen and chlorine are adsorbed to oxygen vacant sites at the bridge sites, mentioned as the most favorable adsorption sites (Wang, Deo et al. 1999). On both $Cu_2O(001)$ and $RuO_2(110)$ surface, chlorine and oxygen atoms compete for vacant sites according to results of investigations based on atomic adsorption of these two species as adsorption energies of both chlorine and oxygen are around -60kcal/mol to both of surfaces. The next step is propylene adsorption on the surface. On both of the surfaces, propylene is physically adsorbed as adsorption energies are small, less than 5kcal/mol.

Propylene epoxidation reaction is investigated on chlorinated surfaces of $Cu_2O(001)$ and $RuO_2(110)$. Besides, formations of other products of propylene partial oxidation reactions as acetone, acrolein and allyl-radical on chlorinated $Cu_2O(001)$ surface

and propionaldehyde, acetone and allyl-radical are studied on chlorinated RuO_2(110) surface are investigated. Reaction path analyses are made by CI-NEB analysis and the activation barriers for each path are obtained with this method. Furthermore, transition state analyses are performed to confirm the structures.

Reaction mechanisms are investigated through stable surface intermediates as the existence of them are proved in the literature by both surface science studies with LEED, EXAFS etc and DFT studies (Medlin, Mavrikakis et al. 1999; Linic, Piao et al. 2004; Torres, Lopez et al. 2007; Roldan, Torres et al. 2009). Different than metal surfaces under scarce oxygen, OMMP1 formation does not occur on chlorinated Cu_2O(001) surface; rather OMMP2 is possible. The reason might be the inclined feature of bridge structure that brings allyl hydrogen and one bridge oxygen on the surface closer to each other and hence enhances allyl hydrogen stripping reaction. On chlorinated RuO_2(110) surface, existence of undercoordinated Ru atoms that are not part of the bridge structure provide more binding site and makes OMMP1 formation possible on this surface. Additionally, direct propylene oxide production path without formation of surface intermediate is also studied on both of the surfaces. But direct PO formation does not occur on chlorinated Cu_2O(001) surface, spontaneous OMMP2 formation is observed in CI-NEB analysis of reaction path. Therefore, only PO formation method on chlorinated Cu_2O(001) is the PO formation via OMMP2 surface intermediate while on chlorinated RuO_2(110) surface there are three possible paths which increases the possibility of PO formation.

The results of all reaction path analyses on chlorinated Cu_2O(001) and chlorinated RuO_2(110) are discussed in section 4.3. The results on chlorinated Cu_2O(001) revealed that PO, acetone and acrolein are the most probable products on this surface. High desorption energy of allyl radical from the surface makes it unfavorable. Actually, it is advantageous since gas phase allyl radical is known to react with gas phase oxygen and combust. Acetone is also slightly less favorable than PO because of the same reason; high desorption energy to gas phase although activation barrier of acetone is less than PO formation. When the dominant phase of chlorinated copper oxide catalyst is Cu_2O(001), probably product stream will comprised of PO, acetone and acrolein.

On chlorinated RuO_2(110) surface, the most favorable elementary reaction is allylic hydrogen stripping reaction which generates adsorbed allyl-radical on the surface. Although allyl-radical formation has very low activation barrier, its desorption energy from the surface is high. The most favorable PO formation method is direct formation without surface intermediates. Formations of side products propionaldehyde and acetone are not so favorable as PO formation.

On chlorinated Cu_2O(001) surface, the rate limiting steps of paths to gas phase products are mostly desorption step of products from the surface whereas on chlorinated RuO_2(110) surface generally desorption of products are easier. The rate limiting steps are mostly formation of the products from either surface intermediates or adsorbed propylene on this surface.

Not an important surface reconstruction is observed on the surfaces in the adsorption of chlorine or propylene investigations, in CI-NEB analysis or even after desorption of products which takes oxygen from the surface and leaves an oxygen vacancy behind.

Comparison of activation barriers of elementary reactions on non-chlorinated Cu_2O(001) surface (Onay; expected January 2012) with chlorinated Cu_2O(001) surface in this study revealed that chlorine addition has a slight improving effect on propylene oxide production by introducing an activation barrier of 4kcal/mol to the side reaction allylic hydrogen stripping which occurs without a barrier on non-chlorinated Cu_2O(001). Other than that, chlorine addition does not have significant effect on activation barriers of reactions on the surface. When chlorine is adsorbed on a closer site to the reaction site, allylic hydrogen stripping reaction occur harder i.e. activation barrier is higher. The first idea of the reason that comes to mind is the electronic effect of chlorine. The charges of the bridge oxygens at reaction sites should be different on two surfaces to propose the electronic effect while they are slightly different; charge of oxygen on the most selective surface i.e. chlorine at the closer position to the reaction site, is calculated slightly less negative than the corresponding charges on nonchlorinated surface and chlorinated surface where the chlorine is far to the oxygen at reaction site. Less negative charge means less electronegativity. According to the hypothesis of Torres et al. (Torres, Lopez et al.

2007) lower Lewis basicity of the oxygen at reaction site has less affinity towards allylic hydrogen stripping reaction which is in parallel with our findings.

Addition of chlorine on RuO_2(110) surface makes PO production by OMMP2 easier but decreases the barrier of side reaction allyl-radical formation. Also, it decreases the probability of direct PO formation. Although chlorine is introduced to a site more closer to the reaction site on RuO_2(110) than Cu_2O(001) it has worsening effect on partial oxidation reaction on this surface.

REFERENCES

APPE. "Propylene Oxide." from http://www.petrochemistry.net/propylene-oxide-and-glycols.html 27 October 2011.

Blöchl, P. E. (1994). "Projector augmented-wave method." Phys. Rev. B **50**: 17953.

Bracey, C. L., A. F. Carley, et al. (2011). "Understanding the effect of thermal treatments on the structure of CuAu/SiO2 catalysts and their performance in propene oxidation." Catalysis Science & Technology **1**(1): 76-85.

Buijink, J. K. F., J.-P. Lange, et al. (2008). Chapter 13 - Propylene Epoxidation via Shell's SMPO Process: 30 Years of Research and Operation. Mechanisms in Homogeneous and Heterogeneous Epoxidation Catalysis. S. T. Oyama. Amsterdam, Elsevier**:** 355-371.

Campbell, C. T. (1986). "Chlorine promoters in selective ethylene epoxidation over Ag(111): A comparison with Ag(110)." Journal of Catalysis **99**(1): 28-38.

Campbell, C. T. and B. E. Koel (1985). "Chlorine promotion of selective ethylene oxidation over Ag(110): Kinetics and mechanism." Journal of Catalysis **92**(2): 272-283.

Cavani, F. and J. H. Teles (2009). "Sustainability in Catalytic Oxidation: An Alternative Approach or a Structural Evolution?" ChemSusChem **2**(6): 508-534.

Chorkendorff, I. and J. W. Niemantsverdriet (2007). Concepts of modern catalysis and kinetics, Wiley-VCH.

Cornils, B. (2003). Catalysis from A to Z: a concise encyclopedia, Wiley-VCH.

Cramer, C. J. (2004). Essentials of computational chemistry: theories and models, Wiley.

Deutschmann, O., H. Knözinger, et al. (2000). Heterogeneous Catalysis and Solid Catalysts. Ullmann's Encyclopedia of Industrial Chemistry, Wiley-VCH Verlag GmbH & Co. KGaA.

Dever, J. P., K. F. George, et al. (2000). Ethylene Oxide. Kirk-Othmer Encyclopedia of Chemical Technology, John Wiley & Sons, Inc.

Dronskowski, R. (2005). Computational chemistry of solid state materials: a guide for materials scientists, chemists, physicists and others, Wiley-VCH.

Duma, V. and D. Hönicke (2000). "Gas Phase Epoxidation of Propene by Nitrous Oxide over Silica-Supported Iron Oxide Catalysts." Journal of Catalysis **191**(1): 93-104.

Ertl, G., H. Knözinger, et al. (1997). Handbook of heterogeneous catalysis, VCH.

Fierro, J. L. G. (2006). Metal oxides: chemistry and applications, Taylor & Francis.

Force, E. L. and A. T. Bell (1976). "The effect of dichloroethane moderation on the adsorbed species present during the oxidation of ethylene over silver." Journal of Catalysis **44**(2): 175-182.

Ghijsen, J., L. H. Tjeng, et al. (1988). "Electronic structure of Cu2O and CuO." Physical Review B **38**(16): 11322.

Hayashi, T., K. Tanaka, et al. (1998). "Selective Vapor-Phase Epoxidation of Propylene over Au/TiO2Catalysts in the Presence of Oxygen and Hydrogen." Journal of Catalysis **178**(2): 566-575.

Henkelman, G. and H. Jónsson (2000). "Improved tangent estimate in the nudged elastic band method for finding minimum energy paths and saddle points." Journal of Chemical Physics **113**(22): 9978-9985.

Henrich, V. E. and P. A. Cox (1996). The surface science of metal oxides, Cambridge University Press.

Jensen, F. (1999). Introduction to computational chemistry, Wiley.

Kahlich, D., U. Wiechern, et al. (2000). Propylene Oxide. Ullmann's Encyclopedia of Industrial Chemistry, Wiley-VCH Verlag GmbH & Co. KGaA.

Kahn, M., A. Seubsai, et al. (2010). "High Throughput Synthesis and Screening of New Catalytic Materials for the Direct Epoxidation of Propylene." Combinatorial Chemistry & High Throughput Screening **13**(1): 67-74.

Kim, Y. D., A. P. Seitsonen, et al. (2001). "Characterization of Various Oxygen Species on an Oxide Surface: RuO2(110)†." The Journal of Physical Chemistry B **105**(18): 3752-3758.

Kirk-Othmer and J. I. Kroschwitz (1992). Kirk-Othmer Encyclopedia of Chemical Technology, John Wiley & Sons.

Kizilkaya, A. C., S. Senkan, et al. (2010). "Investigation of ruthenium-copper bimetallic catalysts for direct epoxidation of propylene: A DFT study." Journal of Molecular Catalysis A: Chemical **330**(1-2): 107-111.

Koch, W. and M. C. Holthausen (2001). A chemist's guide to density functional theory, Wiley-VCH.

Kresse, G. and J. Furthmuller (1996). "Efficiency of ab-initio total energy calculations for metals and semiconductors using a plane-wave basis set." Computational Materials Science **6**(1): 15-50.

Kresse, G. and J. Hafner (1994). "Ab initio molecular-dynamics simulation of the liquid-metal-amorphous-semiconductor transition in germanium." Phys. Rev. B **49**: 14251.

Kresse, G. and D. Joubert (1999). "From ultrasoft pseudopotentials to the projector augmented-wave method." Phys. Rev. B **59**: 1758.

Kung, H. H. (1989). Transition metal oxides: surface chemistry and catalysis, Elsevier.

Lambert, R. M., R. L. Cropley, et al. (2003). "Halogen-induced selectivity in heterogeneous epoxidation is an electronic effect-fluorine, chlorine, bromine and iodine in the Ag-catalysed selective oxidation of ethene." Chemical Communications(10): 1184-1185.

Le, D., S. Stolbov, et al. (2009). "Reactivity of the Cu2O(1 0 0) surface: Insights from first principles calculations." Surface Science **603**(10-12): 1637-1645.

Linic, S., H. Piao, et al. (2004). "Ethylene Epoxidation on Ag: Identification of the Crucial Surface Intermediate by Experimental and Theoretical Investigation of its Electronic Structure." Angewandte Chemie International Edition **43**(22): 2918-2921.

Lu, G. and X. Zuo (1999). "Epoxidation of propylene by air over modified silver catalyst." Catalysis Letters **58**(1): 67-70.

Lu, J., J. J. Bravo-Suárez, et al. (2006). "Direct propylene epoxidation over modified Ag/CaCO3 catalysts." Applied Catalysis A: General **302**(2): 283-295.

Lu, J., J. J. Bravo-Suárez, et al. (2005). "In situ UV-vis studies of the effect of particle size on the epoxidation of ethylene and propylene on supported silver catalysts with molecular oxygen." Journal of Catalysis **232**(1): 85-95.

Lu, J., M. Luo, et al. (2002). "Epoxidation of Propylene on NaCl-Modified VCe1-x Cux Oxide Catalysts with Direct Molecular Oxygen as the Oxidant." Journal of Catalysis **211**(2): 552-555.

Lu, J., M. Luo, et al. (2002). "Epoxidation of propylene on NaCl-modified silver catalysts with air as the oxidant." Applied Catalysis A: General **237**(1-2): 11-19.

LyondellBasell. "Propylene oxide technical information." from http://www.lyondellbasell.com/Products/ByCategory/basic-chemicals/IntermediateChemicalsAndGlycols/PropyleneOxide/ 27 October 2011.

McKetta, J. J. (1993). Encyclopedia of chemical processing and design, Marcel Dekker.

Medlin, J. W., M. Mavrikakis, et al. (1999). "Stabilities of Substituted Oxametallacycle Intermediates: Implications for Regioselectivity of Epoxide Ring Opening and Olefin Epoxidation." The Journal of Physical Chemistry B **103**(50): 11169-11175.

Monkhorst, H. J. and J. D. Pack (1976). "Special points for Brillouin-zone integrations." Physical Review B **13**(12): 5188.

Monnier, J. R. and G. W. Hartley (2001). "Comparison of Cu and Ag Catalysts for Epoxidation of Higher Olefins." Journal of Catalysis **203**(1): 253-256.

Monnier, J. R., J. L. Stavinoha, et al. (2004). "Effects of chlorine and chlorine dynamics during silver-catalyzed epoxidation of butadiene." Journal of Catalysis **226**(2): 321-333.

Nijhuis, T. A., M. Makkee, et al. (2006). "The Production of Propene Oxide: Catalytic Processes and Recent Developments." Industrial & Engineering Chemistry Research **45**(10): 3447-3459.

Nijhuis, T. A., S. Musch, et al. (2000). "The direct epoxidation of propene by molten salts." Applied Catalysis A: General **196**(2): 217-224.

Onal, I., D. Düzenli, et al. (2010). "Propylene Epoxidation: High-Throughput Screening of Supported Metal Catalysts Combinatorially Prepared by Rapid Sol–Gel Method." Topics in Catalysis **53**(1): 92-99.

Onay;, D. (expected January 2012). Application of Density Functional Theory to Propylene to Propylene Oxide Catalytic Reaction (to be submitted). Master of Science, Middle East Technical University.

Over, H., Y. D. Kim, et al. (2000). "Atomic-Scale Structure and Catalytic Reactivity of the RuO2(110) Surface." Science **287**(5457): 1474-1476.

Özbek, M. O., I. Önal, et al. (2011). "Ethylene Epoxidation Catalyzed by Silver Oxide." ChemCatChem **3**(1): 150-153.

Pacchioni, G., J. M. Ricart, et al. (1994). "Ab Initio Cluster Model Calculations on the Chemisorption of CO2 and SO2 Probe Molecules on MgO and CaO (100) Surfaces. A Theoretical Measure of Oxide Basicity." Journal of the American Chemical Society **116**(22): 10152-10158.

Parr, R. G. and W. Yang (1994). Density-functional theory of atoms and molecules, Oxford University Press.

Paulus, U. A., Y. Wang, et al. (2004). "Adsorption and Interaction of Ethylene on RuO2(110) Surfaces†." The Journal of Physical Chemistry B **109**(6): 2139-2148.

Perdew, J. P., J. A. Chevary, et al. (1992). "Atoms, Molecules, Solids, and Surfaces: Applications of the Generalized Gradient Approximation for Exchange and Correlation." Phys. Rev. B **46**: 6671.

Pinnaduwage, D. S., L. Zhou, et al. (2007). "Chlorine Promotion of Styrene Epoxidation on Au(111)." Journal of the American Chemical Society **129**(7): 1872-1873.

Ramachandran, K. I., G. Deepa, et al. (2008). Computational chemistry and molecular modeling: principles and applications, Springer.

Richardson, H. W. (2000). Copper Compounds. Ullmann's Encyclopedia of Industrial Chemistry, Wiley-VCH Verlag GmbH & Co. KGaA.

Rodriguez, J. A., J. Y. Kim, et al. (2003). "Reduction of CuO in H2: in situ time-resolved XRD studies." Catalysis Letters **85**(3): 247-254.

Roldan, A., D. Torres, et al. (2009). "On the effectiveness of partial oxidation of propylene by gold: A density functional theory study." Journal of Molecular Catalysis A: Chemical **306**(1-2): 6-10.

Rothenberg, G. (2008). Catalysis: concepts and green applications, Wiley-VCH.

Santen, R. A. and M. Neurock (2006). Molecular heterogeneous catalysis: a conceptual and computational approach, Wiley-VCH.

Schulz, K. H. and D. F. Cox (1991). "Photoemission and low-energy-electron-diffraction study of clean and oxygen-dosed Cu2O (111) and (100) surfaces." Physical Review B **43**(2): 1610.

Seitsonen, A. P., D. Crihan, et al. (2009). "Reaction mechanism of ammonia oxidation over RuO2(1 1 0): A combined theory/experiment approach." Surface Science **603**(18): L113-L116.

Serafin, J. G., A. C. Liu, et al. (1998). "Surface science and the silver-catalyzed epoxidation of ethylene: an industrial perspective." Journal of Molecular Catalysis A: Chemical **131**(1-3): 157-168.

Seubsai, A., M. Kahn, et al. (2011). "New Catalytic Materials for the Direct Epoxidation of Propylene by Molecular Oxygen." ChemCatChem **3**(1): 174-179.

SHELL. "Propylene oxide product overview." from http://www.shell.com/home/content/chemicals/products_services/our_products/propylene_oxide_derivatives/propylene_oxide/product_overview/ 27 October 2011.

Su, W., S. Wang, et al. (2009). "A molecular insight into propylene epoxidation on Cu/SiO2 catalysts using O2 as oxidant." Journal of Catalysis **268**(1): 165-174.

Sumitomo Chemical Co., L. "Development of New Propylene Oxide Process." from http://www.sumitomochem.co.jp/english/rd/report/theses/docs/20060100_ely.pdf 27 October 2011.

Tang, W. and et al. (2009). "A grid-based Bader analysis algorithm without lattice bias." Journal of Physics: Condensed Matter **21**(8): 084204.

Thomas J.M. , T. J. W. (1997). Principles and Practice of Heterogeneous Catalysis. Weinheim, VCH Verlagsgesellschaft mbH.

Torres, D., F. Illas, et al. (2008). "Towards an understanding of promoter action in heterogeneously catalyzed ethene epoxidation: Why chlorine is the best halogen." Journal of Catalysis **260**(2): 380-383.

Torres, D., N. Lopez, et al. (2007). "Low-Basicity Oxygen Atoms: A Key in the Search for Propylene Epoxidation Catalysts." Angewandte Chemie International Edition **46**(12): 2055-2058.

Trent, D. L. (2000). Propylene Oxide. Kirk-Othmer Encyclopedia of Chemical Technology, John Wiley & Sons, Inc.

Vaughan, O. P. H., G. Kyriakou, et al. (2005). "Copper as a selective catalyst for the epoxidation of propene." Journal of Catalysis **236**(2): 401-404.

Wang, C.-B., G. Deo, et al. (1999). "Interaction of Polycrystalline Silver with Oxygen, Water, Carbon Dioxide, Ethylene, and Methanol: In Situ Raman and Catalytic Studies." The Journal of Physical Chemistry B **103**(27): 5645-5656.

Wang, Y., H. Chu, et al. (2008). "Copper-based efficient catalysts for propylene epoxidation by molecular oxygen." Catalysis Today **131**(1-4): 496-504.

Werner, A. and H. D. Hochheimer (1982). "High-pressure x-ray study of Cu2O and Ag2O." Physical Review B **25**(9): 5929.

Yap, N., R. P. Andres, et al. (2004). "Reactivity and stability of Au in and on TS-1 for epoxidation of propylene with H2 and O2." Journal of Catalysis **226**(1): 156-170.

Young, D. C. (2001). Computational chemistry: a practical guide for applying techniques to real world problems, Wiley.

Zemichael, F. W., A. Palermo, et al. (2002). "Propene Epoxidation over K-Promoted Ag/CaCO₃ Catalysts: The Effect of Metal Particle Size." Catalysis Letters **80**(3): 93-98.

Zhu, W., Q. Zhang, et al. (2008). "Cu(I)-Catalyzed Epoxidation of Propylene by Molecular Oxygen." **112**(20): 4.